MAGNETIC PROPERTIES OF MANGANESE AND COPPER PYROPHOSPHATES

MAGNETIC PROPERTIES OF MANGANESE PYROPHOSPHATE AND COPPER PYROPHOSPHATE

by

JAMES A. R. STILES, B.Sc.

A Thesis

Submitted to the School of Graduate Studies

in Partial Fulfillment of the Requirements

for the Degree

Doctor of Philosophy

McMaster University

November 1972

DOCTOR OF PHILOSOPHY (1973) McMASTER UNIVERSITY
(Physics) Hamilton, Ontario

TITLE: Magnetic Properties of Manganese Pyrophosphate and Copper Pyrophosphate

AUTHOR: James A. R. Stiles, B.Sc. (University of British Columbia, Vancouver, B.C.)

SUPERVISOR: Professor C. V. Stager

NUMBER OF PAGES: ix, 117

SCOPE AND CONTENTS:

The magnetic structure of manganese pyrophosphate and copper pyrophosphate have been determined by single crystal neutron diffraction studies. More detailed information about the magnetic structure is determined from nuclear magnetic resonance data. The origin of the magnetic anisotropy energy in $Cu_2P_2O_7$ is discussed.

Abstract

The magnetic structures of antiferromagnetic manganese pyrophosphate and copper pyrophosphate have been determined by single crystal neutron diffraction techniques. More detailed features of the magnetic structure have been determined by nuclear magnetic resonance (NMR). A discrepancy between previous NMR measurements on $Mn_2P_2O_7$ and the single crystal neutron measurements was resolved by postulating a low temperature crystallographic phase transition. Information about the dependence of the transferred hyperfine interaction upon the separation of the relevant ions is obtained for $Cu_2P_2O_7$ from the NMR data and from previously determined deviations from a higher symmetry phase. The origin of the magnetic anisotropy energy in $Cu_2P_2O_7$ is discussed.

ACKNOWLEDGEMENTS

I would like to thank my supervisor, Dr. C. V. Stager, for his assistance with this work.

I am also indebted to Dr. C. Calvo, for help in aligning the crystals, to Dr. M.F. Collins and Dr. D. A. Goodings for their helpful suggestions, to D. Twiney for growing the crystals and to Dr. S. H. Choh for assistance with the experimental work.

Finally, I would like to thank the National Research Council of Canada for their financial support of this work.

TABLE OF CONTENTS

LIST OF FIGURES

LIST OF TABLES

CHAPTER I

INTRODUCTION

The purpose of this work is to examine the magnetic properties of manganese pyrophosphate ($Mn_2P_2O_7$) and copper pyrophosphate ($Cu_2P_2O_7$) in their magnetically ordered phases. Previous work on these compounds has left a number of unresolved problems. In manganese pyrophosphate, the spin configuration has been determined (Collins et al, 1971) by neutron diffraction from a powdered sample. Choh and Stager (1970) have proposed a number of possible spin configurations on the basis of nuclear magnetic resonance (NMR) experiments. None of their proposals are in agreement with the configuration determined by Collins et al. One of the purposes of the present work is to resolve this discrepancy. Single crystal neutron diffraction techniques were used to confirm the work of Collins et al and the NMR results are explained by postulating a crystallographic phase transition in this compound.

In copper pyrophosphate a similar crystallographic phase transition is known to exist (Robertson and Calvo, 1967). The techniques employed in the present work to study this compound include NMR and single crystal neutron diffraction. The single crystal neutron diffraction results were used to

determine the gross features of the magnetic structure, that is the spin configuration. NMR was employed to look for more detailed features of the magnetic structure including small deviations from the structure determined by neutron and X-ray diffraction techniques. The known crystallographic phase transition, in conjunction with the NMR data, is used to obtain information about the dependence of spin transfer between ions upon the separation of the ions. Also, previous work on this compound has left unanswered the question of the origin of the anisotropy energy determined from antiferromagnetic resonance (AFMR) data (Fowlis, 1970). Several terms in the equations for the anisotropy energy are examined in an attempt to explain the data.

The remainder of Chapter I is devoted to a brief discussion of magnetic ordering in transition metal compounds using the molecular field approximation. In addition there are some references to earlier work on similar magnetic systems. Chapter II contains an outline of the crystallography of the compounds studied. Chapter III describes the neutron diffraction experiments and the method used to obtain the spin configurations. Chapter IV describes the NMR experiments and the associated analysis of the data. Finally, Chapter V is a theoretical discussion of the origin of the anisotropy energy in $Cu_2P_2O_7$.

The magnetic character of the compounds studied arises from the "unpaired spins" which result from the incomplete filling of the 3d electron levels in the transition metal series

of elements of which copper and manganese are members. In an isolated ion Hunds rule says that the states are filled with parallel spins until the maximum number allowed by the Pauli exclusion principle is reached, after which electrons with antiparallel spins are added, until all states are filled. Thus Mn^{++} with five 3d electrons has a total spin of s = 5/2, while Cu^{++} with nine 3d electrons has a total spin of s = 1/2, that is it can be represented as a complete 3d shell plus one hole.

In the absence of any external perturbations, the 3d energy levels are degenerate. However, in the environment of the surrounding crystal, the degeneracies are lifted by strong electric fields, resulting from the surrounding ions, that is a strong Stark splitting is observed. Given a knowledge of the symmetry of the ion sites, one can determine the manner in which the degeneracies are lifted, by group theoretical arguments. From this can be obtained information about the magnetic moment on the ions (Ballhausen, 1962).

The neutron scattering experiments rely on the scattering of neutrons via the dipole-dipole interaction between the magnetic moment on the neutrons and that associated with the unpaired spins on the magnetic ions. If these spins exhibit long range order, as in the magnetically ordered state, then this interaction leads to a contribution to the intensity of Bragg diffraction peaks. Above the ordering temperature this

contribution disappears. It may be determined by measuring the intensity of the Bragg peaks above and below the ordering temperature. The remaining contribution to the Bragg peaks is due to scattering by the nuclei. Generally speaking, the magnetic symmetry of the crystals is different from the crystallographic symmetry, so that some Bragg peaks which are forbidden by symmetry for nuclear scattering, are not forbidden for magnetic scattering. Where the magnetic scattering is much weaker than the nuclear scattering, this effect results in a considerable saving in the time required to obtain the desired statistical accuracy for magnetic scattering, as there is not a large background count due to nuclear scattering with an attendant large statistical uncertainty.

The NMR experiments measure the internal magnetic fields present at the nuclear sites in the samples. These internal fields arise from two main sources. The first of these is the classical dipole field, arising from the magnetic moments localized on the other magnetic ions. The field due to a single neighbouring moment is given by the classical dipole equation. If the site at which the fields is measured is labelled by i and if the magnetic sites are associated with a magnetic moment $\bar{m}_j$ separated from site i by the distance $\underline{r}_{ij}$, it follows that the field at site i due to the rest of the ions in the sample is given by

$$\bar{H} = \sum_{j \neq i} \left(\frac{\bar{m}_j}{|r|^3_{ij}} - \frac{3\bar{r}_{ij}}{|r_{ij}|^5} (\bar{m}_j \cdot \bar{r}_{ij}) \right) \qquad (1)$$

where we have summed over all the magnetic moments in the crystal. In general this sum depends upon the sample shape, however for distances sufficiently far from the site in question, one can replace the discrete moments by a continuous distribution of magnetic moment density. Thus for ease of computation, one can perform the discrete sum for moments contained within a radius R of the site i, and replace the remaining terms with an integral. This integral contains the Lorentz and demagnetizing fields. The demagnetizing field depends upon the sample shape, but for a spherical sample it is equal in magnitude and opposite in sign to the Lorentz field, therefore these terms cancel. It should be noted that for an antiferromagnet, both of these terms are identically zero, since in this case the macroscopic magnetic moment density is zero.

The second contribution to the internal fields is the transferred hyperfine effect. In an iron series transition metal, some of the 3d wavefunction resides on the non-magnetic ions, resulting in a fractional unpaired spin on the non-magnetic ions. The magnitude of the fractional spin depends upon the degree of covalency. Typical values for the fractional unpaired spin in iron series transition metal compounds are in the range .5% to 5% (Owen and Thornley, 1966). This transferred hyperfine effect is closely related to the exchange interaction which is responsible for magnetic ordering.

The transferred hyperfine interaction was first observed

by Owens and Stevens (1953). They interpreted the electron spin resonance spectrum of Ir^{+4} in the complex $(IrCl_6)^{-2}$ by assuming that there were hyperfine lines produced by an interaction with the neighbouring chlorine nuclei. For the iron series transition metal group, the interaction was first observed by Tinkham (1956) in the ESR spectra of Mn^{++}, Fe^{++}, Co^{++}, and Cr^{+++} introduced as impurities in ZnF_2. The first NMR measurements were made by Shulman and Jaccarino (1956) who observed field shifts in the nuclear magnetic resonances of ^{19}F in MnF_2 from their predicted free ion values. They also showed that the shifts were proportional to the magnetic suscepbitility of the sample, and hence to the thermal average of the manganese ion spins (Shulman and Jaccarino, 1957). The only magnetically ordered system with a similar structure to that of the pyrophosphates that has been studied by NMR is antiferromagnetic $LiMnPO_4$ (Mays, 1963). Numerous dissimilar magnetically ordered compounds have been studied,however.

Choh and Stager (1970) have observed the transferred hyperfine effect in $Mn_2P_2O_7$. They have also shown that it is necessary to include a term proportional to the susceptibility in the nuclear Hamiltonian when the system is magnetically ordered. The resulting field shifts in the ^{31}P resonances become non negligible for high applied magnetic fields. In this case the shift shows an angular dependence related to that of the susceptibility tensor.

In the current work, the NMR of $Mn_2P_2O_7$ is reanalyzed in the light of neutron diffraction measurements determining the spin configurations of the compound. The NMR of $Cu_2P_2O_7$ is also analyzed, again with a knowledge of the spin configuration as determined from neutron diffraction.

The systems studied both order magnetically at sufficiently low temperatures. The dominant contribution to the mechanism responsible for magnetic order may be represented by the Heisenberg Hamiltonian, which may be written as follows.

$$H = \sum_{i<j} \bar{\bar{J}}_{ij} \bar{S}_i \cdot \bar{S}_j \qquad (2)$$

where $\bar{S}_i$ and $\bar{S}_j$ are the spins located on the i^{th} and j^{th} ions. $\bar{\bar{J}}_{ij}$ is the exchange parameter and is related to the overlap integral of the wave functions on adjacent ions. The sign of J determines whether the ordering will be ferromagnetic or antiferromagnetic. A commonly used approximation is the molecular field approximation where S_i is replaced by its thermal average. This ignores spin-spin correlations, so the approximation is not valid at very low temperatures. In this case spin wave theory is employed. A commonly used concept in the molecular field approximation is the exchange field, defined by the following equation.

$$H_i = -g\beta \bar{S}_i \cdot \bar{H}_{ex} \qquad (3)$$

H_i is now a single ion Hamiltonian and H_{ex} is the exchange field. This may be interpreted as a magnetic field which acts

on adjacent spins to keep them colinear. The ordering temperature is reached when the exchange energy becomes comparable with the thermal energy of the spins. Above this temperature thermal energy dominates and the material is paramagnetic, and below it, the exchange energy predominates and the material becomes magnetically ordered. The ordering temperature may be determined by several methods. One method is to observe the specific heat. The phase transition is second order and the specific heat shows a λ type anomaly. Other methods include observing the temperature at which the electron paramagnetic resonance signal disappears and by measuring the temperature dependence of the magnetic susceptibility. Fowlis (1969) has measured the Néel temperature of $Mn_2P_2O_7$ by the latter method and determined it to be 13(1)°K. The number in parentheses is the uncertainty in the data. For copper pyrophosphate Fowlis (1970) determined the Néel temperature to be 26(1)°K from magnetic susceptibility data.

As the compounds studied in this work order antiferromagnetically, we discuss briefly the antiferromagnetic state. This state may be characterized by a number of interpenetrating sublattices, each of which has all its spins parallel. The case where there are two sublattices, with antiparallel spins is discussed at length in an article by Nagamiya et al (1955). They derive the antiferromagnetic equations of motion in the molecular field approximation. If + denotes the "up" sublattice

and - denotes the "down" sublattice, then the exchange field can be written as

$$\bar{H}_{ex}^{\pm} = - A\bar{M}^{\mp} - \Gamma\bar{M}^{\pm} \qquad (4)$$

where M^+ and M^- denote the magnetization of their respective sublattices. A and Γ are second rank interaction tensors which represent inter sublattice and intra sublattice exchange interactions respectively. Their dominant parts are isotropic. With this assumption, the direction of the spins with respect to the crystallographic axes is undetermined so a phenomenological anisotropy energy is introduced which is denoted by E_A. In a system with no higher than orthorhombic symmetry, this energy takes the form

$$E_A = \frac{1}{2} K_1(\beta_+^2 + \beta_-^2) + \frac{1}{2} K_2(\gamma_+^2 + \gamma_-^2), \quad K_2 > K_1 > 0. \qquad (5)$$

where K_1 and K_2 are anisotropy constants and $\beta_\pm$, $\gamma_\pm$ are the direction cosines of the respective sublattice magnetization vectors with respect to the crystallographic axes. The equilibrium spin direction is then determined by minimizing the expression for the anisotropy energy. An anisotropy field is defined by the relationship

$$\delta E_A = - \bar{H}_A^{+} \cdot \delta\bar{M}^{+} - \bar{H}_A^{-} \cdot \delta\bar{M}^{-}. \qquad (6)$$

The assumption is usually made that the exchange energy is much larger than the anisotropy energy, and therefore the magnitude of the sublattice magnetization vectors is not affected

by the anisotropy energy. In tensor notation we can write

$$\bar{H}_a^{\pm} = -A'\bar{M}^{\mp} - \Gamma'\bar{M}^{\pm}. \qquad (7)$$

In the principle axis system one principle value can be set to zero, because only differences in the principle values are considered. In a biaxial system, the remaining two are non zero and different in magnitude.

There are several possible contributions to the anisotropy energy. The first of these is the magnetic dipole interaction. For values of the spin greater than one half there are crystal field contributions to the anisotropy energy, as for example in $Mn_2P_2O_7$ where s = 5/2. This contribution does not arise in the case of $Cu_2P_2O_7$ as we have a ground state doublet and an effective spin of one half. The remaining contributions arise from the Heisenberg Hamiltonian. These contributions may be further subdivided into those due to anisotropy in s and into those attributable to anisotropy in the exchange tensor $\bar{\bar{J}}_{ij}$ which couples adjacent spins. Kanamori (1963), gives an outline of various sources of anisotropy energy arising from the exchange Hamiltonian. Another possible source of anisotropy lies in magnetostrictive effects, but without a detailed knowledge of the elastic constants of the materials, very little can be said about this contribution.

For low symmetry crystals, the spin direction is determined experimentally from the angular dependence of the magnetic susceptibility. The exchange field may also be obtained from

susceptibility data and the anisotropy fields are obtained from AFMR data. Specifically, one obtains the exchange field from the perpendicular susceptibility, that is the susceptibility $\chi_{\perp}$ measured with an external field applied perpendicular to $M^{\pm}$. Molecular field theory gives $\chi_{\perp} = 1/A$ so that, neglecting intra sublattice interactions, the exchange field is given by.

$$\bar{H}_{ex}{}^{\pm} = - \frac{\bar{M}^{\mp}}{\chi_{\perp}} \quad . \tag{8}$$

For sufficiently large external fields, the spins in an antiferromagnet rotate to orient themselves perpendicular to the applied field. This phenomenum is referred to as "spin-flop". This effect arises from the fact that the susceptibility for an antiferromagnet is greater for spins aligned perpendicular to the applied field than for spins parallel to the applied field. Thus the energy of interaction with the external field, given by

$$E = - \frac{1}{2} \int \chi \cdot H^2 dv \tag{9}$$

where the integral is over the volume of the sample, is lower when the applied field is perpendicular to the spins. Spin flop occurs when this energy difference overcomes the anisotropy energy of the crystal. The spin-flop field is given by

$$H_{SF} = (2H_{ex}H_{Al})^{1/2} \tag{10}$$

where H_{Al} is the lower of the two anisotropy fields. The spin flop field can be measured by observing a discontinuity

in the parallel susceptibility as a function of applied field and by AFMR.

From AFMR measurements two resonant frequencies can be measured for a biaxial system. Assuming that both anisotropy fields are much less than the exchange field, these frequencies are given at T = 0 by

$$\frac{\omega_1}{\gamma} = (2H_E \times HA_1)^{1/2} \quad \text{and} \quad \frac{\omega_2}{\gamma} = (2H_E \times H_{A2})^{1/2} \qquad (11)$$

from which both anisotropy fields H_{A1} and H_{A2} can be obtained. γ is the gyromagnetic ratio.

There are a number of deviations from true antiferromagnetic behaviour. One of these involves a canting, or tipping, towards one another of the spins on opposing sublattices. The interaction may be represented by the following Hamiltonian.

$$H = \sum_{i<j} \bar{d} \cdot (\bar{S}_i \times \bar{S}_j) \qquad (12)$$

and is referred to as the Dzialoshinski interaction. The symbol $\bar{d}$ is a constant vector and $\bar{S}_i \times \bar{S}_j$ represents the vector cross product of the spins on adjacent sites. Dzialoshinski first used this interaction to explain weak ferromagnetism in Fe_2O_3 (Dzialoshinski, 1958). Moriya (1963) discusses this, and other sources of weak ferromagnetism in nearly antiferromagnetic compounds. Another phenomenum worthy of note is the existence of two dimensional antiferromagnets above the temperature where one finds true three dimensional ordering. This effect is noted when the exchange coupling within planes is strong, but the

exchange coupling between planes is small. Lines (1967) has investigated such systems, for example K_2NiF_4 . The iron series transition metal pyrophosphate compounds might be expected to exhibit this effect, since planes of magnetic ions defined by the crystallographic axes a and b lie relatively far apart as compared to ions contained within the planes.

Several previous measurements have been made on the pyrophosphates. Atkinson and Stager (1969) and Atkinson et al. (1970) have measured the ^{31}P NMR shift for $Mn_2P_2O_7$, $Cu_2P_2O_7$, $Ni_2P_2O_7$, and $Co_2P_2O_7$ in the paramagnetic phases, thus measuring the transferred hyperfine interaction in these compounds. Fowlis (1970) has observed the magnetic susceptibility of $Mn_2P_2O_7$, $Cu_2P_2O_7$, $Co_2P_2O_7$ and $Ni_2P_2O_7$. In addition he has made AFMR measurements on $Mn_2P_2O_7$ and $Cu_2P_2O_7$. Choh and Stager have observed the ^{31}P NMR in antiferromagnetic $Mn_2P_2O_7$. Their results are reinterpreted in the present work. Collins et al (1971) have determined by powder neutron diffraction measurements the spin configuration of $Mn_2P_2O_7$. In this work their results are confirmed, using single crystal neutron diffraction techniques and the reported discrepancies between their work and the NMR results of Choh and Stager (1970) are reconciled by postulating a low temperature crystallographic phase transition in that compound.

The g values of Mn^{++}, Cu^{++}, and Co^{++} have been determined in the pyrophosphate structure by substituting them as dilute impurities in a non-magnetic host pyrophosphate compound, for

example $Zn_2P_2O_7$ (Chambers et al. 1964, Calvo et al. 1967, and Atkinson et al. 1970).

The crystallographic structure of $Cu_2P_2O_7$ was determined by Robertson and Calvo (1967). Lukaszewicz and Smajkiewicz (1961) and Tondon (1971) have done the crystallographic work on $Mn_2P_2O_7$.

CHAPTER II

CRYSTALLOGRAPHY OF THE COMPOUNDS STUDIED

A. $Mn_2P_2O_7$

The crystal structure of $Mn_2P_2O_7$, at room temperature, has been determined by Lukaszewicz and Smajkiewicz (1961). It is monoclinic with space group C2/m and contains two molecules in a unit cell. Tondon (1971) has ascertained that there is no phase transitiondown to 100°K. He gives the lattice parameters at 100°K as a = 6.598(5)Å, b = 8.558(5)Å, c = 4.516(5)Å and β = 102.74(5)°. Among a series of pyrophosphates that have the C2/m structure at high temperatures, $Mn_2P_2O_7$ is unique in that there is no X-ray evidence for a different low temperature phase (Robertson and Calvo, 1970). The other compounds in the series all lose the mirror plane in the low temperature phase.

The four manganese ions in the c-centered unit cell are crystallographically equivalent. They are located on a two fold axis and are related by the mirror plane and the c-centered operation. The four phosphorus ions are also equivalent and are located on the mirror plane. The oxygen atoms are of three types. Two of them are designated O_I and form the bridging link between the two phosphorus ions in the anion. These are located both on the mirror plane and on a two fold axis. The second type, designated O_{II}, are terminal

ions on the anion group and are located on the mirror plane, but not on a two fold axis. There are 4 of these. The remaining eight are designated O_{III}. These are also terminal ions on the anion and are not located at points of symmetry. The lattice coordinates of the ions are listed in Table 1, as are some of the important bond lengths.

B. $Cu_2P_2O_7$

$Cu_2P_2O_7$ is monoclinic and is known to exist in two phases. The high temperature or β phase has the C2/m structure and is isomorphous with $Mn_2P_2O_7$. The low temperature or α phase has the c axis doubled. Robertson and Calvo (1967) report the lattice parameters of the α phase as a = 6.876(5)Å, b = 8.115(5)Å, c = 9.162(5)Å and β = 109.54(6)°. They refined the structure in the space groups C2/c and Cc, and chose C2/c as being the most probable. In either case the structure does not differ by much from the C2/m phase. The atomic coordinates for α $Cu_2P_2O_7$ are listed in Table 2, as are some important bond lengths. A schematic diagram of the pyrophosphate molecule is shown in Fig. 1.

In both compounds the magnetic ions occur in layers which lie in planes containing the b and a axes. The ions in adjacent planes are relatively far apart, and are separated by layers of anions.

TABLE 1

Atomic Coordinates for Manganese Pyrophosphate

ion[a]	x/a	y/b	z/c
Mn	0	.3096	1/2
P	.2155	0	.9092
O_I	0	0	0
O_{II}	.3742	0	.2082
O_{III}	.2209	.1489	.7258

Selected Bond Lengths for $Mn_2P_2O_7$

Mn-O distance (Å)	O-P distance (Å)	Mn-O-P angle (deg.)
2.098(10)	1.525(11)	136.6
2.343(10)		118.1
2.098(10)	1.525(11)	136.6
2.343(10)		118.1
2.138(7)	1.540(11)	130.1
2.138(7)		130.1

[a]The remaining atomic coordinates are obtained by applying the symmetry operations of the space group C2/m.

TABLE 2

Atomic Coordinates for α $Cu_2P_2O_7$

ion[a]	x/a	y/b	z/c
Cu	-.0183(2)	.3133(2)	.5138(3)
P	.1978(4)	.0086(4)	-.0878(5)
O_I	0	.0480(24)	0
O_{II}	.3768(11)	-.0019(15)	.2254(18)
O_{III}	.2223(11)	.1556(12)	.2714(15)
	.1782(13)	.1530(10)	.2634(10)

Bond Lengths in α $Cu_2P_2O_7$ for a Single Cu^{++} Ion

Cu-O_{II}	1.990(6) Å
Cu-O_{II}	1.986(6) Å
Cu O_{III}	1.907(6) Å
Cu O_{III}	1.935(6) Å
Cu O_{III}	2.322(6) Å
Cu O_{III}	2.947(6) Å

[a]The remaining coordinates are generated using the symmetry operations of the space group C2/c.

Fig. 1

A schematic diagram of a transition metal ion pyrophosphate compound. The unmarked circles correspond to metal ions and the intra anion bonds are marked in black.

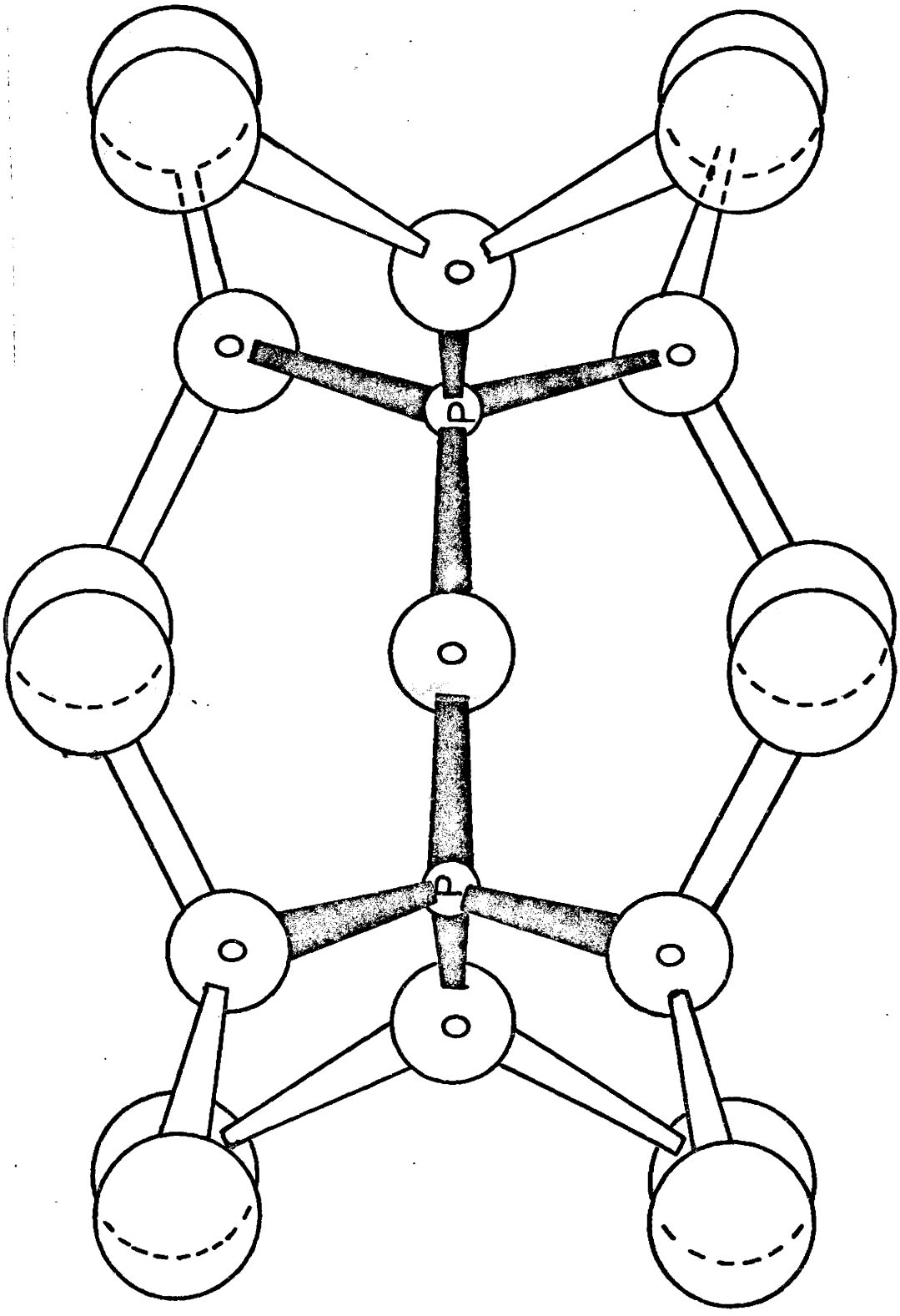
P
P

CHAPTER III

Neutron Diffraction. Experimental Apparatus

Neutrons have associated with themselves an intrinsic wavelength given by $\lambda = h/mv$ where h is Planck's constant and m and v are the mass and velocity of the neutron. If one considers that the neutrons in a reactor have made a large number of collisions with atoms at a temperature T before being extracted from the reactor thus they will have a root mean square velocity $\bar{v}$ related to the absolute temperature by the following equation.

$$\frac{1}{2} m\bar{v}^2 = \frac{3}{2} kT \qquad (13)$$

where k is Boltzman's constant. The associated wavelength of these neutrons is then given by

$$\lambda^2 = h^2/3mkT. \qquad (14)$$

It is fortuitous that the wavelengths, for typical reactor temperatures of approximately 100°C, are of the same order of magnitude as a typical lattice constant for the compounds studied. There will be a spread of neutron velocities given by the Maxwellian distribution. If $N_\lambda d_\lambda$ is the number of neutrons extracted from the reactor per second with wavelength between λ and $\lambda + d_\lambda$, then

$$N_\lambda = \frac{2N_1}{\lambda} \left(\frac{E}{kT}\right)^2 e^{-E/kT} \qquad (15)$$

where N_1 is the number of neutrons per second integrated over all velocities, and E is the energy of a neutron of wavelength λ (Bacon and Thewlis, 1949). The white beam from the reactor must be monochromated. This is accomplished by using a Bragg reflection from a copper crystal. The monochromated beam is collimated by using cadmium apertures. The resulting beam has a wavelength given by

$$\lambda = 2d(h,k,\ell)\sin\theta_m \qquad (16)$$

where $d(h,k,\ell)$ is the interplanar spacing of those planes corresponding to Miller indices h, k and ℓ. The angle θ_M is shown in Fig. 2. The wavelength desired can be selected by making an appropriate choice for θ_M. It is apparent that neutrons of wavelength λ/n will be diffracted at the same angle from the set of planes characterized by nh, nk, and $n\ell$, where n is an integer. To reduce this harmonic contamination of the monochromated beam it is necessary to select a wavelength sufficiently near the high energy end of the Maxwellian distribution so that the spectral density of the white beam for $n_\lambda (n \geq 2)$ is negligible.

The bandwith $\Delta\lambda$ is determined by the mosaic spread of the monochromating crystal, and by the finite divergence of the incident beam. The intensity of the monochromated beam increases as $\Delta\lambda$ is increased but the spectral resolution decreases so a compromise must be reached between the two factors.

Fig. 2

A schematic diagram of the McMaster triple axis spectrometer at Chalk River, Ont.

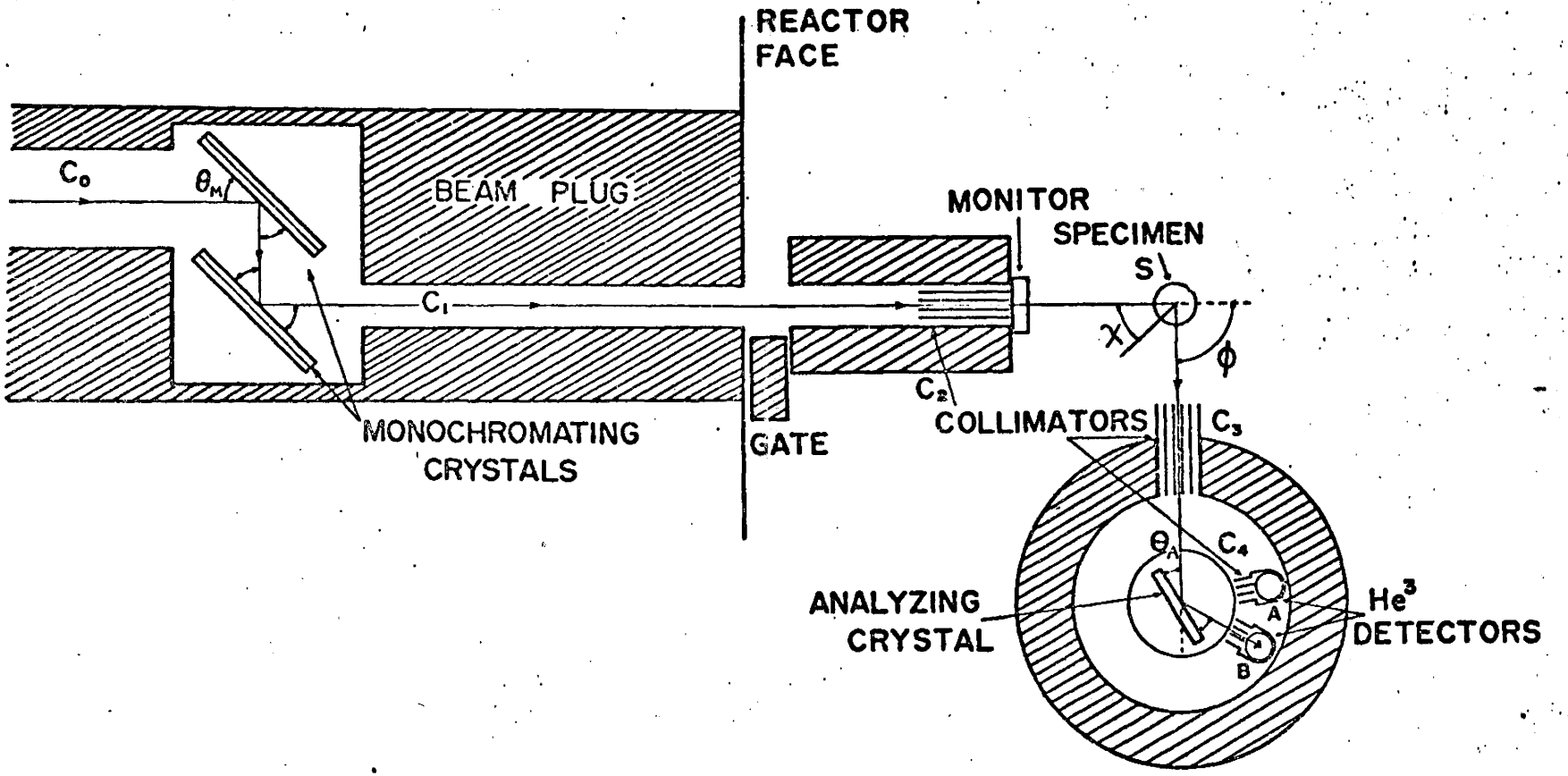
REACTOR
FACE
C_0
θ_M
BEAM PLUG
MONITOR
SPECIMEN
S
C_1
χ
ϕ
C_2
COLLIMATORS
C_3
MONOCHROMATING
CRYSTALS
GATE
θ_A
C_4
ANALYZING
CRYSTAL
He^3
DETECTORS
A
B

The monochromatic beam is diffracted by the sample crystal and a proportional counter is used to measure the diffracted neutrons from the sample. The diffraction angles for the sample are denoted by ϕ and the orientation of the crystal axes with respect to the incident beam is denoted by χ. Both of these angles are shown in Fig. 2. A monitor counter is used to determine the intensity of the incident monochromatic beam. The count rate is defined as the number of diffracted neutrons for a fixed number of monitor counts. The neutron diffraction experiments employed two spectrometers. Where the count rates were sufficiently high, it was possible to use the double axis spectrometer at the McMaster University reactor. A schematic diagram of the spectrometer is shown in Fig. 3. A boron trifluoride proportional counter was employed as a detector. The monochromator for this experiment utilized the (220) reflections of a copper crystal and provided a neutron beam with wavelength 1.048 Å. Where small sample size, and very weak magnetic scattering necessitated the use of a higher flux reactor, use was made of the McMaster University triple axis spectrometer at the NRU reactor of Atomic Energy of Canada Ltd. at Chalk River, Ontario. The spectrometer was used in a two axes mode, that is the analyzer crystal was removed so that the detector directly counted the diffracted beams from the sample. In this case the detector was a ^{3}He proportional counter. This spectrometer employs a double monochromator which enables the wavelength of the monochromated beam to be

Fig. 3

A schematic diagram of the McMaster University double axis spectrometer.

R	REACTOR CORE
B	BISMUTH PLUG
D	BEAM TUBE
G	IRON GATE
L	LATHE BED
C	COUNTER
M	MONITOR
T	BEAM STOPPER
X_1	MONOCHROMATOR
X_2	MONOCHROMATOR
S	SAMPLE TABLE

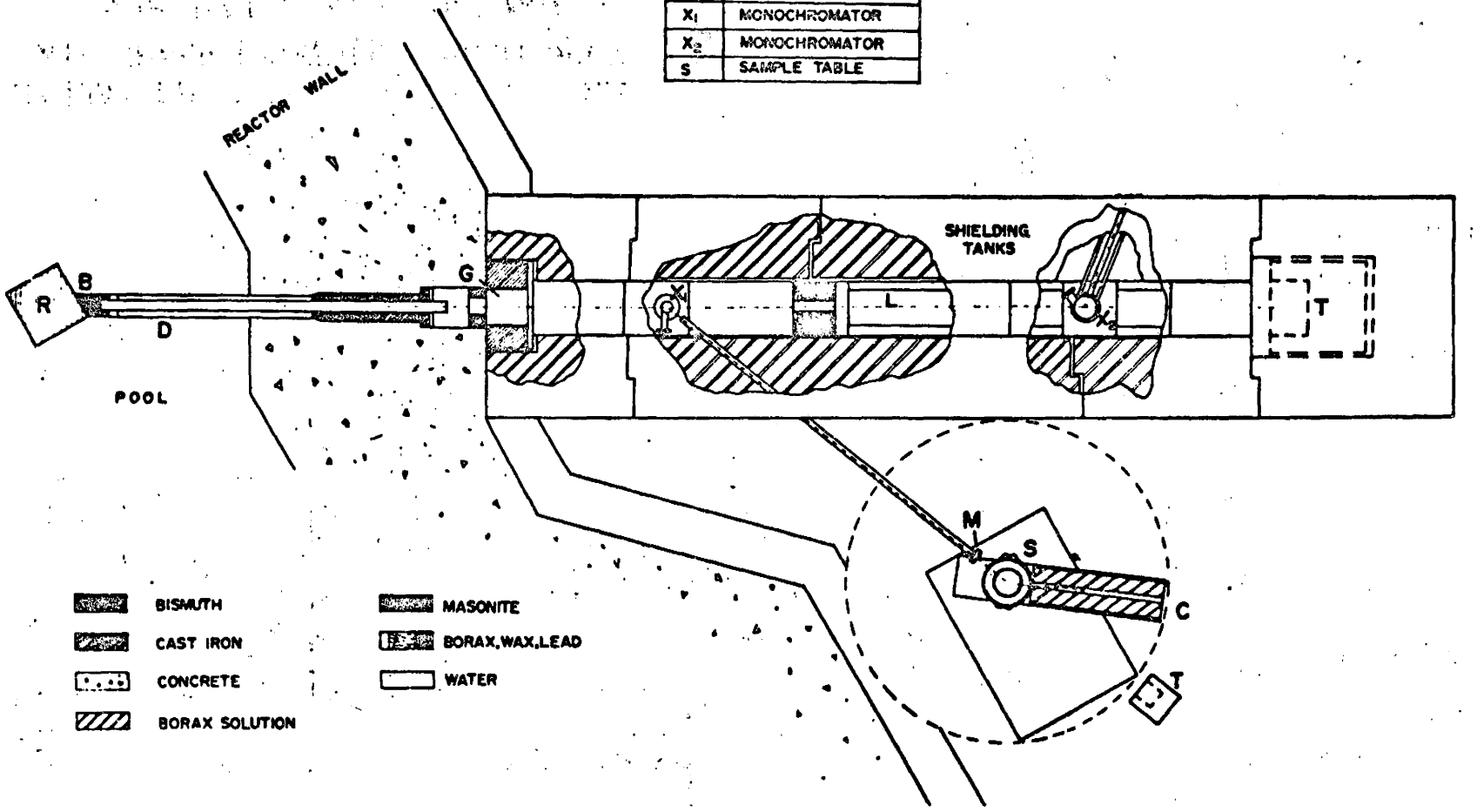

changed easily, wtihout moving the entire spectrometer with its heavy machinery and shielding. A schematic diagram of this spectrometer is shown in Fig. 2. The wavelength used for this experiment was 1.190 Å.

The cryostat used for these experiments was of conventional design and used helium exchange gas to cool the sample. An ultimate temperature of 6°K was reached. A schematic diagram of the cryostat is shown in Fig.4 . The crystal was mounted on a tripod inside the exchange gas chamber so that small adjustments to the alignment of the crystal could be made while it was in the cryostat.

Samples

The $Mn_2P_2O_7$ and $Cu_2P_2O_7$ crystals were obtained by slowly cooling a melt of the desired compound through the melting point. The crystals were extracted from the resulting solidified mass. For $Mn_2P_2O_7$ the compound was melted and cooled under vacuum and for $Cu_2P_2O_7$ the powder was sealed in an evacuated silica tube before heating. The $Mn_2P_2O_7$ crystal was shaped into a rough ellipsoid with principal diameters of 3.5, 5.5, and 5.5 mm along the a, b, and c* crystallographic axes. The $Cu_2P_2O_7$ crystal was approximately a rectangular parallelopiped with dimensions 2 mm×1 mm×1 mm.

The crystals were aligned to within 1° along a specific crystallographic axis before being inserted into the cryostat. This was done with an X-ray precession camera. Once aligned in this manner, they were glued to a quartz rod and mounted on the

Fig. 4

A schematic diagram of the cryostat used for neutron diffraction studies.

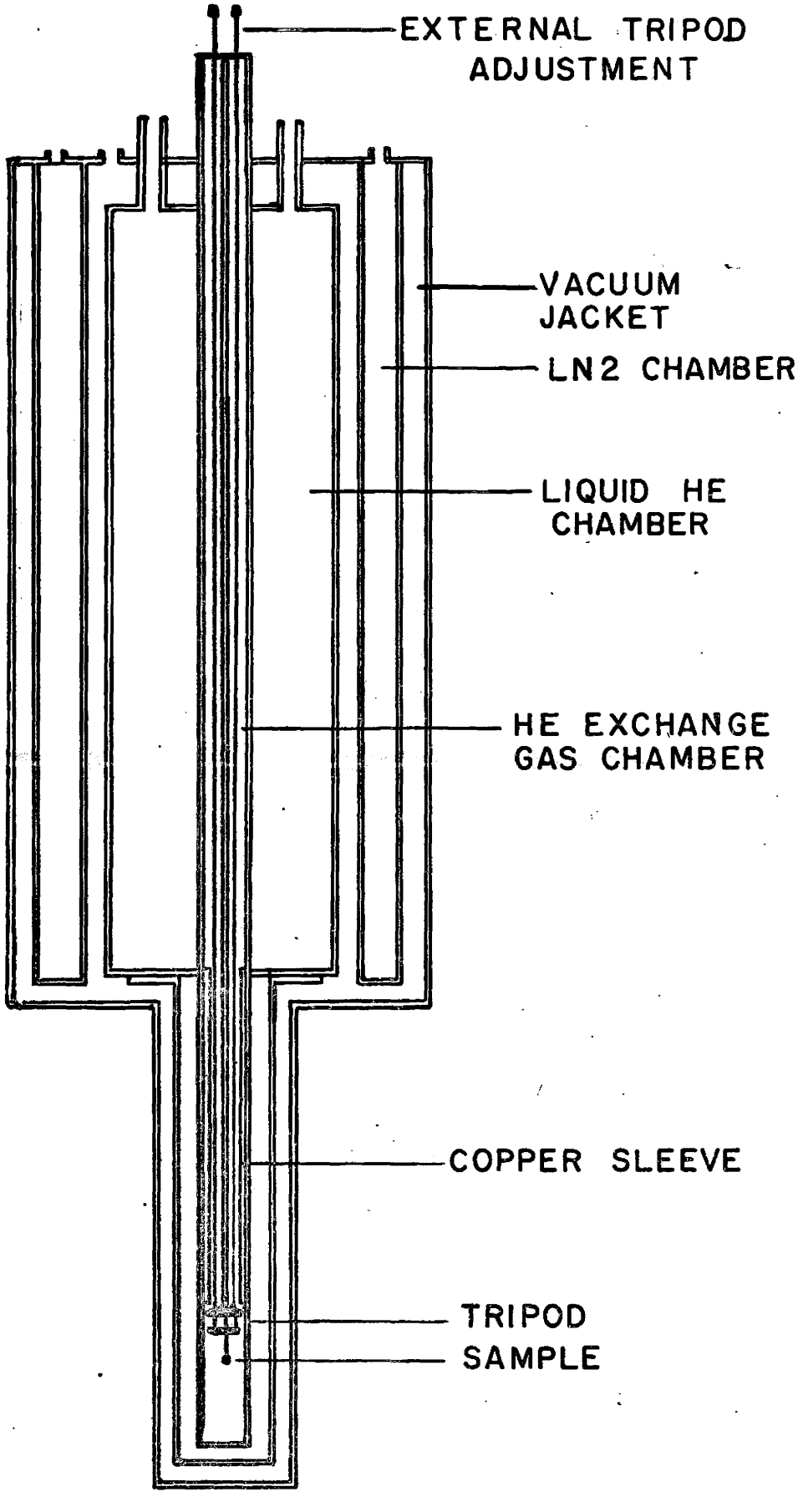
EXTERNAL TRIPOD ADJUSTMENT
VACUUM JACKET
LN2 CHAMBER
LIQUID HE CHAMBER
HE EXCHANGE GAS CHAMBER
COPPER SLEEVE
TRIPOD
SAMPLE

tripod within the cryostat. They could then be aligned to greater precision using the neutron beam. A further adjustment was necessary after the samples were cooled due to differential thermal expansion of the sample holder.

Theory of elastic neutron scattering by solids

Scattering by nuclei

If we represent an incoming plane wave of neutrons by $\Psi = e^{ikz}$ where $k = 2\pi/\lambda$ and if this wave is incident upon a single nucleus the scattered wave will be of the form $\Psi = -(b/r)e^{ik\,r}$, where r is the distance from the scattering nuclei, b is defined as the scattering length which is in general a complex number. We write $b = \alpha + i\beta$. The imaginary part becomes important only for materials with a large neutron absorption coefficient, such as cadmium, and may be ignored for the types of atoms considered in this work. Therefore we may consider b to be real. The resultant neutron wave is given by

$$\Psi = e^{ikz} - (b/r)e^{ikr} \qquad (17)$$

The scattering cross section is defined as the ratio of the outgoing current of scattered neutrons to the incident neutron flux. It is therefore given by the following relation

$$\sigma = 4\pi r^2 v \frac{\left|(b/r)e^{ikr}\right|^2}{v\left|e^{ikz}\right|^2} = 4\pi b^2 \ . \qquad (18)$$

If we now consider the scattering of neutrons from a regular lattice of atoms, the amplitude of the scattered wave is given by

$$\Psi = \sum_{\rho} (b_\rho/r) e^{i\bar{k}\cdot\bar{r}} e^{i\bar{\rho}\cdot(\bar{k}-\bar{k}')} \qquad (19)$$

where ρ labels the atoms and $\bar{\rho}$ is the vector from the origin to the ρ^{th} atom. k and k' are the wave vectors of the incident and scattered waves respectively. For the case of a regular lattice the term $e^{i\rho(k-k')}$ which takes into account the phase difference between the scattered waves from different nuclei, is replaced by $\exp\{2\pi i(hx + ky + \ell z)\}$. In this expression, h, k and ℓ are the Miller indices appropriate to the scattering direction being considered and x, y, and z are fractions of the lattice vectors $\bar{a}$, $\bar{b}$ and $\bar{c}$.

In a regular lattice diffraction is is only possible at discrete angles which are determined by the Bragg condition.

$$\bar{\kappa}-\bar{\kappa}' = \bar{G}(h\ k\ \ell). \qquad (20)$$

$\bar{G}(hk\ell)$ is referred to as a reciprocal lattice vector and is given by

$$\bar{G}(h\ k\ \ell) = h\bar{a} + k\bar{b} + \ell\bar{c}. \qquad (21)$$

The intensity of the Bragg peak corresponding to the direction $(hk\ell)$ is proportional to the following expression.

$$|F(hk\ell)|^2 = \left|\sum_{\rho} b_\rho \exp 2\pi i(hx + ky + \ell z)\right|^2. \qquad (22)$$

The assumption is made that the incident beam is not significantly attenuated by the crystal. Also lattice vibrations are neglected, but since the compounds studied have a high melting temperature, this effect should be negligible at the temperatures of interest.

The Bragg condition contains two requirements for scattering. The first concerns the angle 2ϕ which the scattered beam makes with the incident beam. This is given by

$$\lambda = 2d(hk\ell)\sin\phi \qquad (23)$$

where $d(hk\ell)$ is the interplanar spacing associated with h, k and ℓ . The angle ϕ is shown in Fig. 2. The second concerns the direction of the reciprocal lattice vector $\bar{G}(hk\ell)$ which must be in the same direction as $\bar{\kappa}-\bar{\kappa}'$. This is also shown in Fig. 2. In addition to the intensity due to the Bragg peaks, there is a background intensity which is independent of the orientation of $\bar{G}$ with respect to the beam. This background arises from several sources. These include incoherent scattering due to different isotopes of the same element being distributed randomly through the crystal. They include as well the effect of the different nuclear spins on atoms of the same element.

In single crystal diffraction experiments, the usual experiment is to set the scattering angle at the prescribed angle for a particular Bragg peak and rotate the crystal by varying the angle χ to produce a rocking curve. The intensity is then taken to be proportional to the area under the curve. This procedure introduces an additional geometric factor into the expression for the scattered intensity. In this case we have for the intensity of the peak

$$I = \frac{\lambda^3 N_c^2}{\sin 2\phi} V|F|^2 \ . \qquad (24)$$

V is the volume of the crystal and N_c is the number of unit cells per unit volume.

Magnetic scattering

Neutrons may be scattered from unpaired electrons in a crystal via the dipole-dipole interaction. The scattering amplitude for nuclear scattering is replaced by the following expression for an antiferromagnet with a single magnetic species.

$$F_M = |\bar{q}|\bar{S}\,\frac{e^2\gamma}{mc^2}\,f\sum_{\rho_M}\exp 2\pi i(hx + ky + \ell z)\ . \qquad (25)$$

q is the magnetic interaction vector defined by

$$\bar{q} = \bar{\varepsilon}(\bar{\varepsilon}\cdot\bar{K}) - \bar{K} \qquad (26)$$

where $\bar{K}$ is a unit vector in the direction of the atomic magnetic moment and $\bar{\varepsilon}$ is a unit vector along the reciprocal lattice vector for the appropriate h, k and ℓ. S is the spin on the magnetic ions, γ is the magnetic moment of the neutron expressed in nuclear magnetons, and f is an atomic form factor given by

$$f = 4\pi\int d\rho n(\rho)\ \rho^2\,\frac{\sin\mu\rho}{\mu\rho}\ , \qquad (27)$$

The factor $n(\rho)$ is the density of unpaired electrons in a single ion normalized so that the total number of unpaired electrons per magnetic ion is unity. The symbol ρ is the distance from the nucleus of the ion in question and $\mu = (4\pi/\lambda)\sin\theta$. To a first approximation this quantity is given for Mn^{++} as

$$f = e^{-.075\mu^2} \text{ (Shull et al, 1951)} \qquad (28)$$

and for Cu^{++} is given by

$$f = e^{-.04\mu^2} \text{ (Alperin, 1960).} \qquad (29)$$

The sum over ions includes only magnetic ions.

If we consider both nuclear and magnetic scattering, the intensity of the Bragg peaks is given by the following expression.

$$d\sigma = b^2 + 2bp\bar{q}\cdot\bar{\lambda} + p^2q^2 \qquad (39)$$

where $p = \frac{e^2\gamma}{2mc^2} Sf$, and $\bar{\lambda}$ is the neutron polarization vector (Halpern and Johnson, 1939). For an unpolarized neutron beam, the dot product $\bar{q}\cdot\bar{\lambda}$ averages to zero, therefore

$$d\sigma = b^2 + p^2q^2 \ . \qquad (31)$$

As a result, the magnetic and nuclear scattering contributions to the intensity of a Bragg peak are additive. In those cases where symmetry permits both nuclear and magnetic scattering, the magnetic scattering intensity can be obtained by subtracting from the intensity observed below the magnetic ordering temperature, the intensity of the nuclear scattering observed above the ordering temperature. Above the ordering temperature there is no coherent magnetic scattering in the absence of an external magnetic field.

The Bragg conditions are expressed in terms of the following coordinate system for the monoclinic systems of interest. The direction of G(hkℓ) is given in spherical polar coordinates with respect to the following choice of axes. The x-axis is chosen

to be along the crystallographic a axis, the y axis is chosen to be along b, which makes the Z axis along the direction of the reciprocal lattice vector c*.

The d spacings for a monoclinic system are given by the following expression

$$d(hk\ell) = \frac{1}{\sqrt{\frac{h^2}{a^2} + \frac{k^2}{b^2} + \left(\frac{a\ell - ch\cos\beta}{ac\sin\beta}\right)^2}} \qquad (32)$$

With the above choice of axes the polar angle θ is given by the following expression

$$\theta = \cos^{-1}\left(\left[\frac{\ell}{c}\csc\beta - \frac{h}{a}\cot\beta\right]d(hk\ell)\right) . \qquad (33)$$

The azimuthal angle ϕ may be obtained from the following expression

$$\phi = \cos^{-1}\left(\frac{\frac{h}{a}}{\sqrt{\frac{h^2}{a^2} + \frac{k^2}{b^2}}}\right). \qquad (34)$$

Selected values of $1/d(hk\ell)$, and the spherical polar angles for the reciprocal lattice vectors are given in Table 3 for $Mn_2P_2O_7$, and in Table 4 for $Cu_2P_2O_7$.

The structure factors for the compounds studied are as follows. For $Mn_2P_2O_7$ it is given, for nuclear scattering, by

$$\begin{aligned} F(hk\ell) = {} & b_{Mn} \sum_{i=1}^{4} \exp 2\pi i(hx_i + ky_i + \ell z_i) \\ & + b_P \sum_{j=1}^{4} \exp 2\pi i(hx_j + ky_j + \ell z_j) \\ & + b_O \sum_{k=1}^{14} \exp 2\pi i(hx_k + ky_k + \ell z_k) \end{aligned} \qquad (35)$$

TABLE 3

Selected Values of 1/d(hkℓ) and Spherical Polar Angles for the Reciprocal Lattice Vectors in $Mn_2P_2O_7$

h k ℓ	1/d(hkℓ)	θ	ϕ
0 2 0	.2331	90.00	90.00
0 0 1	.2258	0.00	0.00
0 0 2	.4516	0.00	0.00
0 1 0	.1166	90.00	90.00
0 1 2	.4664	14.47	90.00
0 3 0	.3497	90.00	90.00
0 1 1	.2541	27.30	90.00

TABLE 4

Selected Values of $1/d(hk\ell)$ and Spherical Polar Angles for the Reciprocal Lattice Vectors in $Cu_2P_2O_7$

h k ℓ	$1/d(hk\ell)$	θ	ϕ
0 6 0	.7396	90.00	90.00
0 6 1	.7486	81.10	90.00
0 6 4	.8727	57.94	90.00
0 0 8	.9265	0.00	0.00
0 2 2	.3383	46.78	90.00
0 4 2	.5447	64.84	90.00
0 2 1	.2724	64.84	90.00
0 0 1	.1158	0.00	0.00
0 1 0	.1233	90.00	90.00
0 1 1	.1691	46.78	90.00
0 1 3	.3687	19.53	90.00
0 3 0	.3698	90.00	90.00
0 3 1	.3875	72.61	90.00
0 3 3	.5074	46.78	90.00

For $Cu_2P_2O_7$ the nuclear structure factor is

$$F(hk\ell) = b_{Cu} \sum_{i=1}^{8} \exp 2\pi i(hx_i + ky_i + \ell z_i)$$

$$+ b_p \sum_{j=1}^{8} \exp 2\pi i(hx_j + ky_j + \ell z_j)$$

$$+ b_o \sum_{k=1}^{28} \exp 2\pi i(hx_k + ky_k + \ell z_k) \quad . \qquad (36)$$

The coherent nuclear scattering lengths are given as follows: $b_{Mn} = -.36\times10^{-12}$ cm, $b_p = .53\times10^{-12}$ cm, $b_o = .577\times10^{-12}$ cm and $b_{Cu} = .79\times10^{-12}$ cm (Bacon, 1962). The indices j and k in the above expressions refer to the atomic positions of the phosphorus and oxygen atoms respectively. The index i refers to the magnetic atoms.

For magnetic scattering the structure factors are given by

$$F_M(hk\ell) = \sin\alpha \frac{e^2\gamma S}{mc^2} f \sum_{i=1}^{n} \exp 2\pi i(hx + ky + \ell z). \qquad (37)$$

The sum i runs over all magnetic ions in the respective materials. The angle α arises from the magnetic interaction vector and is defined as the angle between the direction of the magnetic moments and the reciprocal lattice vector. It is given by

$$\sin\alpha = \left(1-\left(\frac{h\cos\beta\cos\delta}{a\sin\beta} + \frac{\ell\cos\delta}{c\sin\beta}\right)^2 d(hk\ell)^2\right)^{1/2} \qquad (38)$$

where δ is the angle between the magnetic moment direction and the Z axis. For $Mn_2P_2O_7$ $\beta = 102°$ and $\delta = 80°$ and for $Cu_2P_2O_7$ $\beta = 109°$ and $\delta = 15°$. The δ angles are determined from magnetic susceptibility measurements.

Experimental Results

A. Manganese Pyrophosphate

A typical rocking curve for a magnetic reflection in $Mn_2P_2O_7$ is shown in Fig. 5. The double peak is presumed to be due to the sample consisting of two crystals with a small (0.8°) misorientation of the crystal axes. The double peak is present for both magnetic and nuclear reflections. Table 5 gives the intensities of a selected number of Bragg peaks both at 100°K and 6°K. These temperatures are respectively above and below the the Néel temperature of 13(1)°K as determined from magnetic susceptibility measurements (Fowlis and Stager 1969). The intensities are obtained by integrating the Bragg peak after subtraction of background counts. Fig. 6 shows the temperature dependence of the peak intensity for the (010) reflection. From Fig. 6 and Table 5 it is evident that the (010), (011), (030) and (012) reflections are magnetic in character. The Miller indices used here and below are referred to the chemical unit cell. It should be noted that the Néel temperature of 12°K obtained from the temperature dependence is a lower limit due to the existence of temperature gradients in the dewar, and does not conflict with the previously reported value (Fowlis and Stager 1969) of 13(1)°K.

Assuming that the magnetic unit cell is either identical to the chemical unit cell, or is doubled along the c axis , there are 35 possible colinear antiferromagnetic spin configurations possible. The intensities of the magnetic reflections

Fig. 5

Rocking curve for the (010) magnetic reflection in $Mn_2P_2O_7$. The solid line is drawn as a visual guide through the points.

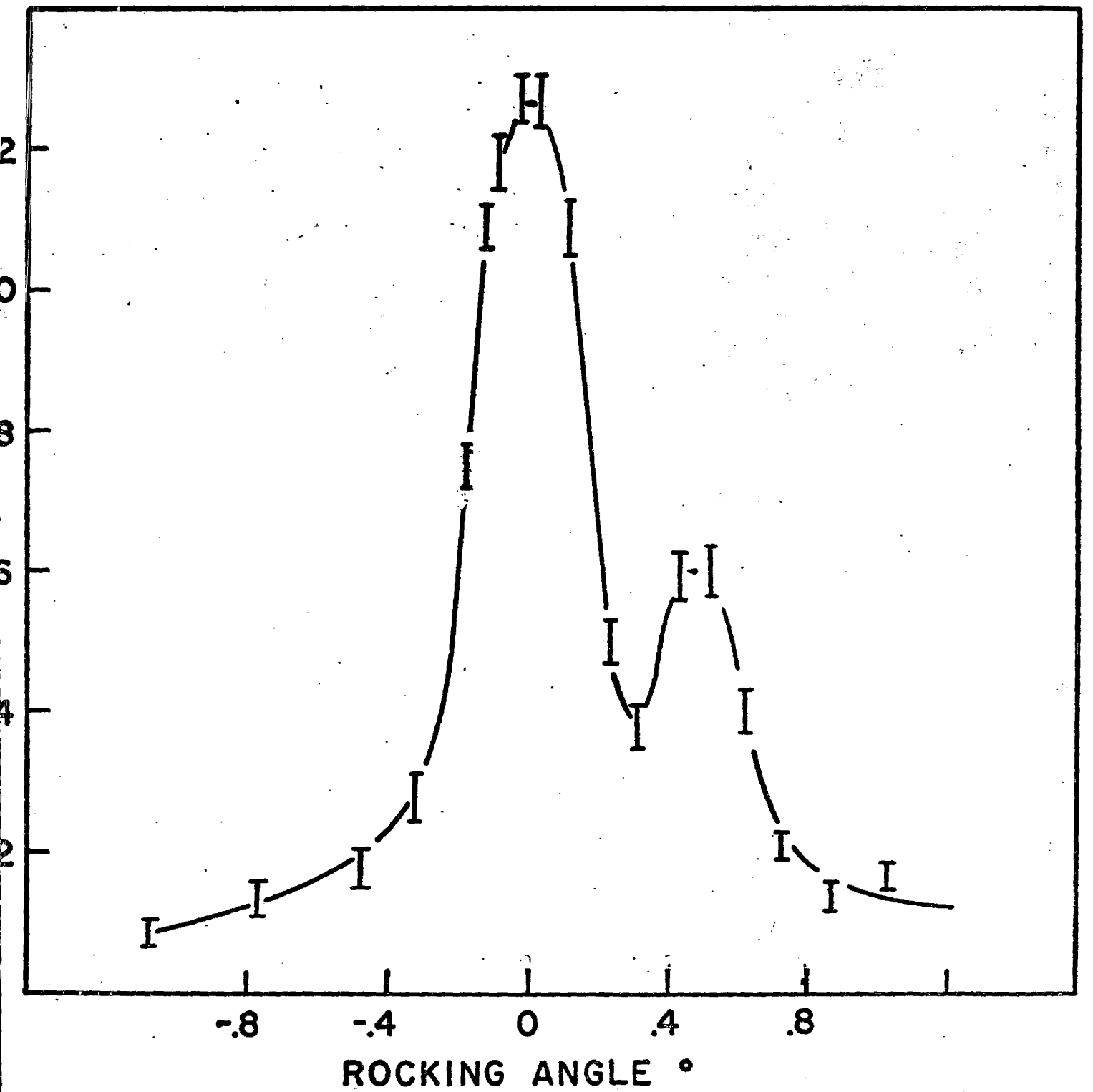
2
0
8
6
4
2
-.8
-.4
0
.4
.8
ROCKING ANGLE °

Fig. 6

Temperature dependence of the counting rate at the center of the (010) peak in $Mn_2P_2O_7$.

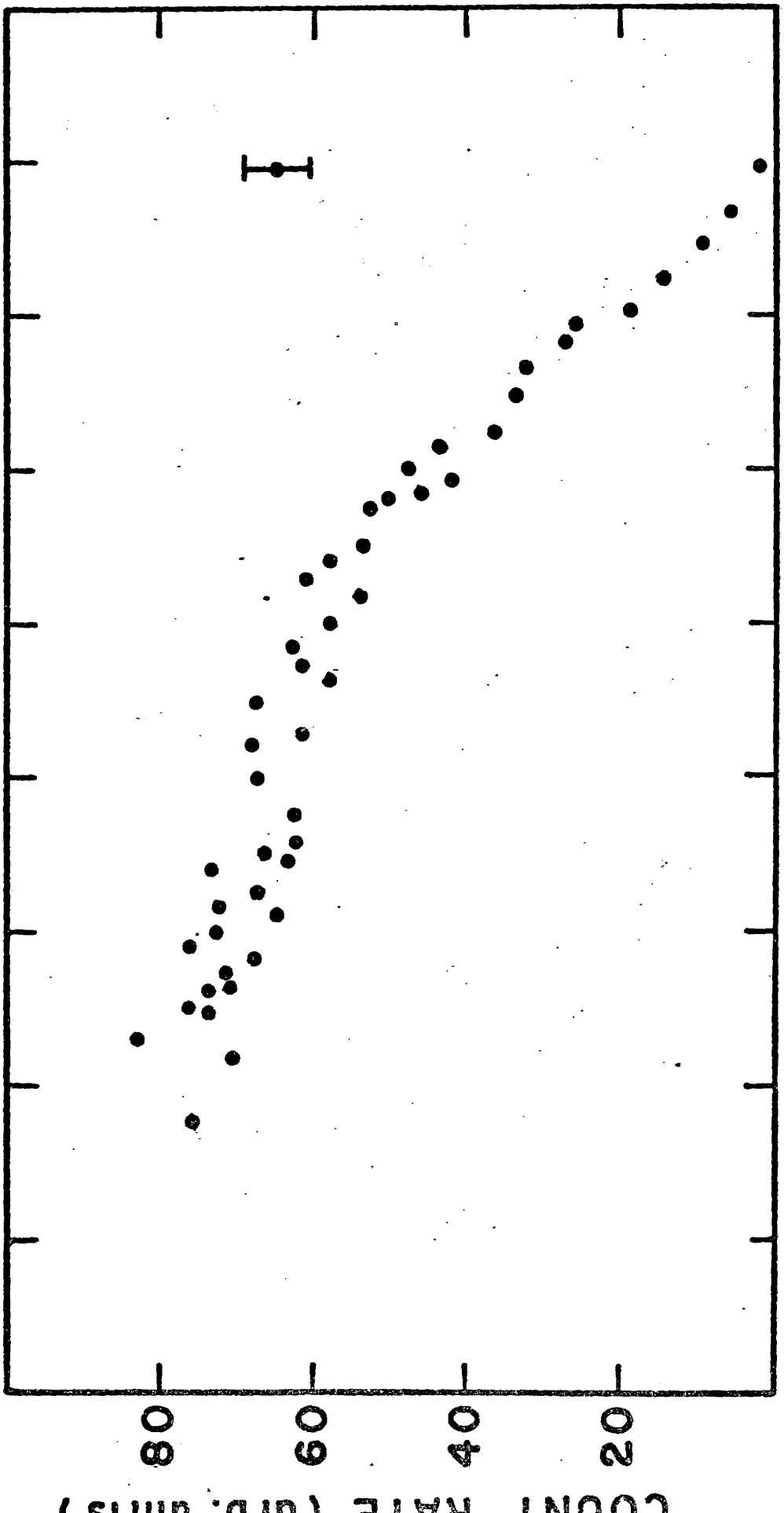
COUNT RATE (arb. units)
80
60
40
20
TEMPERATURE (°K)
5
6
7
8
9
10
11
12

TABLE 5

Observed and Calculated Intensities for $Mn_2P_2O_7$

h k ℓ	Observed Intensity (100°K)	Observed Intensity (6°K)	Calculated Intensity	Type (Nuclear or Magnetic
0 2 0	28	-	28	N
0 0 1	17	-	18	N
0 0 2	26	-	33	N
0 1 0	<1	14 (2)	18	M
0 1 2	<1	4 (1)	5	M
0 3 0	<1	2 (1)	2	M
0 1 1	<1	10 (2)	12	M

The calculated intensities have been normalized to the observed intensity for (020).

The mesured integrated intensities have been multiplied by the geometrical factor sin 2θ (Bacon 1962, p. 57).

were calculated relative to the intensity of the (020) nuclear reflections for all 35 configurations. These calculations do not take into account spin transfer onto non magnetic ions.

Of the 35 configurations, only one has a sufficiently strong (010) reflection to account for the experimental results. There are a number of other configurations with non zero intensities at (010) but they are at most one-quarter of the observed value. The remainder of the observed magnetic peaks are in good agreement with the calculated values as shown in Table 5. There was some ambiguity in the powder results obtained by Collins et al (1970) as to whether the peak was indeed (010) and not $(00\frac{1}{2})$ or possibly a superposition of both as the d spacings for these reflections are almost identical. The present work removes the uncertainty and confirms the spin configuration suggested by Collins et al (1970). The spin configuration for $Mn_2P_2O_7$ is shown in Fig. 7.

The c centering operation in the chemical unit cell is lost in the magnetic unit cell, but the axes lengths are identical. The very strong (010) reflection is caused by the antiferromagnetically ordered layers in the ac plane that are separated by $\frac{1}{2}$ b. As a result there is almost perfect constructive interference for scattering vectors along b. It may be also noted that the (010) intensity is slightly smaller than the calculated value, but this may be attributed to extinction effects which become important for large peaks at low scattering angles. This effect was also apparent in the powder data.

Fig. 7

Spin configuration for $Mn_2P_2O_7$. The mirror plane is cross-hatched. The anti two-fold axis is a two-fold axis rotation followed by the time reversal operation. This constrains the spins to be perpendicular to the two fold axis. Dark circles are up spins, aligned 23° away from a* towards c*, and open circles are down spins.

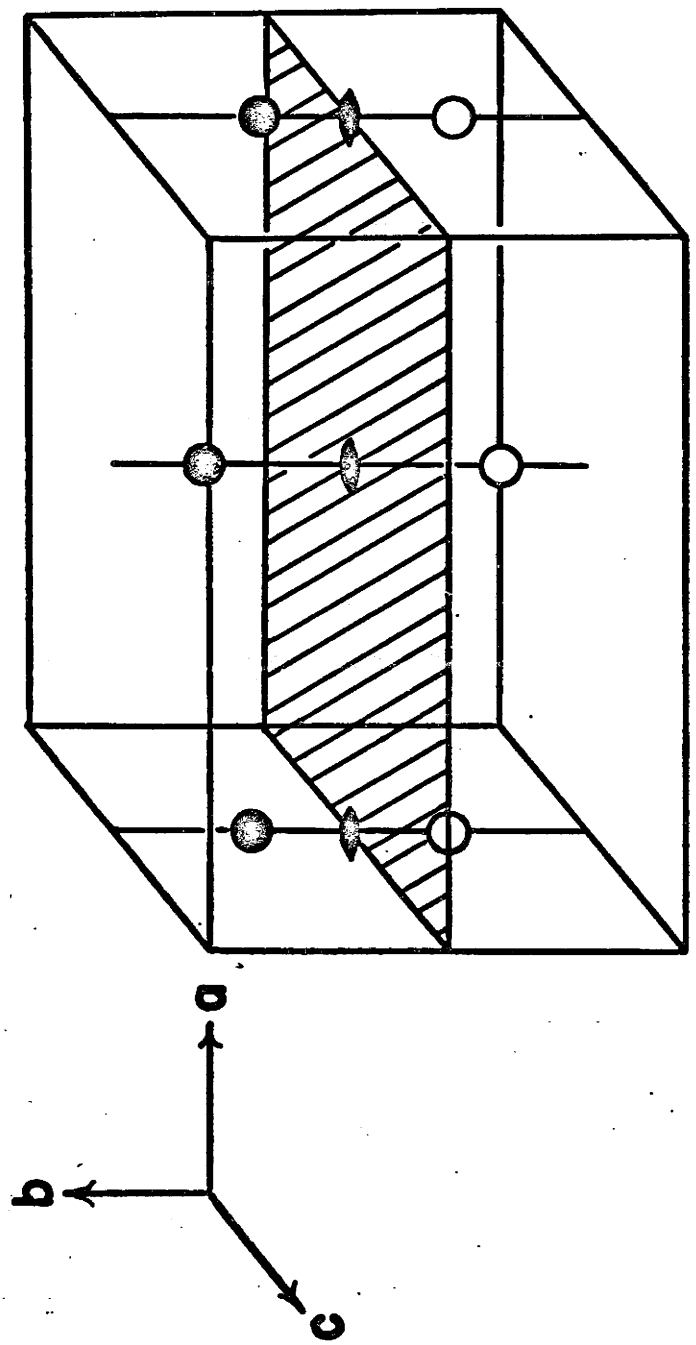
a
b
c
ANTI 2-FOLD AXIS

B. Copper Pyrophosphate

In $Cu_2P_2O_7$ the magnetic reflections are predicted to be two orders of magnitude weaker than the nuclear ones. It was therefore necessary to look for magnetic scattering where the nuclear reflections are absent because of symmetry or where the intensity of the nuclear scattering is very small, either accidentally or due to small deviations from a higher symmetry.

A typical scan of a Bragg peak for $Cu_2P_2O_7$ is shown in Fig. 8. The integrated intensities for selected Bragg peaks are shown in Table 6. The calculated intensities are normalized to the measured (060) peak. Again the calculations have not included the effect of spin transfer onto the non magnetic ions. The space group of the chemical unit cell is either C2/c or Cc. In either case the c centering operation prohibits nuclear reflections if h+k is odd and the c glide plane prohibits nuclear reflections of the form (00ℓ) for ℓ odd. These prohibited nuclear reflections were examined at 6°K for magnetic scattering. None was observed. This means that the magnetic unit cell preserves these two symmetry operations. The remaining nuclear peaks with ℓ odd are relatively weak, as the chemical unit cell is almost the same as in the high temperature β phase where the c axis is halved. The low angle peak of this type with the smallest nuclear intensity was examined as a function of temperature from 6°K to above the Néel temperature. The count rate at the middle of the (021) Bragg peak is shown in Fig. 9. A rocking

Table 6

Observed Calculated Intensities for $Cu_2P_2O_7$

h k ℓ	Observed Intensity (100°K)	Observed Intensity (6°K)	Calculated Intensity	Type (Nuclear or Magnetic
0 6 0	444	-	444	N
0 6 1	38	-	14	N
0 6 4	47	-	43	N
0 0 8	395	-	333	N
0 2 2	88	-	121	N
0 4 2	76	-	36	N
0 2 1*	<0.1	1.0(2)	1.2	M
0 0 1	<0.1	<0.1	0	M
0 1 0	<0.05	<0.05	0	M
0 1 1	<0.05	<0.05	0	M
0 1 3	<0.1	<0.1	0	M
0 3 0	<0.1	<0.1	0	M
0 3 1	<0.1	<0.1	0	M
0 3 3	<0.1	<0.1	0	M

The calculated intensities are normalized to the observed intensity for (060)
The observed intensities are multiplied by the geometrical factor sin 2θ
*The nuclear intensity has been subtracted from the total intensity for (021)

Fig. 8

Rocking curve for the (060) nuclear reflection in $Cu_2P_2O_7$. The error bars in this case are smaller than the points on the figure.

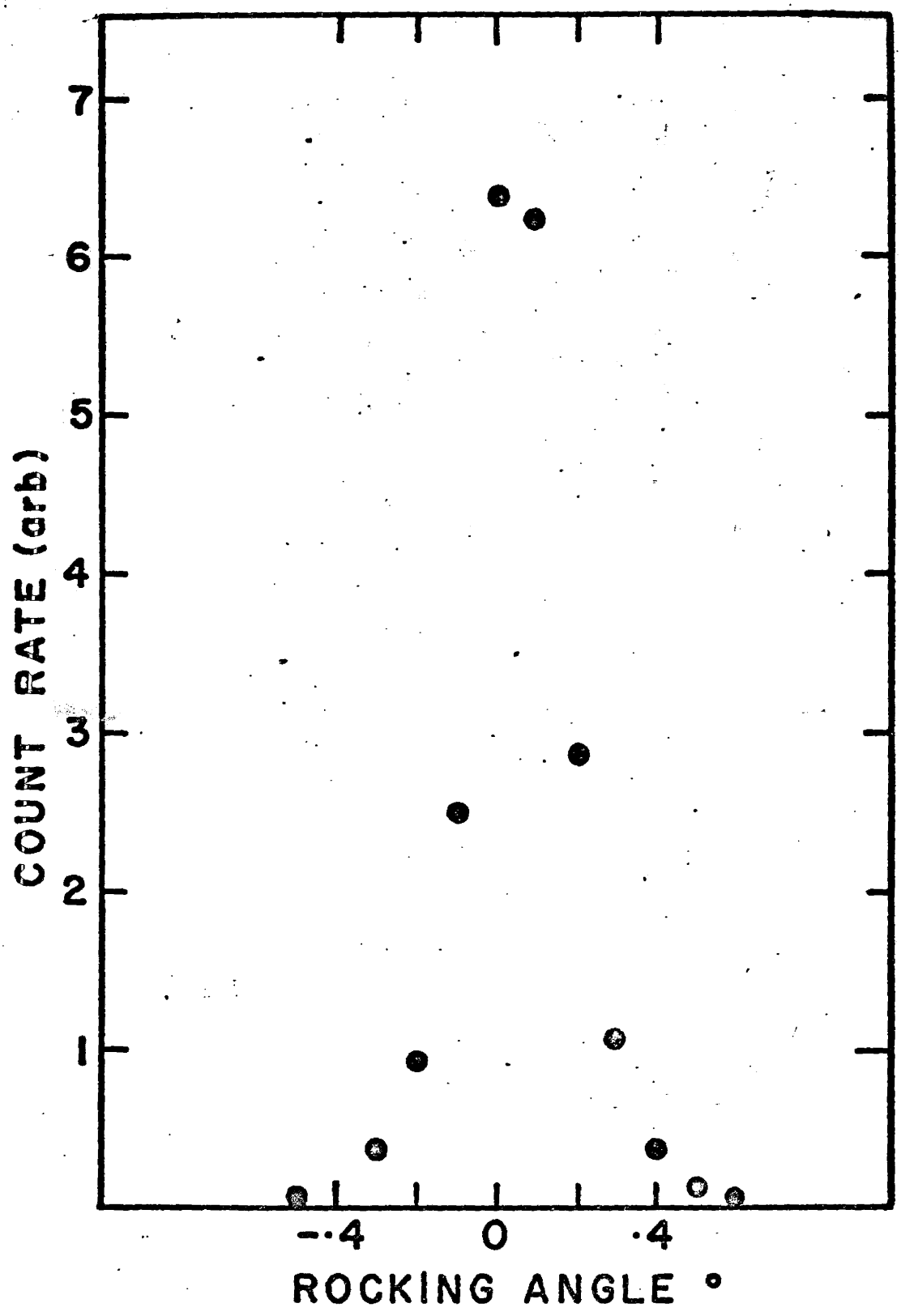
7
6
5
4
3
2
1
COUNT RATE (arb)
-.4
0
.4
ROCKING ANGLE °

Fig. 9

Temperature dependence of the counting rate at the center of the (021) peak in $Cu_2P_2O_7$. The intensity above T_N is attributed to nuclear scattering, which is not prohibited by symmetry.

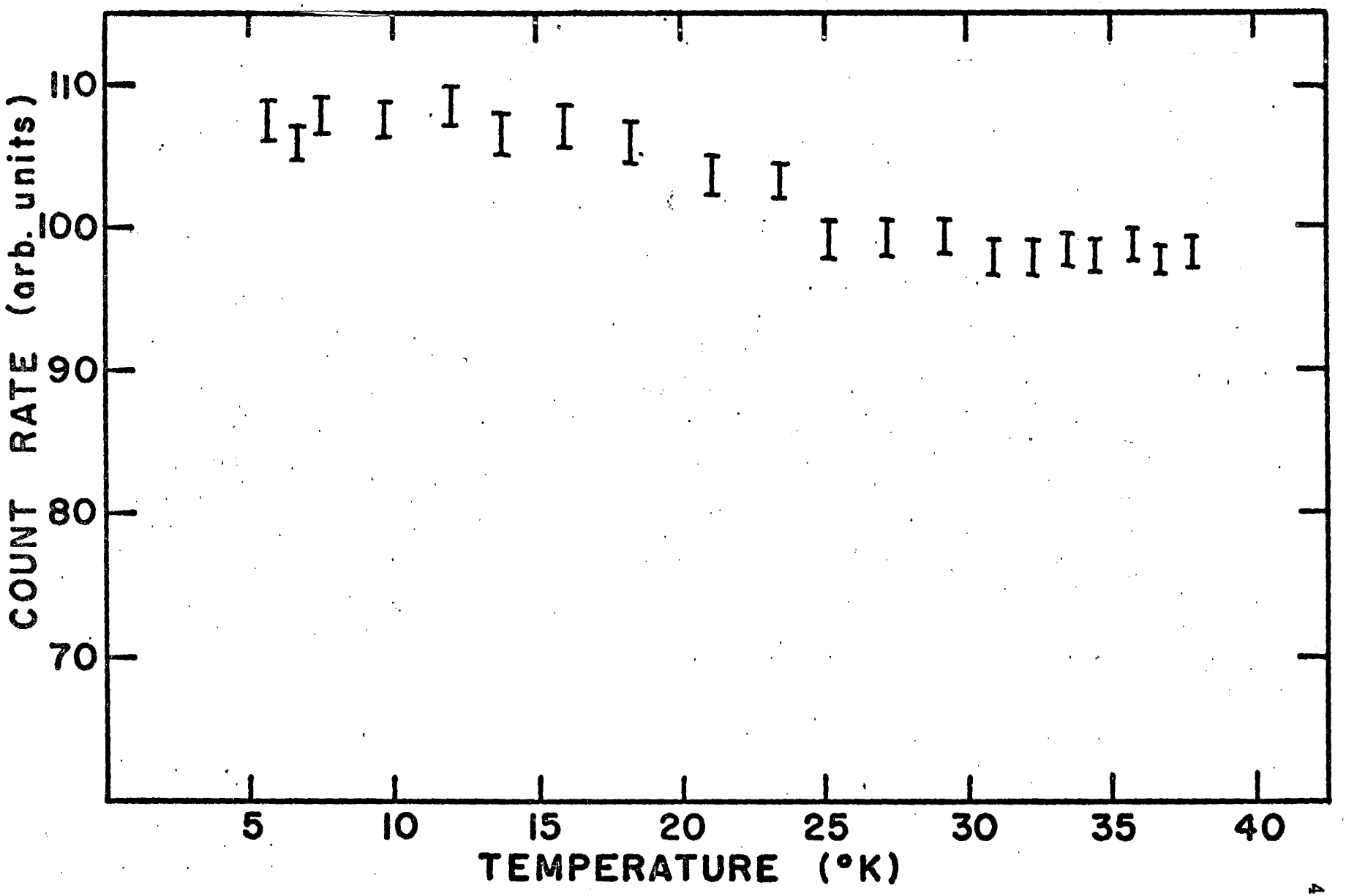
COUNT RATE (arb. units)
110
100
90
80
70
5
10
15
20
25
30
35
40
TEMPERATURE (°K)

curve was done at 4.2°K and 77°K to ensure that the counts taken were at the center of the Bragg peak. This was done to ensure that the crystal did not move due to thermal expansion as the temperature was raised. Because of the very weak scattering and resulting long counting times, it was not possible to check the rocking curve at other temperatures. The 8% difference in the count rate at 6°K and at 26°K is attributed to magnetic scattering. If the magnetic unit cell is commensurate with the chemical unit cell there are 35 possible colinear spin configurations. Eliminating those that do not preserve the c centering only three remain. Of these only 2 preserve the c clide plane and only one of these has magnetic scattering at the (021) Bragg reflection. It is concluded that this is the correct spin configuration. It should be noted here that the change in intensity for (021) may be due also to a crystallographic distortion at the Néel temperature. We are unable to rule out this possibility, but note that the change in intensity is in good agreement with the predicted magnetic intensity for this reflection. The spin arrangement consists of antiferromagnetic sheets in the ab plane which are coupled antiferromagnetically to neighbouring sheets. The favoured spin configuration for $Cu_2P_2O_7$ is shown in Fig. 10(a). The alternate configuration, which does not show magnetic reflection at (021), is shown in Fig. 10(b) and consists of an identical arrangement except that neighbouring sheets are coupled ferromagnetically rather than antiferromagnetically.

Fig. 10

Spin configurations for $Cu_2P_2O_7$. The planes drawn through the middle of the unit cell and the lines joining magnetic ions do not represent symmetry elements, but are drawn for visual assistance. The top configuration represents the one most favoured by the neutron diffraction results, but the bottom configuration is not ruled out.

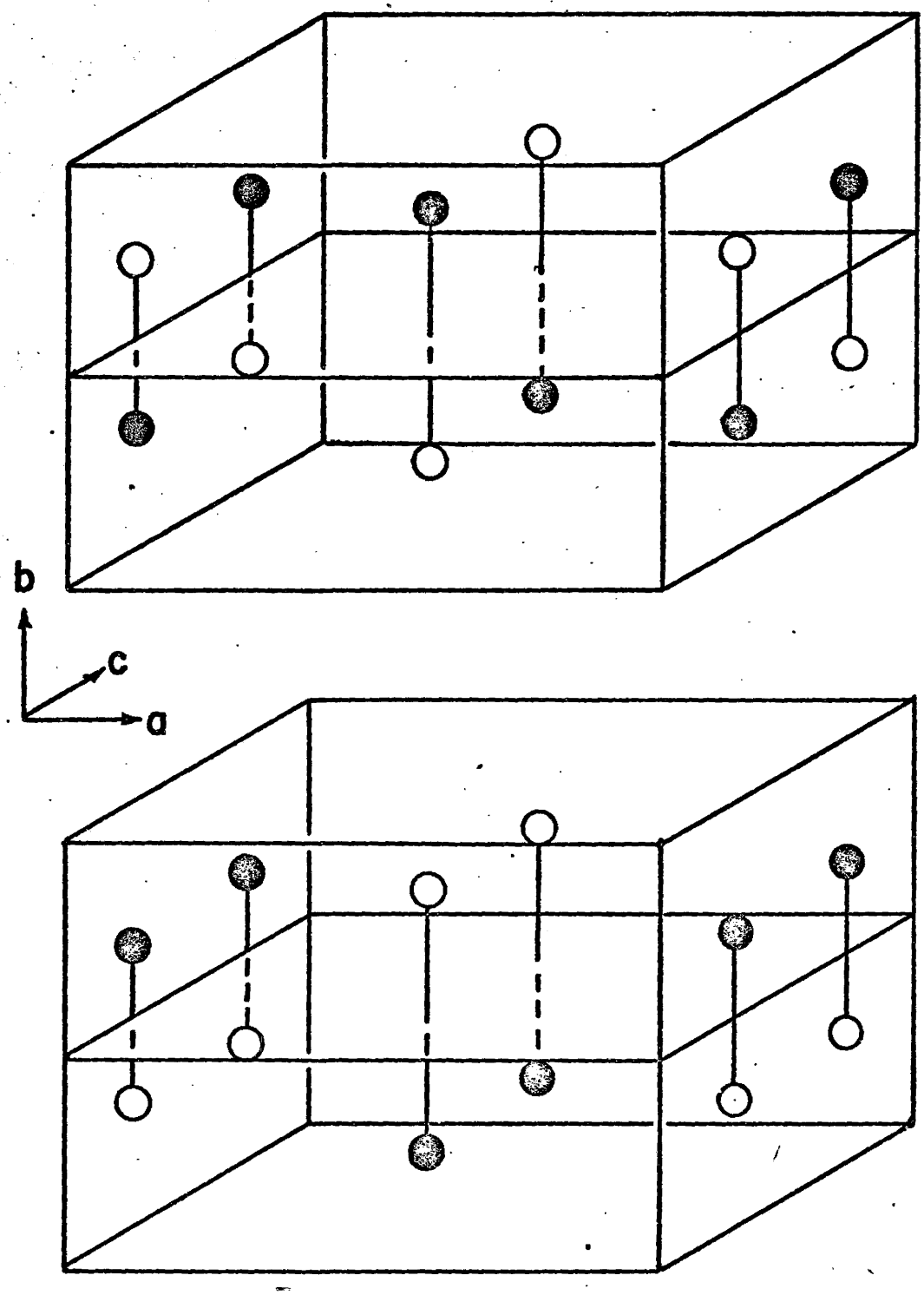
b
c
a

CHAPTER IV

NUCLEAR MAGNETIC RESONANCE

Experimental Procedure

The samples used for the NMR measurements were the same samples used for the neutron diffraction studies. The crystals were aligned along known crystallographic axes using an X-ray precession camera. Once aligned, the crystals were transferred to the end of a glass tube containing diamagnetic $Mg_2P_2O_7$. The $Mg_2P_2O_7$ was used as a standard sample for the ^{31}P resonance, since no resonance shifts are expected for this compound. Once mounted in this manner the alignment of the crystals was rechecked using the precession camera, and mounted inside the radio frequency (r.f.) coil. The coil consisted of a copper coil of diameter 3 mm and length 4 mm, wound with about 20 turns inside a teflon sleeve for rigidity. The sample alignment was accurate to within about 2° at low temperatures, as determined from the mutual consistency of data obtained in several planes.

The rf coil was incorporated in the tank circuit of a marginal oscillator. A circuit diagram of the oscillator is shown in Fig. 11. The frequency of the oscillator was kept constant while the magnetic field was swept linearly with time. Conventional field modulation and phase sensitive detection

Fig. 11

Circuit diagram for the marginal oscillator used for the NMR studies.

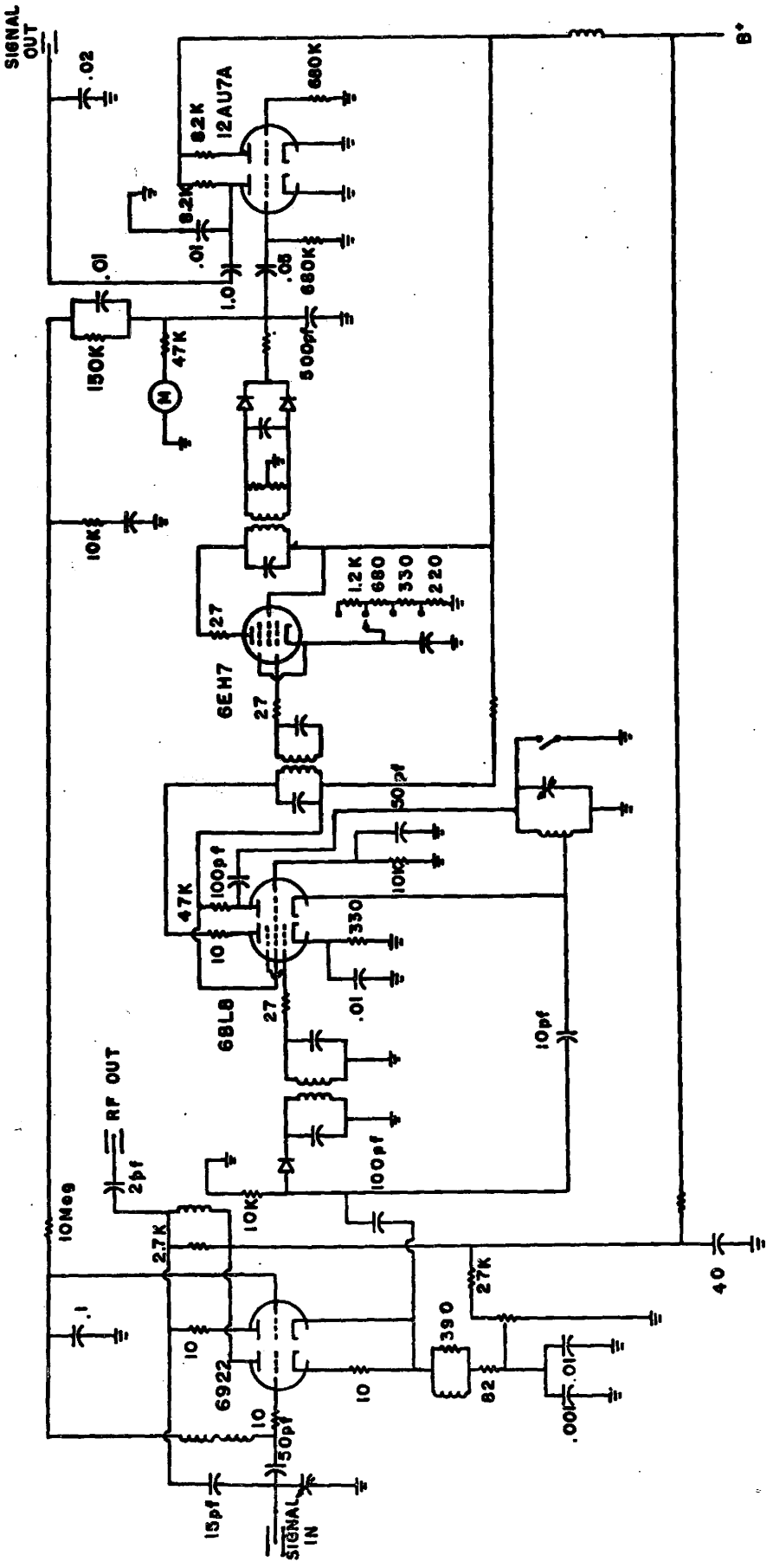
SIGNAL OUT
.02
12AU7A
82K
82K
.01
.01
1.0
.05
680K
680K
500pf
150K
47K
M
10K
1.2K
680
330
220
27
6EH7
27
50pf
100pf
47K
10K
10
330
.01
6BL8
27
10pf
RF OUT
2pf
100pf
10K
10Meg
2.7K
27K
40
.1
10
6922
10
10
390
82
.01
.001
150pf
15pf
SIGNAL IN
B+

techniques were employed. The 100 Hz field modulation was variable from 0 - 100 gauss peak to peak and for the low temperature measurements, values ranging from 20 gauss to 100 gauss were found to be optimal, depending upon the orientation of the sample. A time constant of 3 seconds was used for the filter on the output signal. The DC magnetic field was measured with a Varian Fieldial Mark I magnetic field regulator.

The cryogenic system was also of conventional design, enabling measurements to be made at 4.2°K. The sample was immersed in the liquid helium. Provision was made for pumping on the liquid helium so that an ultimate temperature of 1.5°K could be reached.

A typical first derivative resonance curve for the ^{31}P resonance in $Mg_2P_2O_7$ and in $Cu_2P_2O_7$ at room temperature is shown in Fig. 12. The resonance in $Cu_2P_2O_7$ is shifted with respect to that in $Mg_2P_2O_7$ as a result of the transferred hyperfine interaction in the paramagnetic state. A typical ^{31}P resonance from $Cu_2P_2O_7$ at 4.2°K, in the antiferromagnetic state is shown in Fig. 13. It should be noted that the linewidth observed varied widely as a function of the orientation of the crystal, from about 30 Oe to 100 Oe. The integrated intensity of the resonance varied considerably as well. In fact for some orientation of the crystal, the resonance due to certain crystallographic sites was too weak to be observed. This variation was first thought to be due to mosaic spread in the crystal but this

Fig. 12

Field derivative of the ^{31}P NMR in $Cu_2P_2O_7$ and in $Mg_2P_2O_7$ at room temeprature. The frequency at which the resonances were observed is 22.49 MHz.

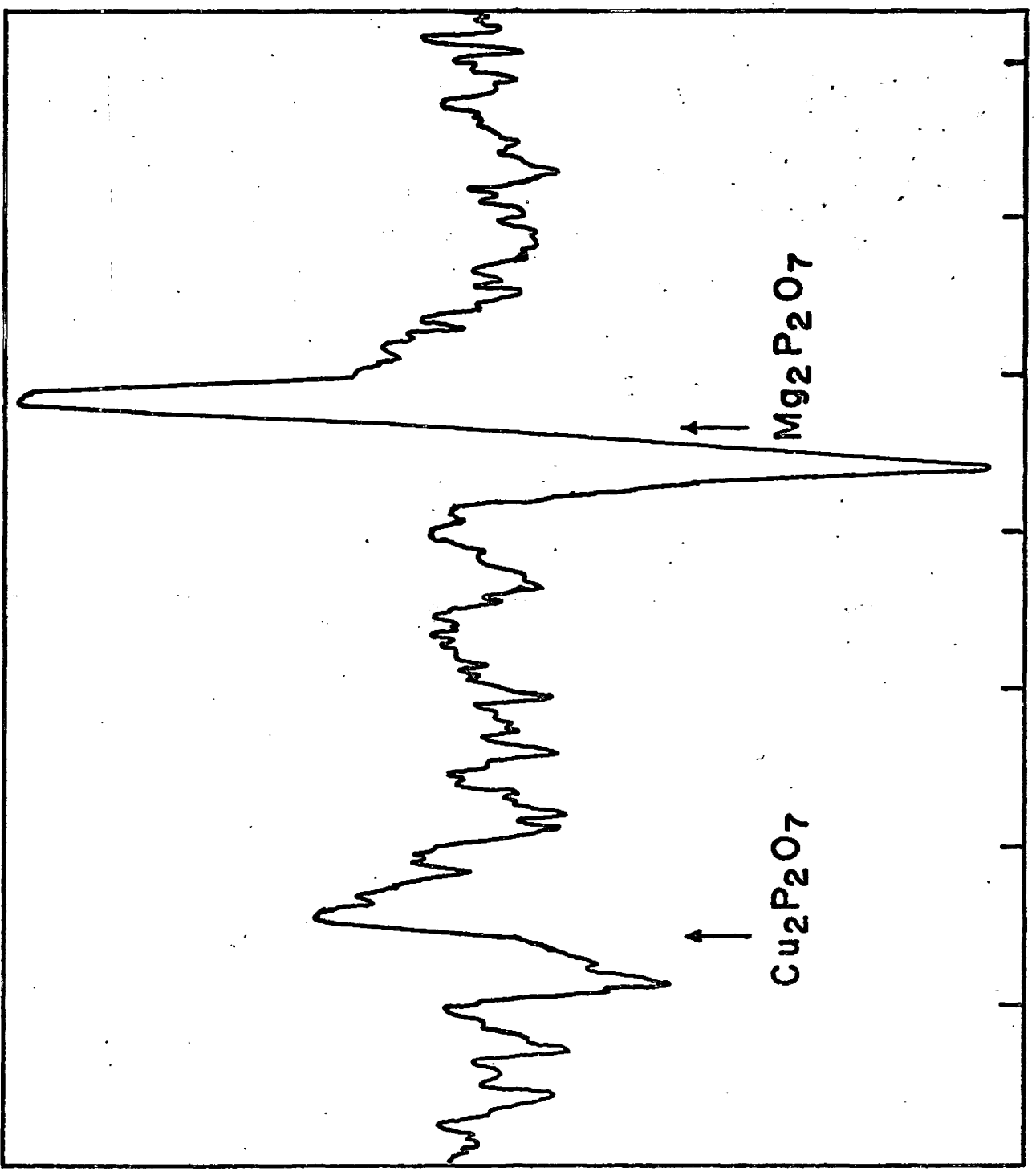
$Mg_2P_2O_7$
$Cu_2P_2O_7$
13.96
13.98
14.00
14.02
APPLIED FIELD IN kOe

Fig. 13

Field derivatives of the ^{31}P NMR in $Cu_2P_2O_7$ and $Mg_2P_2O_7$ at 4.2°K. The linewidth for $Cu_2P_2O_7$ varies from about 25 Oe observed in this case to 100 Oe, depending upon the orientation of the crystal with respect to the external field.

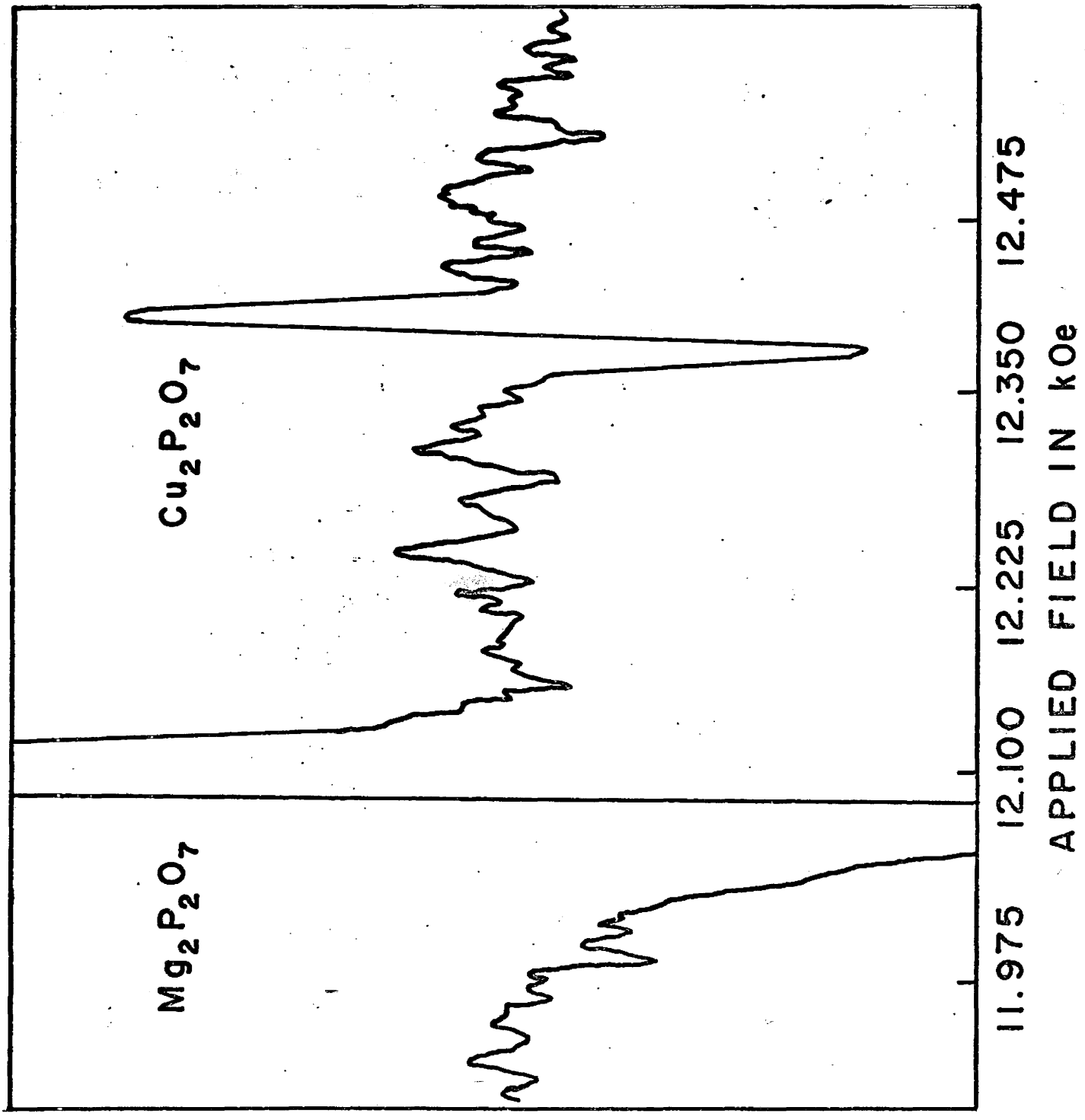
$Cu_2P_2O_7$
$Mg_2P_2O_7$
11.975
12.100
12.225
12.350
12.475
APPLIED FIELD IN kOe

possibility was ruled out because in this case the linewidth should increase in those regions where the resonance field changes rapidly with orientation. This was not the case experimentally.

Theory of NMR in the Ordered State

The Hamiltonian for the i^{th} phosphorus nucleus may be written in the following form.

$$H_M = \sum_j \bar{S}^j \cdot \bar{\bar{A}}^{ij} \cdot \bar{I}^i \quad . \tag{39}$$

For phosphorus the nuclear spin I = 1/2. The second rank tensor $\bar{\bar{A}}^{ij}$ couples the i^{th} nucleus to the j^{th} magnetic ion. The sum runs over all magnetic ions. $\bar{S}^j$ represents the spin on the j^{th} atom. For a simple two sublattice antiferromagnet, the sum can be divided into two parts, one for up spins, the other for down spins. Hence we can write.

$$H_M = \sum_l \bar{S}_\uparrow^k \cdot \bar{\bar{A}}_\uparrow^{ki} \cdot \bar{I}^i + \sum_k \bar{S}_\downarrow^k \bar{\bar{A}}_\downarrow^{ki} \bar{I}^i . \tag{40}$$

Because the up spins and down spins are all the same in a two sublattice model, we can write.

$$H_M = \bar{S}_\uparrow \cdot \bar{\bar{A}}_\uparrow \cdot I^i + \bar{S}_\downarrow \cdot \bar{\bar{A}}_\downarrow \cdot \bar{I}^i \quad . \tag{4}$$

$\bar{\bar{A}}_\uparrow$ and $\bar{\bar{A}}_\downarrow$ are the coupling tensors between all of the spins on the respective sublattice and the i^{th} nucleus. If the following definitions are made:

$$\bar{S}^\pm = \frac{1}{2}(\bar{S}_\uparrow \pm \bar{S}_\downarrow) \tag{42}$$

$$\bar{\bar{A}}^\pm = (\bar{\bar{A}}_\uparrow \pm \bar{\bar{A}}_\downarrow) \text{ where } A_{\uparrow,\downarrow} = \sum_k \bar{\bar{A}}^k_{\uparrow,\downarrow} \tag{43}$$

then the above Hamiltonian may be written as

$$H_M = \bar{S}^+ \cdot \bar{\bar{A}}^+ \cdot \bar{I}^i + \bar{S}^- \cdot \bar{\bar{A}}^- \cdot I^i. \qquad (44)$$

$\bar{S}_\uparrow(T,H)$ and $\bar{S}_\downarrow(T,H)$ are functions of temperature and the external magnetic field. These vectors are shown graphically in Fig. 14. In the absence of an external field.

$$\bar{S}^o_{\downarrow,\uparrow}(T,0) = \pm \bar{k} S M_s(T)/M_s(0) \qquad (45)$$

where $M_s(T)$ is the sublattice magnetization at T°K and $\bar{k}$ is a unit vector along the spin direction. Using the appropriate g tensor and the relation $\bar{M} = \bar{\bar{\chi}} \cdot \bar{H}$ we may write

$$\bar{S} \cdot \bar{\bar{A}}^+ \cdot \bar{I}^i = \frac{\bar{H}}{2Ng\beta} \left(\bar{\bar{\chi}} \cdot \bar{\bar{A}}^+ + \bar{\bar{A}}^+ \cdot \bar{\bar{\chi}}\right) \bar{I}^i \qquad (46)$$

where $\bar{\bar{\chi}}$ is the susceptibility tensor expressed in units of e.m.u./mole and N is Avogadro's number. The Hamiltonian may now be written as

$$H^i = -g_N \beta_N \bar{H} \cdot \bar{I}^i + \frac{\bar{H}}{2N\beta} \cdot \bar{\bar{g}}^{-1} \cdot \left(\bar{\bar{\chi}} \cdot \bar{\bar{A}}^+ + \bar{\bar{A}}^+ \cdot \bar{\bar{\chi}}\right) \bar{I}^i + \bar{S}^- \cdot \bar{\bar{A}}^- \cdot \bar{I}^i \qquad (47)$$

where the usual nuclear Zeeman term has been included. The factor $\bar{\bar{g}}^{-1}$ is the inverse of the g tensor, g_N is the nuclear g factor and β and β_N are the Bohr magneton and the nuclear magneton respectively.

The task remains to determine the vectors $\bar{S}^+$ and $\bar{S}^-$ as a function of applied field. We will define these in terms of $\bar{M}^+$ and $\bar{M}^-$ where

$$\bar{M}^\pm = \bar{\bar{g}} \cdot \mu_B \cdot \bar{S}^\pm = \bar{M}_o^\uparrow \pm \bar{M}_o^\downarrow . \qquad (48)$$

Fig. 14

An illustration of the spin vectors $\bar{S}^{o}_{\uparrow}$ and $\bar{S}^{o}_{\downarrow}$ at zero field and $S_{\downarrow}$ and $S_{\downarrow}$ in the presence of an applied field H. $\bar{S}^{\pm} = \frac{1}{2}(\bar{S}_{\uparrow} \pm \bar{S}_{\downarrow})$.

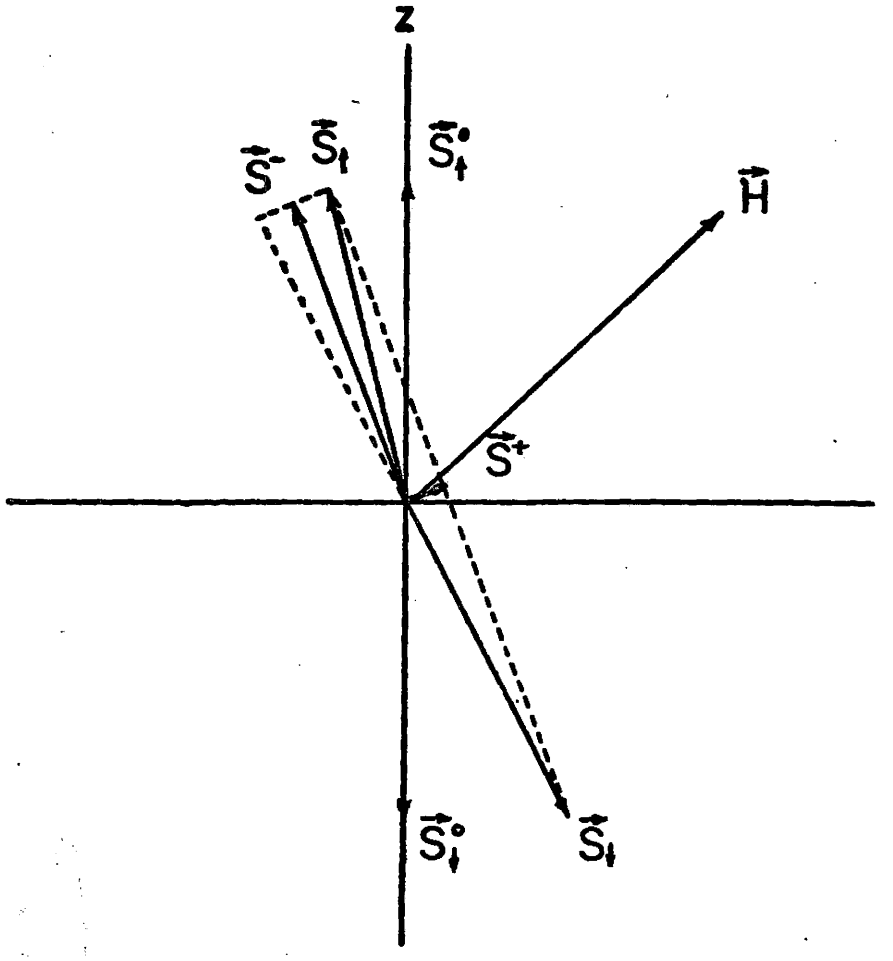
z
$\vec{S}$
$\vec{S}_1$
$\vec{S}_1^{\circ}$
$\vec{H}$
$\vec{S}^{+}$
$\vec{S}_1^{\circ}$
$\vec{S}_1$

Nagamiya et al (1955) have outlined a method for calculating the magnitude and direction of $\bar{M}^+$ and $\bar{M}^-$ in the molecular field approximation. The following expression for M^+ is given

$$|\bar{M}^+| \simeq \frac{|\bar{H}|}{|\bar{H}_{ex}|} \cdot |2\bar{M}_o\uparrow| . \qquad (49)$$

$\bar{H}_{ex}$ is the molecular exchange field and $\bar{M}_o$ is the zero field value of the sublattice magnetization. The existence of $\bar{M}_+$ is attributed to the tipping of spins on opposing sublattices towards one another to result in a net macroscopic magnetization in an applied field.

It is slightly more complicated to compute $\bar{M}^-$. Nagamiya et al (1955) give the following expression for the free energy of the system.

$$F = -\frac{1}{2}\chi_{||}H_{||}^2 - \frac{1}{2}\chi_{\perp}H_{\perp}^2 + E_A . \qquad (50)$$

Nagamiya et al (1955) assume that the two principle values of the susceptibility which correspond to eigenvectors perpendicular to the direction of the sublattice magnetization are equal. Experimentally, this is not true for $Cu_2P_2O_7$ but the values are sufficiently close to one another that the assumption is a valid approximation. The perpendicular susceptibility is denoted by $\chi_{\perp}$, and the parallel susceptibility is denoted by $\chi_{||}$. The anisotropy energy is defined phenomenologically as follows.

$$E_a = \frac{1}{2} K_1(\beta_+^2 + \beta_-^2) + \frac{1}{2} K_2(\alpha_+^2 + \alpha_-^2), K_2 > K_1 > 0. \quad (51)$$

$\alpha\pm$ and $\beta\pm$ are the direction cosines of the respective sublattice magnetization vectors. The z axis is therefore the easy direction. The free energy of the system is expressed by the following equation.

$$F = -\frac{1}{2} \chi_{||} H^2 (\alpha\alpha_H + \beta\beta_H + \gamma\gamma_H)^2 - \frac{1}{2} \chi_{\perp} H^2 [1 - (\alpha\alpha_H + \beta\beta_H + \gamma\gamma_H)^2] + K_1\beta^2 + K_2\gamma^2 \quad (52)$$

where α_H, β_H and γ_H are the direction cosines of the external field. The expression has been simplified by assuming that the sublattice magnetization vectors are colinear so that $|\alpha_+| = |\alpha_-|$, $|\beta_+| = |\beta_-|$ and $|\gamma_+| = |\gamma_-|$. This is a good approximation if the induced magnetization of the sample is small. From equation (49) it can be seen that this condition is satisfied if the exchange field is very large compared to the external field. The magnetization direction in a finite external field is obtained by minimizing the above expression for the free energy, subject to the constraint $\alpha^2 + \beta^2 + \gamma^2 = 1$. This is equivalent to solving the following equation.

$$\begin{vmatrix} \alpha_H^2 + \kappa_2 - \lambda & \alpha_H\beta_H & \alpha_H\gamma_H \\ \alpha_H\beta_H & \beta_H^2 + \kappa_1 - \lambda & \beta_H\gamma_H \\ \alpha_H\gamma_H & \beta_H\gamma_H & \gamma_H^2 - \lambda \end{vmatrix} = 0 \quad (53)$$

The constants κ_1 and κ_2 are defined as follows

$$\kappa_1 = 2K_1/[(\chi_{\perp} - \chi_{||})H^2] \quad (54)$$

$$\kappa_2 = 2K_2/[(\chi_\perp - \psi_{||})H^2] \quad . \tag{55}$$

The smallest value of the eigenvalue λ corresponds to the condition of minimum free energy and the associated eigenvector corresponds to the desired values of α, β and γ that is the direction cosines of the sublattice magnetization. The coordinate system for the above equation has been defined so that the z direction corresponds to the easy direction, the y direction corresponds to the intermediate direction, and the x axis corresponds to the hard direction, with reference to the principal values of the free energy.

Now that we have obtained the vectors $\bar{M}^+$ and $\bar{M}^-$ and hence $\bar{S}^+$ and $\bar{S}^-$, the only unknown parameters in the Hamiltonian are the tensors $\bar{\bar{A}}^+$ and $\bar{\bar{A}}^-$. These may be determined from the experimental data. Each of these tensors has two major parts. The first of these is the classical dipole-dipole interaction, and may be calculated given a knowledge of the crystal structure, and the arrangement of the spins in the unit cell. To a first approximation this may be done assuming that all of the spins are localized on the magnetic ions. The dipole-dipole energy is given by

$$E_k = \sum_j \left[\frac{\bar{m}_{Nk} \cdot \bar{m}_j}{r_{kj}^3} - \frac{3(m_{Nk} \cdot r_{kj})(\bar{m}_j \cdot \bar{r}_{kj})}{r_{kj}^5}\right] \tag{56}$$

This is the energy of interaction of the k^{th} site with all of the magnetic ions. m_{N_k} is the nuclear moment at the k^{th} site given by

$$\bar{m}_{N_k} = g_N \mu_N \bar{I} \tag{57}$$

and $\bar{m}_j$ is the electronic magnetic moment at the j^{th} magnetic site. The vector $\bar{r}_{kj}$ connects the j^{th} site to the k^{th} one. In general, a straightforward calculation of the dipole sum is difficult. For the present work, Ewald's method, outlined in Born and Huang (1954) is used. This method involves summation of the series in both real and reciprocal space out to a finite radius R. The dipole energy of interaction with the site k can be written as

$$E_k = \sum_{\alpha} \mu_N \beta_N I_\alpha \sum_{\beta} \sum_{k'} Q_{\alpha\beta}(kk') m_{k,\beta}. \tag{58}$$

The coefficients $Q_{\alpha\beta}(k,k')$ are tensor elements which relate the β component of the magnetic moment associated with the k^{th} ion in the unit cell to the α component of the resulting magnetic field at the k^{th} ion in the unit cell. The sum over unit cells has been incorporated into the tensor elements.

The Ewald method has been used in a computer program, written by E. R. Cowley, to calculate the coefficients $Q_{\alpha\beta}(kk')$.

The dipole sums can be modified to some extent by assuming that some of the spin density is transferred to the non magnetic sites. The degree of transfer can be estimated from NMR studies in the paramagnetic state (Atkinson, 1969) and use of symmetry considerations.

The second major contribution to the tensors $\bar{\bar{A}}^{\pm}$ is the

transferred hyperfine interaction. This effect arises from the presence of a finite spin density on the ^{31}P ions. This spin transfer is a result of the overlap of the wavefunctions of magnetic and non magnetic ions. In the process of orthogonalizing the wavefunction of the magnetic ions and neighbouring non magnetic ions, those wave functions associated with the isolated ions which are not orthogonal, that is those with the same spin, become mixed. This process is approximated by the molecular orbital method which uses linear combinations of atomic orbitals to form bonding and antibonding orbitals. To obtain an understanding of this method, the simple case of a three electron two center case is considered. The bonding and antibonding orbitals have the following form.

$$\psi_B = \frac{(\psi_L+\gamma\psi_M)(\uparrow\downarrow)}{[1+2\gamma\langle\psi_L|\psi_M\rangle+\gamma^2]^{1/2}} \tag{59}$$

$$\psi_{AB} = \frac{(\psi_M-\lambda\psi_L)(\uparrow)}{[1-2\lambda\langle\psi_L|\psi_M\rangle+\lambda^2]^{1/2}} \tag{60}$$

ψ_M is a magnetic ion orbital and ψ_L is a non magnetic ligand orbital. ψ_A and ψ_{AB} are approximately orthogonal if $\lambda \approx \gamma + \langle\psi_L|\psi_M\rangle$. The assumption is made that the overlap integral $\langle\psi_L|\psi_M\rangle$ is small. The bonding orbital ψ_B is lower in energy because its dominant part is ψ_L, which is a lower energy state that ψ_M. As a result ψ_B contains two of the three elec-

trons available from the atomic states, leaving one electron for the antibonding state. It is ψ_{AB} which contributes to the unpaired spin density on the non magnetic ion. The unpaired spin density is then proportional to λ^2.

The remaining part of the transferred hyperfine interaction is the interaction between the unpaired spin on the ^{31}P ions and the nucleus. This is the direct hyperfine interaction, and it consists of two parts. The first is a dipole-dipole interaction between the nuclear and the electron spins. This effect is zero, if the electronic wave function is spherically symmetric. As a result there is no dipole interaction for s electrons. There is however another contribution, the Fermi contact interaction, which depends on the electron density at the nucleus. This is finite only for s electrons, since all others have zero electron density at the origin.

The dipole hyperfine constant for 3p electrons is given by

$$A_{3p} = \frac{2}{5} g\beta\gamma\hbar \left\langle \frac{1}{r^3_{3p}} \right\rangle . \qquad (61)$$

The value for $\left\langle \frac{1}{r^3_{3p}} \right\rangle$ can be obtained from the optical spectrum (Barnes and Smith, 1954).

The Fermi contact contribution is

$$A_{3s} = \frac{8}{3} \pi g\beta\gamma\hbar |\psi_{3s}(o)|^2 . \qquad (62)$$

where $|\psi_{3s}(o)|^2$ is the density of 3s electrons at the nucleus. It can be obtained from the formula

$$|\psi_{3s}(o)|^2 = \frac{Z_i}{Z_o} \frac{1}{\pi a_o^3} \left(\frac{T}{R}\right)^{3/2} \qquad (63)$$

where Z_i is the effective nuclear charge, a_o is the Bohr radius, T is the term value and R is Rydbergs constant. (Crawford and Schawlow, 1949).

The fraction of unpaired 3s electrons at the i^{th} nucleus due to the k^{th} magnetic ion is given by

$$f_{3s} = \frac{2S A_s^{ki}}{A_{3s}} \qquad (64)$$

where A_s^{ki} is the experimental hyperfine constant determined from the field shift at the i^{th} nucleus in the paramagnetic phase. S is the spin on the magnetic ion. A_s^{ki} is given by the following expression

$$\frac{\Delta H_{HF}}{H_o} = - \frac{1}{\gamma \hbar} \sum_k A_s^{ki} \cdot \frac{\langle S \rangle^i}{H_o} \qquad (65)$$

where ΔH_{HF} is the transferred hyperfine field shift of the nuclear magnetic resonance which occurs at H_o in the absence of magnetic interactions. ΔH_{HF} is obtained from the total experimental field shift ΔH by subtracting from ΔH contributions due to dipole fields and the demagnetization field. The above equations is easily solved for A_s^{ki} if the assumption is made that A_s^{ki} is the same for all magnetic ions. $\langle S \rangle^i$ is the thermal average of the spins in the paramagnetic state and is given by

$$\langle S \rangle = SB_s(x) \text{ where } x = \frac{g\mu_B SH}{kT} \qquad (66)$$

$B_s(x)$ is the Brillouin function for spin s. For $s = \frac{1}{2}$ it is given by

$$B_{\frac{1}{2}}(x) = \tanh x \qquad (67)$$

Magnetic symmetry

The chemical unit cell of the compounds studied have the point group 2/m. That is there exists a 2 fold axis along the b axis of the crystal and a mirror plane perpendicular to it. The magnetic symmetry of the crystal involves the additional complication of keeping track of the spin direction of symmetry related sites. To accommodate this additional information a number of additional symmetry operations are defined. The magnetic symmetry elements for a monoclinic system include the follows: 2, 2', m, m', I, and I'. The 2 operation is the usual crystallographic 2 fold axis element, and m is the crystallographic mirror plane operation. I is the identity operation. The 2' operation is a product of the 2 operation and the time reversal operation. Magnetic vectors transform in the same way as angular momentum, and the angular momentum vector can be written as $\bar{r}\times\bar{p}$ where $\bar{r}$ is a position vector and $\bar{p}$ is a linear momentum vector. The time reversal operator transforms $\bar{p}$ into $-\bar{p}$ while leaving $\bar{r}$ unchanged, so the net effect of this operation is to change the sign of a magnetic vector. The m' operation is a product of the mirror plane

and time reversal. I' is a product of the identity and the time reversal operator. Fig. 15 shows the effect of the various operations on a magnetic vector. A number of special cases are worthy of note. If a magnetic site is located on a crystallographic 2 fold axis, then a magnetic 2 axis implies that the magnetic vector associated with that site must lie along the two fold axis. Similarly a magnetic 2' axis implies that the vector must be perpendicular to the axis. If the site is located on a crystallographic mirror plane, then a magnetic m plane implies that the magnetic vector must be perpendicular to the mirror plane, and an m' plane implies that it must lie within the mirror plane. A complete description of the way in which axial or magnetic vectors transform under the magnetic point group operations may be found in a paper by Donnay et al (1958). Methods of applying these groups in the determination of magnetic structures from NMR data is discussed by Riedel and Spence (1960) and Spence and van Dalen (1968). In these papers the magnetic point groups are referred to as Heesch groups, of which there are 122 derivable from the 32 ordinary point groups and the corresponding magnetic space groups are referred to as Shubnikov groups, of which there are 1651, obtainable from the 230 ordinary crystallographic space groups. For a monoclinic system the following Heesch groups are possible. If the crystallographic point group is m, then the Heesch group may be one of 2', m' or 2'/m'. Similarly if the crystallographic point group is 2, the Heesch group may be 2, m, or 2/m. Finally, if the

Fig. 15

The effects of symmetry operations on magnetic vectors.

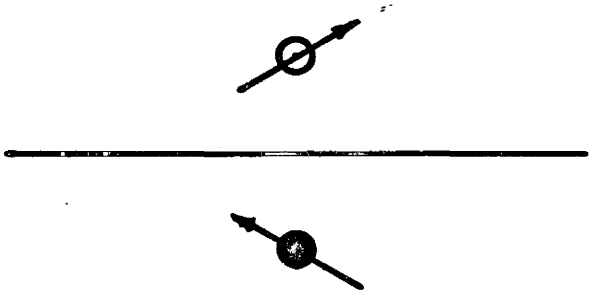

m plane

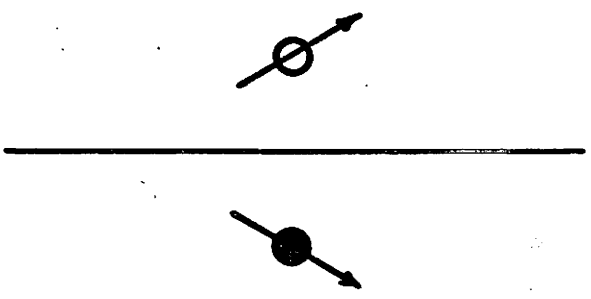

m' plane

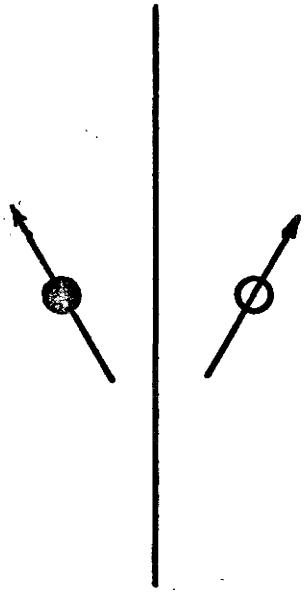

2 axis

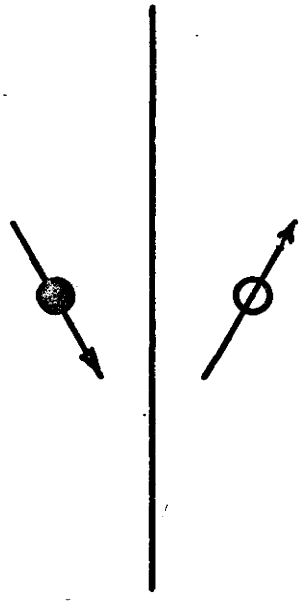

2' axis

point group is 2/m, the Heesch group is one of 21', ml', 2/ml', 2/m' or 2'/m. As a final note it should be stated that the magnetic point groups defined here as Heesch groups differ from those defined by Opechowski and Guccione (1965) in that they remove all translations from the magnetic space groups to obtain the point group whereas here the anti translations, that is those including time reversal, are condensed into the anti identity.

EXPERIMENTAL RESULTS AND DISCUSSION

$Mn_2P_2O_7$

The experimental work on the NMR of this compound in the antiferromagnetic phase has been reported by Choh and Stager (1970). The interpretation of these results in terms of possible spin configurations, using the method of Spence and van Dalen (1968), was not consistent with the spin configuration determined by Collins et al (1970) from powder neutron diffraction data. Since the powdered data was confirmed by single crystal studies in the present work, it becomes necessary to reevaluate the NMR data in light of this information. The ^{31}P NMR in the ordered state has been used to measure the internal field at the phosphorus nuclei. The components of the internal fields at the phosphorus sites are listed in Table 7. Assuming that the space group symmetry of the crystal does not change down to 4.2°K, the magnetic ions are located on a 2 fold axis. Experimentally the spins are determined to be perpendicular to the 2 fold axis

TABLE 7

Internal field components at the phosphorus sites in $Mn_2P_2O_7$

i	H_x	H_y	H_z
1	.005(5)	.259(11)	+1.27(9)
2	-.005(5)	-.259(11)	+1.27(9)
3	+.005(5)	+.259(11)	-1.27(9)
4	-.005(5)	-.259(11)	-1.27(9)

- Fields are given in kiloOersteds.
- The spin direction is along z.
- The two-fold axis is along y.
- i labels the phosphorus ions.

(Fowlis 1970) so the 2 fold axis becomes a magnetic 2' axis. This is consistent with the spin configuration determined by neutron diffraction. The neutron studies determined that spins related by the mirror plane are antiparallel, and because the spins are parallel to the mirror plane, the crystallographic mirror plane must be a magnetic m plane. The phosphorus nuclei are situated on the m plane, so all internal fields measured at the phosphorus sites must be perpendicular to the mirror plane. From Table 7 it is evident that this is not observed experimentally.

The dipole field was calculated and found to be perpendicular to the m plane, as expected from symmetry. If all of the magnetic moment is concentrated on the manganese ions, then the calculated dipole field is approximately twice as large as the measured perpendicular component. This result can be modified significantly by assuming that some of the spin polarization is located on the oxygen ions that are near neighbours to the manganese ions. An order of magnitude estimate with 2% spin transferred to each oxygen ion, where spin polarization is not forbidden by symmetry, would lead to an oxygen contribution to the perpendicular component that is approximately 40% that of the manganese ion contribution. If the oxygen spins are antiparallel to the near neighbour manganese spins this contribution would have the opposite sign to that due to the manganese ions. A detailed calculation would be very sensitive to the atomic positions, which are not accurately known at helium

temperatures, and especially sensitive to the spin direction. As a result it is possible that all of the perpendicular component of the internal field arises from the dipole field.

The parallel component must come from the transferred hyperfine interaction. The experimentally measured component in the plane is parallel to the measured spin direction, as expected for an isotropic transferred hyperfine interaction (Atkinson and Stager, 1969). The contributions to the parallel component should, however, cancel in pairs because of the m plane. We will postulate a very small distortion from C2/m symmetry so that the mirror plane is lost. If the distortion is small it will not strongly affect the dipole contribution with its $1/r^3$ dependence. If we assume that the transferred spin on the phosphorus ions result from the same mechanism responsible for superexchange, then from high pressure studies (Benedek and Kushida, 1960) there is an approximate $1/r^{10}$ radial dependence. The high pressure studies were done on manganese fluoride. The assumption is made that the change in the relevant bond angles is small and does not affect the magnitude of the interaction. A rough estimate of the degree of cancellation of the hyperfine fields can be obtained by comparison with the NMR data in the paramagnetic state. There the expectation value of all spins are parallel and no cancellation occurs. Using the data of Atkinson and Stager(1969) a hyperfine field of 31.8 kOe is predicted for saturated paramagnetic $Mn_2P_2O_7$. The observed value for the antiferromagnetic state is 1.27 kOe. Order of

magnitude calculations are done in the following manner.

The interaction between a magnetic ion and the phosphorus nucleus is given by $H_{HF} = A_{HF}(r) \frac{S}{\mu_N g_N}$ where r is the length of the hyperfine path in the limit of C2/m symmetry. If the phosphorus ion is moved off the mirror plane the length of the hyperfine path for one of the symmetry related magnetic ions becomes r+Δ and for the other r-Δ. Taking into account the functional dependence of the hyperfine interaction and the antiparallel arrangement of the symmetry related spins, the total hyperfine field becomes, for the distorted crystal

$$H_{HF} = \frac{S}{\mu_N g_N} [A_{HF}(r+\Delta) - A_{HF}(r-\Delta)] \tag{68}$$

$$= \frac{S}{\mu_N g_N} [k(r+\Delta)^{-10} - k(r-\Delta)^{-10}] = \frac{kS}{\mu_N g_N} [r^{10} - 10r^9\Delta + \ldots - r^{10} - 10r^9\Delta]$$

$$= \frac{-20kSr^9\Delta}{\mu_N g_N}. \tag{69}$$

k is an appropriate proportionality constant for the transferred hyperfine interaction. Similarly for parallel spins, as in a saturated paramagnet the hyperfine field is given by

$$H'_{HF} = \frac{kS}{\mu_N g_N} [r^{10} + 10r^9\Delta + r^{10} - 10r^9\Delta] = 2r^{10} \frac{kS}{\mu_N g_N}. \tag{70}$$

Taking the ratio H_{HF}/H'_{HF} gives the following result.

$$H_{HF}/H'_{HF} = \frac{-10\Delta}{r}. \tag{71}$$

Δ/r is the fractional change in the transferred hyperfine path.

In general, for an r^n dependence of the transferred hyper-

fine field this is given by

$$H_{HF}/H'_{HF}=\frac{n\Delta}{r} \quad . \qquad (72)$$

Using equation (71) bond length changes of the order of .01 Å are sufficient to explain the result. These changes are too small to have been observed by any neutron or X-ray diffraction experiment carried out so far on $Mn_2P_2O_7$. F. Long (private communication) has examined a powdered sample by X-rays at 6°K and observed no evidence for a symmetry change from the C2/m structure.

The Heesch group above the low temperature phase transition is 2'/m. From the symmetry of the internal fields, it is likely that the Heesch group remains unchanged through the phase transition, at least to within the accuracy of the experimental measurements. If this is indeed the case, the resonances corresponding to the four magnetic sites in the crystal should coincide in pairs if the internal field is oriented perpendicular to the 2 fold axis. The linewidth of the resonances observed was about 80 Oe, and the internal field was approximately 1 kOe, so any splitting of the coincident resonances involving more than 5% difference between the two corresponding internal fields should have been observable. No such splitting was observed experimentally. This 5% limit, taking into account the r^{10} dependence of the transferred hyperfine field would preclude the observance of changes from 2'/m symmetry involving fractional changes in atomic coordinates

of less than 0.5%.

$Cu_2P_2O_7$

Data were taken at 4.2°K with the external field in the ac*, ab and bc* planes. The c* axis is along the direction $\underline{a}\times\underline{b}$. Additional data were taken in a plane which is perpendicular to an axis 30° from the c* axis towards the $\underline{a}$* axis in the ac plane. These data are shown in Figs. 16, 18, 18 and 19 respectively. The first three planes of data were taken at 17.00 MHz, the latter at 16.5 MHz. A total of 4 resonances was observed. The angular dependence of a given resonance shows the characteristic 360° periodicity of NMR in a magnetically ordered system. The four resonances correspond to the vector sum of the external field with 4 different internal fields at the phosphorus nuclei. There is no quadrupole splitting for ^{31}P since the nucleus has $I = \frac{1}{2}$. Measurements were made at a higher frequency (21 MHz) at 4.2°K in the ac plane to determine the field dependence of the resonance pattern. These results are shown in Fig.20 . The additional resonance with a minimum at 14.2 kOe is related to the antiferromagnetic spin flop resonance. As this is a cooperative electronic effect in the crystal, the intensity of this resonance is several orders of magnitude larger than the nuclear resonances. Fowlis (1970) has observed the same resonance using microwave techniques at 35 GHz. The temperature dependence of the internal field was examined with the external field along the direction of easy magnetization.

Fig. 16

Applied fields for the ^{31}P resonances as a function of angle for the external field in the ac* plane. The resonant frequency is 17.00 MHz.

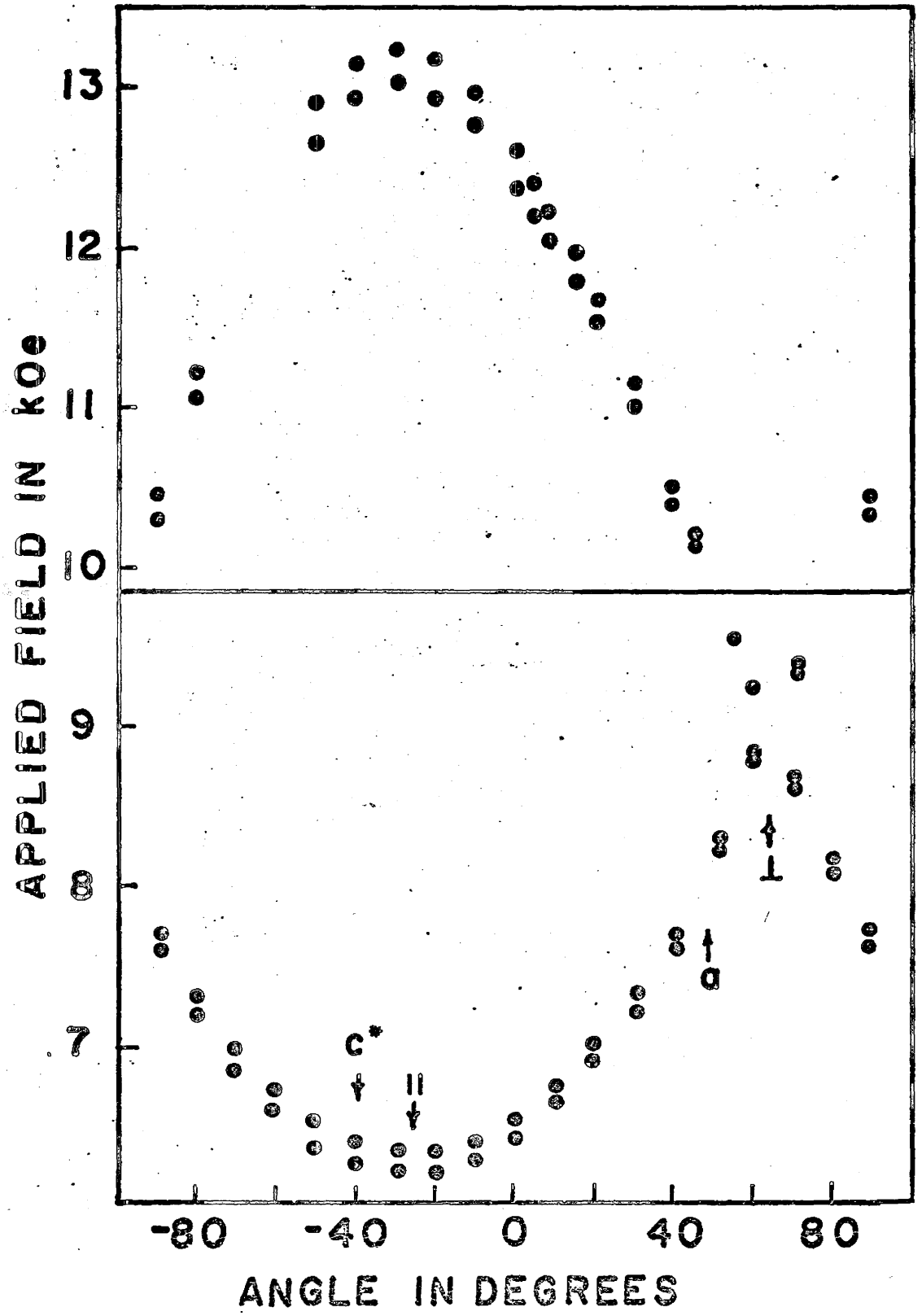
APPLIED FIELD IN kOe
13
12
11
10
9
8
7
c*
II
⊥
a
-80
-40
0
40
80
ANGLE IN DEGREES

Fig. 17

Applied fields for the ^{31}P resonances as a function of angle for the external field in the ab plane. The resonant frequency is 17.00 MHz.

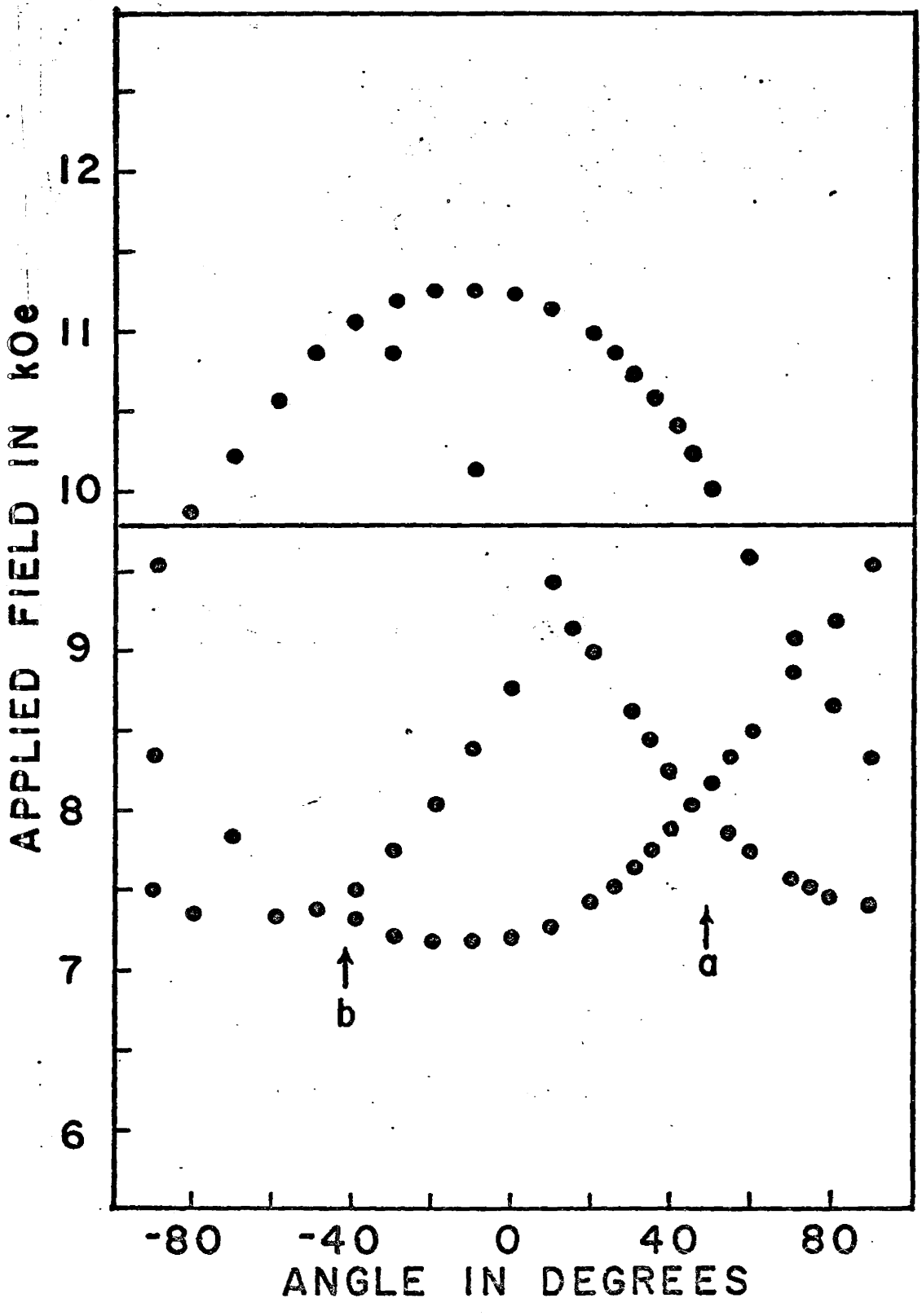
APPLIED FIELD IN kOe
12
11
10
9
8
7
6
b
a
-80
-40
0
40
80
ANGLE IN DEGREES

Fig. 18

Applied fields for the ^{31}P resonances as a function of angle for the external field in the bc* plane. The resonant frequency is 17.00 MHz.

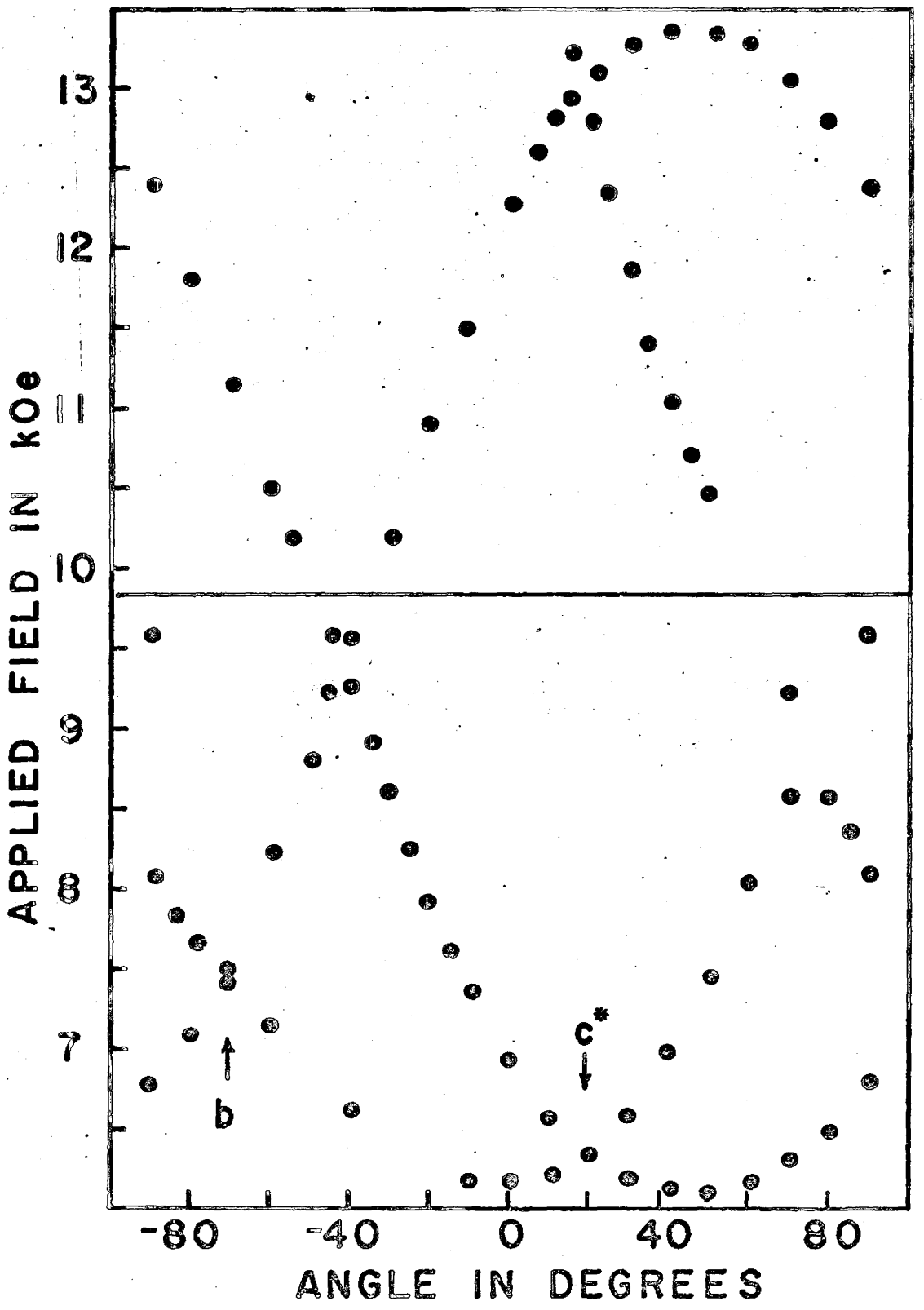
APPLIED FIELD IN kOe
13
12
11
10
9
8
7
b
c*
-80
-40
0
40
80
ANGLE IN DEGREES

Fig. 19

Applied fields for the ^{31}P resonances as a function of angle for the external field in a plane perpendicular to an axis 30° from c* towards the a axis in the ac* plane. The resonant frequency is 16.5 MHz.

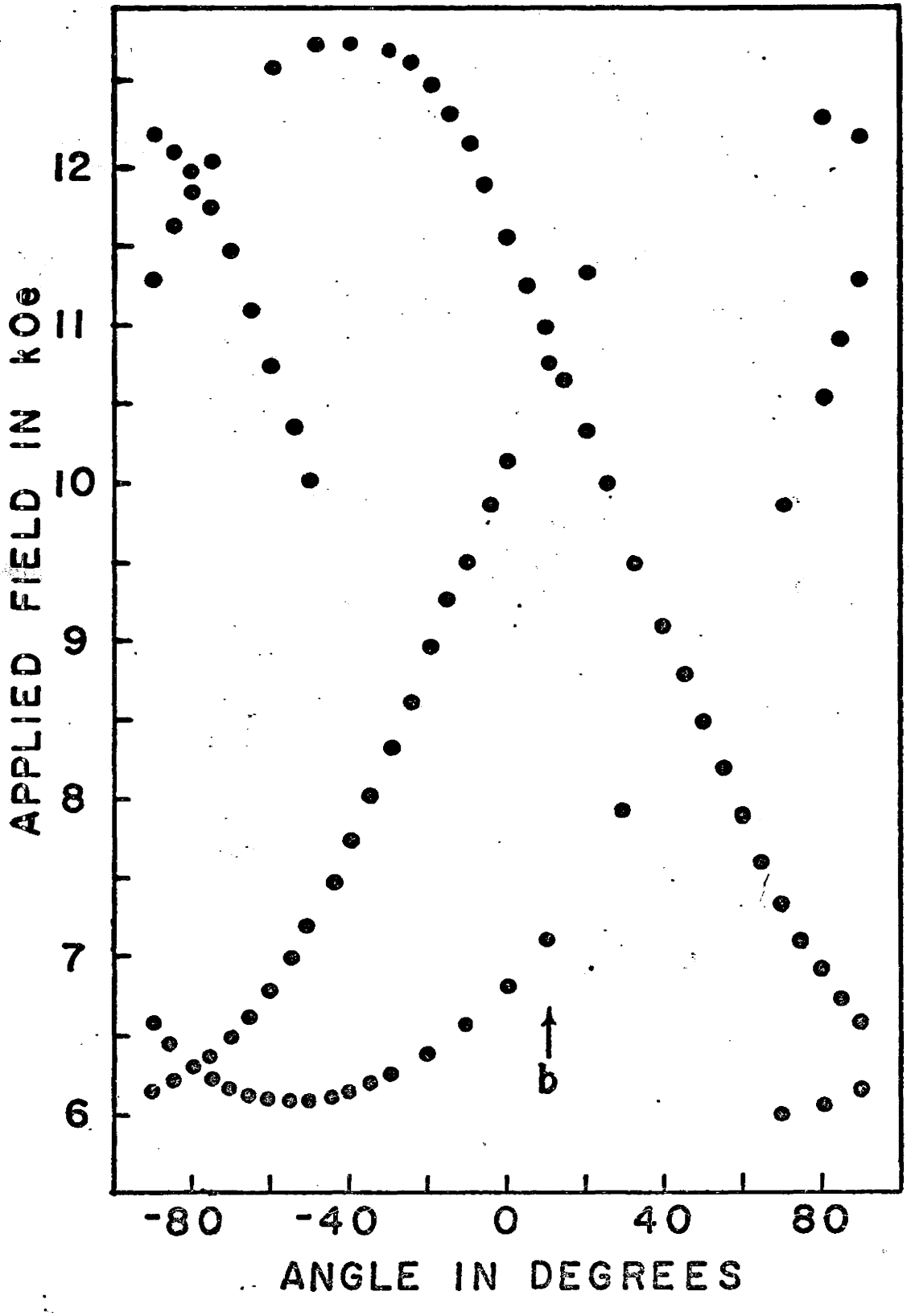
APPLIED FIELD IN kOe
12
11
10
9
8
7
6
b
-80
-40
0
40
80
ANGLE IN DEGREES

Fig. 20

The solid circles are the applied fields for the ^{31}P resonances as a function of angle for the external field in the ac* plane. The resonant frequency is 21 MHz. The open circles are spin flop antiferromagnetic resonances at the same frequency.

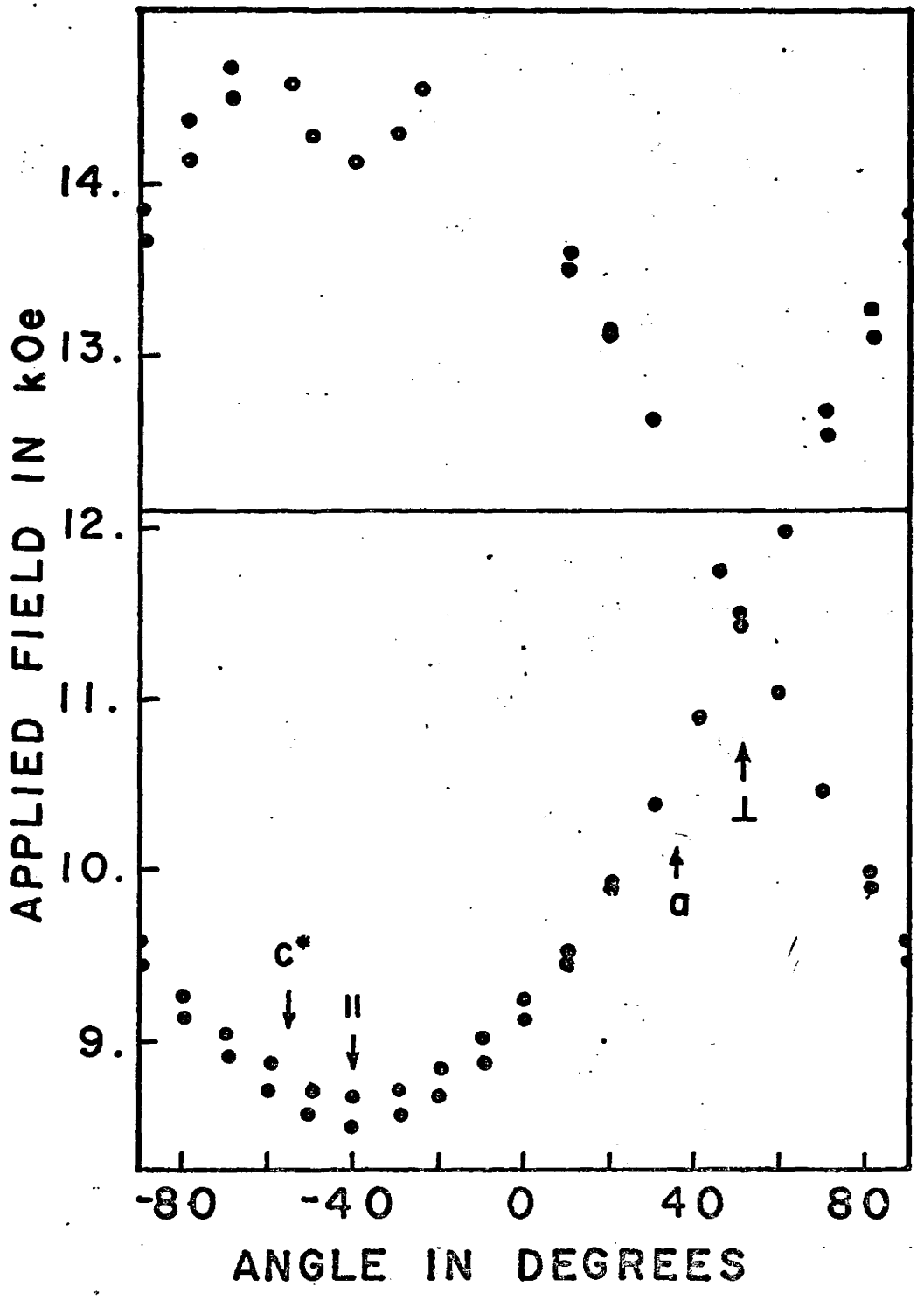
APPLIED FIELD IN kOe
14.
13.
12.
11.
10.
9.
c*
||
a
⊥
-80
-40
0
40
80
ANGLE IN DEGREES

No temperature dependence was observed between 1.5°K and 10°K.

The formalism of Choh and Stager (1970) as developed earlier in this chapter, was used to evaluate the $Cu_2P_2O_7$ data. There are a number of outstanding differences between the experimental results for $Mn_2P_2O_7$ and $Cu_2P_2O_7$. The first is the substantially larger internal field present at the phosphorous sites in $Cu_2P_2O_7$. Secondly the resonance pattern in $Cu_2P_2O_7$ does not exhibit the two maxima per site as a function of angle over 360° as does that in $Mn_2P_2O_7$, but more closely approximates a simple sinusoidal dependence. This is related to the small magnitude of the susceptibility term in the Hamiltonian. There are, however, still significant deviations from sinusoidal behaviour. Exact sinusoidal behaviour would result if the internal magnetic fields are not perturbed by the external field. Finally, there was no temperature dependence of the resonances for fields along the easy direction, in contrast to the results for $Mn_2P_2O_7$.

As was discussed earlier in this chapter, there are two major perturbations on the spins in an antiferromagnetic system upon the application of an external magnetic field. The first, being the tipping of spins on opposing sublattices towards one another, is included in the susceptibility term of the Hamiltonian, since it involves the vector $\bar{S}^+$ defined earlier. As shown previously, this tipping is proportional to H/H_{ex}. In $Mn_2P_2O_7$ this effect is important since the exchange field is 77 kOe, as determined from magnetic susceptibility data (Fowlis

and Stager (1970) and the applied field was of the order of 12 kOe. In $Cu_2P_2O_7$, however, this spin tipping might be expected to be less important, because the exchange field for this compound has been determined to be H_{ex} = 900 kOe as compared to an internal field again of the order of 12 kOe. The exchange field for $Cu_2P_2O_7$ has been determined by Fowlis (1970) from magnetic susceptibility data. The ratio of H/H_{ex} is therefore much smaller for $Cu_2P_2O_7$ than it is for $Mn_2P_2O_7$.

The second effect is the spin rotation effect which depends on H/H_{SF}. This effect was not important in $Mn_2P_2O_7$ because of the relatively large spin flop field of 24.2 kOe. The spin flop field for $Mn_2P_2O_7$ was obtained from antiferromagnetic resonance data (Fowlis 1970). In $Cu_2P_2O_7$, the spin flop field of 14.2 kOe makes the rotation effect considerably larger. In $Mn_2P_2O_7$ the rotation angle was at most about 2° while in $Cu_2P_2O_7$ the rotation was as much as 25°.

In the analysis of the $Cu_2P_2O_7$ data, the full Hamiltonian is used, and it will be shown that the neglect of the susceptibility term is justified. For this system it is not realistic to replace $\bar{S}^-$ in the final term of the Hamiltonian with $\bar{S}^o_\uparrow$ where $\bar{S}^o_\uparrow$ is the unperturbed vector for an up spin in the absence of a magnetic field. This is because at the fields at which some of the experimental results were obtained the spin flop field is approached and the spins are rotated considerably from their equilibrium zero field positions.

In the analysis of the NMR data for $Cu_2P_2O_7$, the following

coordinate system was chosen. The z axis is chosen to be along the measured zero field sublattice magnetization, and the y axis is chosen to be along the b axis of the crystal. This coordinate system then corresponds to the principle axes of the susceptibility tensor. The tensors $\bar{\bar{A}}^+$ and $\bar{\bar{A}}^-$ are assumed to be real and symmetric. In order to evaluate the Hamiltonian it is necessary to determine the direction and magnitude of $\bar{S}^-$ as a function of the magnitude and direction of the external field, using the procedure described earlier in this chapter. This requires a knowledge of the two spin flop fields for this biaxial system and of the ratio of the parallel to perpendicular susceptibilities. The spin flop fields have been determined by Fowlis (1970) from antiferromagnetic data, to be 14.2 kOe and 140 kOe. The latter result is not considered to be reliable since the AFMR data is not very sensitive to the parameter, but fortunately, the rotation of $\bar{S}^-$ is not sensitive to small changes in the magnitude of this parameter either. The susceptibility has also been determined by Fowlis. From these data are obtained the anisotropy fields of 120 Oe and 12 kOe respectively. The anisotropy field of 120 Oe is a measure of the ease with which the spins can be rotated in a plane defined by the easy direction and the b axis, and the field of 12 kOe refers to the ease by which they can be rotated in a plane perpendicular to the b axis. Thus the b axis is the "intermediate" axis and the second perpendicular direction is the "hard" axis.

It is further assumed that the magnitude of $\bar{S}^-$ remains unchanged and is equal to $|\bar{S}^o_\uparrow|$. This is a valid assumption provided the ratio of the spin flop field to the exchange field H_{SF}/H_{ex} is small. Since $H_{ex} = 10^3$ kOe for $Cu_2P_2O_7$, this approximation is reasonable.

Having found the direction of $\bar{S}^-$ under the influence of an external field H, one defines a new coordinate system, (x'y'z') such that z' is along the direction of $\bar{S}^-$. In this new coordinate system the solution of the Hamiltonian involves a straightforward diagonalization of the 2×2 matrix which arises from $I = \frac{1}{2}$.

As mentioned previously, there are four resonances observed experimentally, corresponding to 4 different sites. The values of the tensors $|\bar{S}|\bar{\bar{A}}^-$ and $\bar{\bar{\chi}}\cdot\bar{\bar{A}}^+$ are tabulated in Table 8. Because the z axis is along the measured easy direction, only the xz, yz and zz components of $\bar{\bar{A}}^-$ are measured with any precision. The parameters tabulated were obtained by a least squares fit to the Hamiltonian. From these results it is apparent that to within experimental accuracy the tensor product $\bar{\bar{\chi}}\cdot\bar{\bar{A}}^+$ is zero. The tensor $\bar{\bar{A}}^+$ is easily obtained from NMR in the paramagnetic phase as it couples <S> and I in the paramagnetic phase. Atkinson (1969) has determined $\langle\bar{S}\rangle\bar{\bar{A}}^+$ by measuring the frequency shift of the ^{31}P NMR signal at room temperature (300°K). The thermal average of S' can be calculated, and hence $\bar{\bar{A}}^+$ can be determined. Using this value of $\bar{\bar{A}}^+$ and the experimental uncertainty in $\bar{\bar{\chi}}\cdot\bar{\bar{A}}^+$ one can put an upper

Table 8

Interaction tensor components in units of 10^{-4} cm^{-1} at 4.2°K

i[a]	1	2	3	4
$(\chi \cdot A^+)xx$	.004(.004)[b]	.011(.004)	.011(.003)	.004(.004)
$(\chi \cdot A^+)xy$	.005(.004)	-.002(.004)	-.002(.004)	+.005(.004)
$(\chi \cdot A^+)xz$	.005(.003)	.002(.002)	.002(.002)	.005(.003)
$(\chi \cdot A^+)yy$	-.002(.003)	.006(.003)	+.006(.003)	-.002(.003)
$(\chi \cdot A^+)yz$	-.009(.003)	-.010(.003)	-.010(.004)	-.009(.003)
$(\chi \cdot A^+)zz$	-.004(.003)	-.004(.002)	-.004(.002)	-.004(.003)
$\langle S \rangle \cdot A^-xx$	-41 (24)	31 (14)	-31 (14)	41 (24)
$\langle S \rangle \cdot A^-xy$	1.73 (.53)	1.85 (.42)	-1.85 (.42)	-1.73 (.53)
$\langle S \rangle \cdot A^-xz$	-.03 (.02)	.00 (.02)	.00 (.02)	.03 (.02)
$\langle S \rangle \cdot A^-yy$	-.53 (.28)	.81 (.39)	-.81 (.39)	.53 (.28)
$\langle S \rangle \cdot A^-yz$	1.05 (.02)	1.10 (.02)	-1.10 (.02)	-1.05 (.02)
$\langle S \rangle \cdot A^-zz$	-1.94 (.03)	1.95 (.03)	-1.95 (.03)	1.94 (.03)

[a] i labels the phosphorous ions. The remaining 4 ions in the chemical unit cell are generated by the c centering symmetry operation.

[b] The numbers in parenthesis are the standard deviations.

limit on the magnetic susceptibility tensor elements.

A limit of approximately 10^{-2} emu/mole for the perpendicular susceptibility is calculated. This is consistent with the value 8.0×10^{-3} emu/mole obtained by Fowlis (1970) with a Foner magnetometer at 4.2°K. Our experimental uncertainty is due to the linewidth of the NMR signal. Assuming that any temperature dependence is due to the susceptibility term in the Hamiltonian, the lack of any temperature dependence of the resonance curves in $Cu_2P_2O_7$ is consistent with the above result. It should be noted that there may be an additional temperature dependent term due to the Brillouin function dependence of $|\bar{S}_\uparrow|$, but this is small over the temperature range examined. For a Néel temperature of 26°K the sublattice magnetization normalized to the sublattice magnetization at 0°K is $M_S(T)/M_S(0) = .985$ at T = 10°K which is the highest temperature at which data was taken. It should be noted that for sufficiently low temperatures the magnetization should fall off more sharply according to spin wave theory which is valid in the low temperature region, but at 10°K we are sufficiently high in temperature that the molecular field approximation is valid. Therefore the sublattice magnetization and hence $|\bar{S}_\uparrow|$ varies by at most $\lesssim 1.5\%$ over the temperature range examined. This effect would be masked by the uncertainty in the measurements.

The four resonances observed correspond to four inequivalent phosphorus sites. At high temperature (300°K) the point group of the crystal is 2/m (Robertson and Calvo, 1967). The phosphorus sites are at general positions, and so the

four sites are generated by the 2 fold axis rotation and the mirror plane. Initially it will be assumed that the point group remains 2/m at 4.2°K. The spin configuration has been determined in an earlier section of this work and is shown in Fig. 10(a). There is a possibility of the configuration being that shown in Fig. 10(b) for reasons discussed in Chapter III. Assuming that configuration I of Fig. 10(a) is correct, it can be seen from the figure and from the crystallographic space group that the Heesch group is 2/m'. Using this information the internal fields at the phosphorus sites can be analysed in terms of the crystal symmetry. Figure 21 shows the internal fields as determined from the NMR data. Sites (1) and (2) are related by the 2 fold axis, as are sites (3) and (4), using the above Heesch group as a guide. Sites (1) and (3), as well as (2) and (4) are related by the m' plane. It follows then, that all internal fields have the same magnitude and that the external fields (1) and (4) as well as (2) and (3) are colinear. From this information it is evident that if the external field is applied perpendicular to the 2 fold axis as in Fig. 16 that the magnitude of the vector sum of the internal and external fields should coincide in pairs, and only two resonances should be seen, related to each other by the 2 fold axis. The fact that experimentally, four resonances are observed in this plane indicates that the mirror plane has been lost as an element of the crystallographic point group. In terms of the space group for the crystal, this means that the c glide plane is no

Fig. 21

Internal fields in $Cu_2P_2O_7$ at the phosphorus nuclei.

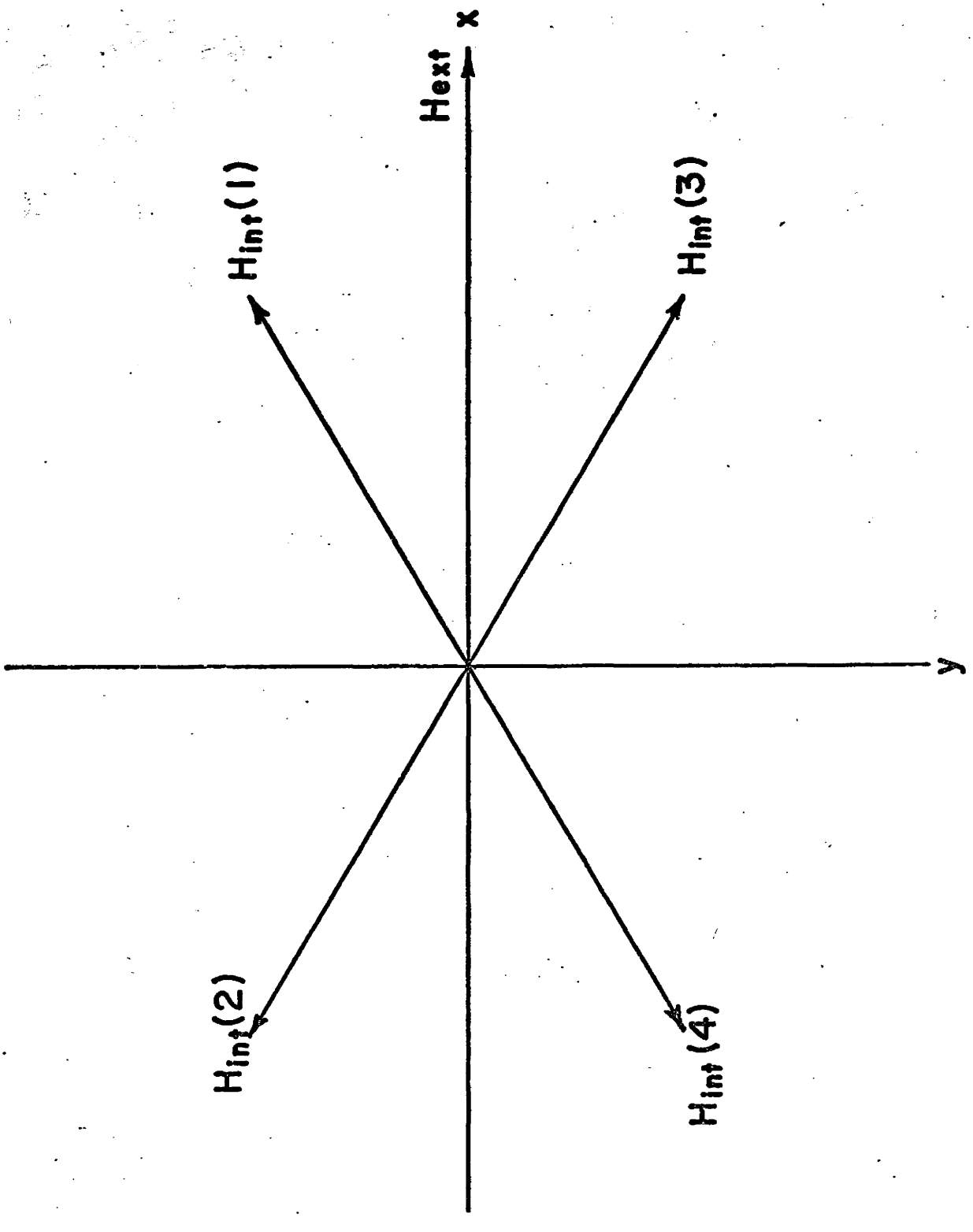
x
Hext
y
Hint(1)
Hint(3)
Hint(2)
Hint(4)

longer a symmetry element, so the space group becomes C2.

If it should be true that configuration II in Fig. 10(b) represents the correct spin configuration, the Heesch group becomes 2'/m. Again with reference to Fig.21 , it is now evident that sites (1) and (3) are related by the 2' axis as are sites (2) and (4). Sites (1) and (4) as well as (2) and (3) are related by the mirror plane. Again it follows that all internal fields are equal in magnitude and that fields (1) and (4) and (2) and (3) are colinear, assuming that the space group is C2/c. In this case the resonances should coincide in pairs as well, if the external field is perpendicular to the 2 fold axis. However, the two observed resonances are not related by the 2 fold axis in this case, but by the mirror plane. Thus the observance of four resonances indicates the loss of the 2' axis as a symmetry element. In terms of the crystallographic symmetry this means that the space group is Cc.

In either case, the degree of deviation from C2/c can be estimated. With the external field along the easy direction, where the splitting of the resonances is greatest, the observed splitting is of the order of 100 Oe. The internal field component in this direction is 3.3 kOe so the fractional internal field difference for the 2 closely related sites is about 3%.

Using the approximate $\frac{1}{r^{10}}$ dependence for the transferred hyperfine field gives a difference of 0.3% in the bond lengths. That is the atomic coordinates of the symmetry related sites in the C2/c approximation are shifted relative to one another by

about .005 Å.

Next the origins of the internal field are discussed. As in $Mn_2P_2O_7$ these consist of two major parts. The dipole field may be calculated using the procedure outlined earlier. As was the case for $Mn_2P_2O_7$, this was done assuming that the magnetic moments are localized on the magnetic ions, and then again, assuming that some of the spin polarization is on those oxygens which are near neighbours to the magnetic ions. The dipole fields for both of these cases, assuming spin configuration I are given in Table 9. For the spin configuration II the dipole fields are given in Table 10. The spin polarization on the oxygens was assumed to be 2% of one unpaired spin, a result estimated from NMR in the paramagnetic phase (Atkinson 1969). From the tables it is evident that the measured components of the internal field perpendicular to the easy direction are not accounted for by the dipole fields, although the latter spin configuration gives a better result than the former. The easy direction of the magnetization was determined by susceptibility measurements (Fowlis 1970) to lie in the ac* plane 15° away from the c* towards the a axis.

Initially, the transferred hyperfine interaction is assumed to be isotropic. If this is the case, the transferred hyperfine contribution to the internal field should lie along the easy direction of the magnetization. The fact that the only

Table 9

Dipole fields in Oe for phosphorous sites in $Cu_2P_2O_7$ for spin configuration most favoured from neutron diffraction results

i^b	1	2	3	4
^aH_y with spins localized on copper ions	48	48	-48	-48
H_y with 2% spin polarization on oxygen sites				
contribution from copper sites	46	46	-46	-46
contribution from oxygen sites	125	125	-125	-125
total dipole field	171	171	171	171
measured field component along y axis	1850(40)	1900(40)	-1900(40)	-1850(40)

[a] Only y components of the dipole fields are tabulated. There is a small perpendicular component to the dipole field arising because the copper ions are located slightly off of a two-fold axis in the crystal.

[b] i labels the phosphorous sites.

Table 10

Dipole fields in Oe for phosphorus sites in $Cu_2P_2O_7$, assuming alternate spin configuration

i[b]	1	2	3	4
a_{H_y} with spins localized on copper ions	1060	1060	-1060	-1060
H_y with 2% spin polarization on oxygen sites				
contribution from copper sites	1000	1000	-1000	-1000
contribution from oxygen sites	125	125	-125	-125
total	1125	1125	-1125	-1125
measured field component along y axis	1850(40)	1900(40)	-1900(40)	-1850(40)

[a]Only y components of the dipole fields are tabulated

[b]i labels the phosphorus sites

other known contribution to the internal field, the dipole field, does not account for the component of internal field perpendicular to the easy direction suggests that there may be an anisotropic contribution to the transferred hyperfine interaction. The discrepancy might also be explained in the following manner. If the point group is indeed Cc or C2, there is no center of inversion symmetry between magnetic ions and the existence of a Dzialoshinsky term in the exchange Hamiltonian is not ruled out. The spins may be canted slightly in this case. This did not manifest itself in the susceptibility measurements (Fowlis, 1970), but the experimental error in the measurements is such that a small canting angle would not have been apparent. Fowlis has shown that $Ni_2P_2O_7$ is a canted antiferromagnet. The resulting component of spins perpendicular to the easy direction would result in a net ferromagnetic moment. The contributions to the transferred hyperfine interactions due to this component of the spins on various sites would not tend to cancel. The spin components along the easy direction do tend to cancel, however. Thus a relatively small perpendicular component of the spins in this direction could produce a large transferred hyperfine field at the phosphorus sites.

It is noted that the transferred hyperfine fields in $Cu_2P_2O_7$ are much larger than those found in $Mn_2P_2O_7$, even though they might be expected to be much smaller, due to the spin of 1/2 on the copper ions compared to s = 5/2 for manganese. To understand this effect it is appropriate to reconsider the origin

of the transferred hyperfine fields in $Mn_2P_2O_7$. In this case the space group was C2/m and the mirror plane was a magnetic m plane, which should result in the transferred hyperfine field at the phosphorus sites, which lie on the mirror plane, to be zero. However, it was postulated that a crystallographic phase transition caused the disappearance of the mirror plane, thus allowing the transferred hyperfine field to be non zero. However, the deviation from symmetry was small, resulting in almost perfect cancellation of the symmetry related fields. In $Cu_2P_2O_7$, however, the deviation from C2/m symmetry is larger so that the cancellation effect is not as pronounced, resulting in a larger net transferred hyperfine field. An approximate calculation can be made of the deviation from C2/m symmetry by using equation (71), as was done for $Mn_2P_2O_7$. As in the previous case, the transferred hyperfine field in the paramagnetic phase can be compared with the measured field for the antiferromagnetic phase, to roughly determine the magnitude of the deviations from C2/m symmetry. From NMR in the paramagnetic phase (Atkinson 1969) an extrapolated field for a saturated paramagnet of 12.6 kOe is obtained. Assuming that the measured transferred hyperfine field consists only of the component of the measured internal field along the easy direction for the magnetization we may take it to be 3.3 kOe. These two results and equation (71) then predict a difference in the transferred path lengths of .08 Å for pairs which are symmetry related in

the C2/m phase, or roughly eight times the distortion predicted for $Mn_2P_2O_7$. This result can be compared with the variations in the Cu-O bond lengths determined by Robertson and Calvo (1967) by X-ray diffraction. They obtained values of 1.907(6)Å and 1.935(6)Å for two bonds which are symmetry related in the β or C2/m phase giving a difference of .03Å and 1.990(6)Å and 1.968(6)Å for the remaining pair giving a difference of .02Å. These differences are smaller, partly because variations in the P-O bond lengths are being ignored. Also any dependence of the transferred hyperfine mechanism on the angle between the P-O bond and the Cu-O bond has been ignored. These differences are small however and should not account for the discrepancy. It is concluded then, that the transferred hyperfine interaction varies more rapidly with increasing separation of the ions than was previously assumed. In fact a value of 20 for the factor n in equation (72) would be more appropriate, that is the functional dependence of the interaction goes like r^{20} where r is the separation of the ions measured along the connecting bonds.

This result may be compared with the temperature dependence of the fraction of unpaired electron on the ^{31}P ion in the paramagnetic phase. Because the excited states for copper in $Cu_2P_2O_7$ are of the order of 2000 cm^{-1} above the ground state doublet, they should not be appreciably occupied at $T \sim 400°K$ or less. Thus any change in the transferred hyperfine field may be attributed to changes in the transferred hyperfine path due to thermal expansion. Atkinson (1969) gives fractions of

unpaired electrons at 400°K of .23%, at 298°K of .25% and at 77°K of .27% in $Cu_2P_2O_7$. The lattice parameters are not accurately known as a function of temperature, but an estimated change of .4% between 400°K and 298°K can be obtained using the r^{20} radial dependence of the unpaired spin. This is a change of approximately .03 Å for the lattice parameters over this temperature difference. This is not inconsistent with the work of Robertson and Calvo (1967), who obtain values for a of 6.827(5)Å at 370°K and 6.876(5)Å at 298°K giving a difference of .04(1)Å. It should be noted that $Cu_2P_2O_7$ is in the α phase at 298°K and in the β phase at 400°K, however, this should not affect the lattice constants appreciably, except for the c axis, which is doubled in the α phase.

CHAPTER V

A DISCUSSION OF THE ORIGIN OF THE ANISOTROPY ENERGIES FOR $Cu_2P_2O_7$

The reader is reminded that the anisotropy energy defines the ease with which the spins can be rotated from the long direction into each of two perpendicular directions. These two energy differences are denoted by E_{A_1} and E_{A_2}. The anisotropy energy may arise from a number of possible sources in a non cubic magnetic material. These include the dipole-dipole interaction, single ion anisotropy energies arising from interaction with the crystal field, and anisotropy arising from the exchange Hamiltonian.

The first of these to be discussed is the dipole anisotropy. The dipole energy can be written in the following form

$$E_D = \frac{-1}{v_a} \sum_{\beta} \sum_{\alpha} \sum_{\substack{kk' \\ k \leq k'}} \mu_\alpha(k) Q_{\alpha\beta}(kk') \mu_\beta(k') \qquad (73)$$

where E_D is the dipole energy per unit volume and the $Q_{\alpha\beta}(kk')$ are the coefficients defined in chapter four. $\mu_\alpha(k)$ and $\mu_\beta(k)$ are the α and β components of the k^{th} and k'^{th} magnetic moments in the unit cell. The magnetic moment is given by

$$\mu_\alpha(k) = \beta \sum_{\beta} g_{\alpha\beta}(k) S_\beta(k) \qquad (74)$$

where $g_{\alpha\beta}(k)$ are the components of the g tensor for the site k and $S_\beta(k)$ is the β component of the spin on the site k. Experimentally, the g tensor is identical for all sites so $\bar{\bar{g}}(k) = \bar{\bar{g}}$. The g tensor is given by

$$\bar{\bar{g}} = \begin{pmatrix} g(x')\cos^2\theta + g(z')\sin^2\theta & 0 & g(z')-g(x'))\sin\theta\cos\theta \\ 0 & g(y') & 0 \\ g(z')-g(x')\sin\theta\cos\theta & 0 & g(z')\cos^2\theta + g(x')\sin^2\theta \end{pmatrix} \quad (75)$$

where g(x'), g(y'), and g(z') are the principal values corresponding to a coordinate system where x' is 30° away from the a axis away from a* and y' is along the b axis. g(x) = 2.480, g (y') = 2.090 and g(z') = 2.095. The angle θ corresponds to a rotation about y'. A rotation of θ = -105° puts the g tensor in the coordinate system xyz where x corresponds to the easy direction for the magnetization. In this coordinate system the g tensor is given by

$$\bar{\bar{g}} = \begin{pmatrix} 2.12 & 0 & .11 \\ 0 & 2.09 & 0 \\ .11 & 0 & 2.45 \end{pmatrix} \quad (76)$$

Combining equations (73) and (74) gives the dipole energy

$$E_D = \frac{-1}{v_a} \sum_{\substack{kk' \\ k \leq k'}} \bar{S}(k) \cdot \bar{\bar{g}} \cdot \bar{\bar{Q}}(kk') \cdot \bar{\bar{g}} \cdot \bar{S}(k') \quad (77)$$

The tensor product $\bar{\bar{g}}\cdot\bar{\bar{Q}}(kk')\cdot\bar{\bar{g}}$ is defined as $\bar{\bar{C}}(kk')$. Use has been made of the fact that $\bar{\bar{g}}\cdot\bar{S} = \bar{S}\cdot\bar{\bar{g}}$ because $\bar{\bar{g}}$ is symmetric. The spin $S(k) = (\pm 1)_k S$. Incorporating the appropriate signs into the tensor $\bar{\bar{C}}(kk')$, the dipole energy is given by

$$E_D = - \begin{pmatrix} S_x \\ S_y \\ S_z \end{pmatrix} \cdot \begin{pmatrix} C_{xx} & X_{xy} & C_{xz} \\ C_{yx} & C_{yy} & C_{yz} \\ C_{zx} & C_{zy} & C_{zz} \end{pmatrix} \cdot \begin{pmatrix} S_x \\ S_y \\ S_z \end{pmatrix} \qquad (78)$$

where

$$\bar{\bar{C}} = \sum_{\substack{kk' \\ k \leq k'}} (\pm 1)k \, \bar{\bar{C}}(kk')(\pm 1)k' \, . \qquad (79)$$

The sign $(\pm 1)_k$ is determined from the spin configuration. The direction of the spins for minimum dipole energy is then found by solving the following eigenvalue problem.

$$\begin{pmatrix} C_{xx}+E & C_{xy} & C_{xz} \\ C_{yx} & C_{yy}+E & C_{yz} \\ C_{zx} & C_{zy} & C_{zz}+E \end{pmatrix} \begin{pmatrix} S_x \\ S_y \\ S_z \end{pmatrix} = 0 \qquad (80)$$

The three eigenvalues, E_0, E_1 and E_2 are the dipole energies with the spins in the three orthogonal directions, with $E_2 > E_1 > E_0$. The spin direction is determined by the spin eigenvector association with E_0. From this vector, the easy direction for the magnetization is easily determined from the relation $\bar{\mu} = \bar{\bar{g}}\cdot\bar{S}$. The dipole anisotropy energies are given by $E^D_{A_1} = E_2 - E_0$ and $E^D_{A_2} = E_1 - E_0$. The calculated easy directions

for the spin configurations shown in Figures 10(a) and 10(b) are shown in Fig.22 . In neither case does the calculated easy direction correspond to the experimental direction. The dipole anisotropy energies $E^D_{A_1}$ and $E^D_{A_2}$ are given by $E^D_{A_1}$ = .172 cm^{-1} and $E^D_{A_2}$ = .163 cm^{-1} for the spin configuration in Fig. 10(a). In this case $E^D_{A_1}$ refers to the anisotropy energy measured in the ac plane and $E^D_{A_2}$ refers to the anisotropy energy in the plane defined by the predicted spin direction and the b axis. For the spin configuration in Fig. 10(b), $E^D_{A_1}$ = .207 cm^{-1} and $E^D_{A_2}$ = .224 cm^{-1}. For both these configurations the ratio of the anisotropy energies is approximately equal to unity, a result in disagreement with a ratio of about 100 to 1 measured by antiferromagnetic resonance (Fowlis 1970). The lack of agreement with experiment suggests that there is another contribution to the anisotropy energy.

At this point it is appropriate to consider the electronic structure of the Cu^{++} ion. The Cu^{++} ion has nine 3d electrons and the free ion ground state is $^2D_{5/2}$. In the absence of a spin orbit coupling term in the single ion Hamiltonian this state is degenerate in energy with the $^2D_{3/2}$ state. Upon the application of spin orbit coupling these levels split, so there are six degenerate levels lowest in energy corresponding to the $^2D_{5/2}$ state and four higher in energy corresponding to the $^2D_{3/2}$ state. In the crystal field resulting from neighbouring ions in $Cu_2P_2O_7$, these states are mixed to form five Kramers

Fig. 22

Calculated easy directions for the anisotropy energy, assuming different mechanisms. The direction labelled 2 is the easy direction for the dipole energy, assuming the spin configuration in Fig. 10(b). The direction labelled 3 is the easy direction for the dipole energy, assuming the configuration most favoured by neutron diffraction measurements as in Fig. 10(a). The direction labelled 1 is the easy direction predicted on the basis of the spin anisotropy. Finally, the direction labelled 4 is the experimental easy direction.

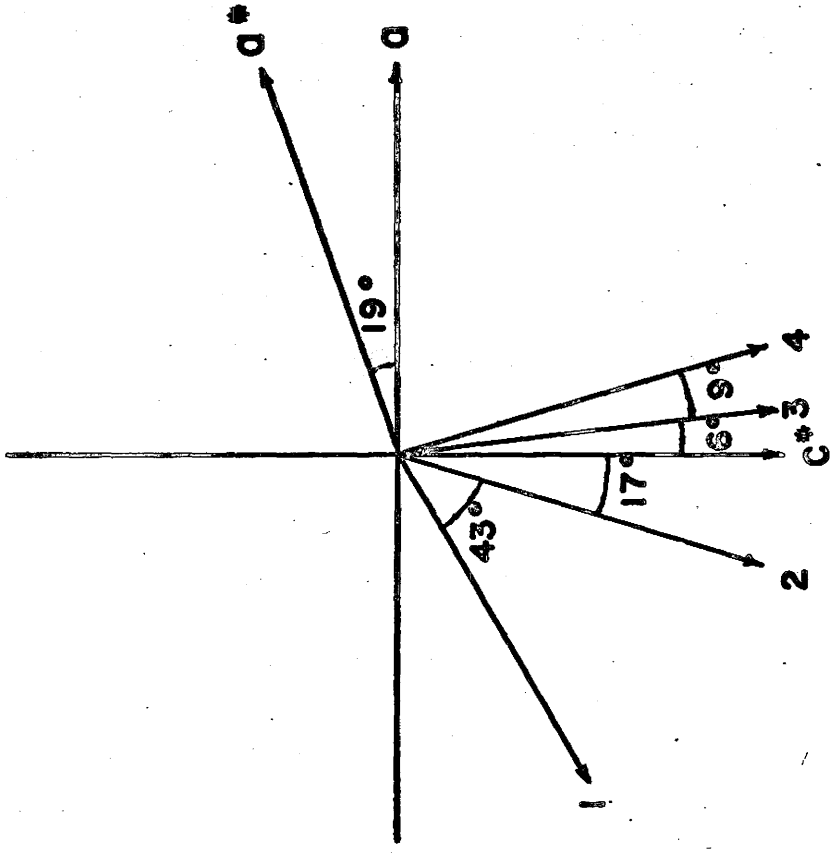
a*
a
19°
4
5°
3
5°
c*
17°
43°
2
1

doublets. The local environment of the Cu^{++} ions is almost tetragonal, as shown by the g values of 2.48, 2.090 and 2.095 (Fowlis,1970) respectively. However, there is a small orthorhombic distortion. Using the measured spin orbit coupling constant for the free ion and the measured g values the angular part of the wavefunctions for Cu^{++} in $Cu_2P_2O_7$ can be obtained.

Since the Kramers doublets are well separated the system can be discussed in terms of the lowest doublet only. A fictitious spin of 1/2 can be applied to this system as a result. This rules out the existence of single ion crystal field terms in the Hamiltonian which contribute to the anisotropy energy, since terms of this type are zero for S = 1/2.

Another source of anisotropy lies in the exchange Hamiltonian

$$H = \sum_{i<j} \bar{\bar{J}}_{ij} \bar{S}_i \cdot \bar{S}_j \ . \qquad (81)$$

This anisotropy may be a result of anisotropy in the exchange tensor $\bar{\bar{J}}_{ij}$ or it may be due to anisotropy in the expectation value for $\bar{S}_i$ and $\bar{S}_j$. The latter case will be discussed first. It is first necessary to calculate the wavefunctions of the Cu^{++} ions. The calculation is done using the basis states $|\ell\ S\ J\ M_J\rangle$. For Cu^{++} $\ell = 2$ and $S = \frac{1}{2}$, leaving two possible values for J, namely $J = \frac{3}{2}$ and $J = \frac{5}{2}$. The following Hamiltonian is used which describes the interaction of the ion with the crystal field.

$$H = \sum_{\ell,m} A_\ell^m \psi_\ell^m + \lambda \bar{L}\cdot\bar{S}. \qquad (82)$$

The sum over ℓ and m may be restricted by noting that $\ell < 5$ since matrix elements of the form $\langle \ell S J M_J | \psi_k^q | \ell S J' M_{J'} \rangle$ must satisfy the triangle inequality $k \leq J + J' < 5$. The odd values are ruled out because they result in non conservation of parity; so the only remaining possibilities are $\ell = 4$, $\ell = 2$ and $\ell = 0$. The allowable values of m may be determined by the symmetry of the site. For cubic symmetry the allowable non zero coefficients are A_4^0 and A_4^4. The existence of the three fold symmetry axis in a cubic system demands that ψ_4^0 and ψ_4^4 are realted by the following equation: $A_4^4 = \sqrt{\frac{5}{14}}\ A_4^0$. In a tetragonal field this restriction is lifted and A_2^0 is non zero as well. In an orthorhombic field, the coefficients A_2^2 and A_4^2 are non zero, but for our case these are small since the local symmetry is almost tetragonal. The spin orbit coupling parameter is denoted by λ. With the above restrictions in mind, the Hamiltonian becomes.

$$H = A_2^0\psi_2^0 + A_4^0\psi_4^0 + A_4^4\psi_4^4 + A_2^2\psi_2^2 + A_4^2\psi_4^2 + \lambda\bar{L}\cdot\bar{S}\ . \qquad (83)$$

The basic states used in this calculation are $|JM_J\rangle$. There are ten of these, but they are paired into Kramers conjugate states which have degenerate energies. As a result the ten by ten matrix obtained by taking matrix elements of the Hamiltonian can be reduced to a five by five matrix. The matrix elements can be calculated by the following method. The Wigner Eckart

theorem can be used to express the matrix elements in terms of a reduced matrix element. That is, one has

$$\langle \ell SJM_J | \psi_k^q | \ell SJ'M_J' \rangle = (1)^{J-M_J} \begin{pmatrix} J & k & J' \\ -M_J & Q & M_J' \end{pmatrix} \langle \ell SJ || \psi_k || \ell SJ' \rangle . \quad (84)$$

The symbol in round brackets is the standard 3j symbol as defined in Rotenberg, The 3j and 6j symbols (1959). $\langle \ell SJ || \psi_k || \ell SJ' \rangle$ is the reduced matrix element. This reduced matrix element can be written in the following form.

$$\langle \ell SJ || \psi_k || \ell SJ' \rangle = (-1)^{J+k+\ell+S} \sqrt{(2J+1)(2J'+1)} \begin{Bmatrix} \ell & J & S \\ J' & \ell' & k \end{Bmatrix} (\ell S ||| \psi_k ||| \ell S) \quad (85$$

where the symbol in curly brackets is the six j symbol defined in Rotenberg and $(\ell S ||| \psi_k ||| \ell S)$ is a doubly reduced matrix element which is independent of J and J'. Because Cu^{++} has only one hole per ion this doubly reduced matrix element has a simple form given by

$$(\ell S ||| \psi_k ||| \ell' S) = (-1)^{\ell} \sqrt{(2\ell+1)(2\ell'+1)} \begin{pmatrix} \ell & k & \ell' \\ o & o & o \end{pmatrix} \quad (86)$$

where again the symbol in round brackets is a 3j symbol. Combining these results gives the following expression for the matrix elements of the Hamiltonian.

$$\langle \ell SJM_J | \psi_k^q | \ell SJ'M_J' \rangle = (-1)^{2J+K+S-M_J} (2\ell+1) \sqrt{(2J+1)(2J'+1)}$$

$$\times \begin{pmatrix} J & k & J' \\ -M_J & q & M_J' \end{pmatrix} \begin{pmatrix} \ell & k & \ell \\ 0 & 0 & 0 \end{pmatrix} \begin{Bmatrix} \ell & J & S \\ J' & \ell & k \end{Bmatrix} \quad (87)$$

The matrix of the Hamiltonian is shown in Table 11. The spin

Table 11

Matrix Elements of the Crystal Field Hamiltonian for Cu^{++}

	$\|5/2\ 5/2\rangle$	$\|5/2\text{-}3/2\rangle$	$\|3/2\text{-}3/2\rangle$	$\|5/2\ 1/2\rangle$	$\|3/2\ 1/2\rangle$
$\|5/2\ 5/2\rangle$	$-\frac{6}{21}A_2^0-\frac{1}{21}A_4^0+\lambda$	$-\frac{2}{3}\sqrt{\frac{1}{14}}A_4^4$	$-\frac{2}{3}\sqrt{\frac{2}{7}}A_4^4$	$-\frac{2}{35}\sqrt{15}A_2^2-\frac{1}{7}A_4^2$	$-\frac{2}{35}\sqrt{10}A_2^2-\frac{1}{21}\sqrt{6}A_4^2$
$\|5/2\text{-}3/2\rangle$	$-\frac{2}{3}\sqrt{\frac{1}{14}}A_4^4$	$\frac{2}{35}A_2^0+\frac{1}{7}A_4^0+\lambda$	$-\frac{6}{35}A_2^0-\frac{2}{21}A_4^0$	$-\frac{6}{35}\sqrt{3}A_2^2+\frac{1}{21}\sqrt{5}A_4^2$	$\frac{4}{35}\sqrt{2}A_2^2-\frac{1}{21}\sqrt{30}A_4^2$
$\|3/2\text{-}3/2\rangle$	$-\frac{2}{3}\sqrt{\frac{2}{7}}A_4^4$	$-\frac{6}{35}A_2^0-\frac{2}{21}A_4^0$	$-\frac{1}{5}A_2^0-\frac{3}{2}\lambda$	$-\frac{2}{35}\sqrt{3}A_2^2+\frac{2}{21}\sqrt{5}A_4^2$	$-\frac{\sqrt{2}}{5}A_2^2$
$\|5/2\ 1/2\rangle$	$-\frac{2}{35}\sqrt{15}A_2^2-\frac{1}{7}A_4^2$	$-\frac{6}{35}\sqrt{3}A_2^2+\frac{1}{21}\sqrt{5}A_4^2$	$-\frac{2}{35}\sqrt{3}A_2^2+\frac{2}{21}\sqrt{5}A_4^2$	$\frac{8}{35}A_2^0-\frac{2}{21}A_4^0+\lambda$	$\frac{\sqrt{6}}{35}A_2^0-\frac{2\sqrt{6}}{21}A_4^0$
$\|3/2\ 1/2\rangle$	$-\frac{2}{35}\sqrt{10}A_2^2-\frac{1}{21}\sqrt{6}A_4^2$	$\frac{4}{35}\sqrt{2}A_2^2-\frac{1}{21}\sqrt{30}A_4^2$	$-\frac{\sqrt{2}}{5}A_2^2$	$\frac{\sqrt{6}}{35}A_2^0-\frac{2}{21}\sqrt{6}A_4^0$	$\frac{1}{5}A_2^0-\frac{3}{2}\lambda$

orbit terms are calculated by noting that

$$\mathbf{L}\cdot\mathbf{S} = \frac{1}{2}\{J(J+1)-\ell(\ell+1)-S(S+1)\}. \qquad (88)$$

Since J, ℓ, and S are all good quantum numbers of the basis states, this term contributes only to diagonal elements of the matrix. The wavefunctions are given by the following expressions.

$$\psi = a_1|5/2,5/2>+a_2|5/2,-3/2>+a_3|3/2,-3/2>+a_4|5/2,1/2>+a_5|3/2,1/2> \qquad (89)$$

$$\psi^* = a_1|5/2,-5/2>+a_2|5/2,3/2>-a_3|3/2,3/2>+a_4|5/2,-1/2>-a_5|3/2,-1/2> \qquad (90)$$

Use has been made of the fact that $|J,M_J> = (-1)^{J-M_J}|J-M_J>$ to determine the Kramers conjugate state ψ^*. The coefficients a_i are determined by the diagonalization of the above matrix. It is necessary to determine the parameters A_ℓ^m to get a numerical solution for the wavefunctions. This is done by calculating the principle values of the g tensors in terms of the lowest energy wavefunctions with arbitrary A_ℓ^m's. A best fit is then obtained for the measured g values, and the corresponding values for the parameters A_ℓ^m are taken to be the correct ones.

The g values may be calculated from the following formula.

$$\bar{g} = \bar{\ell} + 2\bar{S}. \qquad (91)$$

The orbital and spin angular momentum vectors may be expressed in terms of spherical tensor components of the first rank as follows.

$$\ell_z = \ell_o \qquad (92)$$

$$-\ell_+ = \frac{-\sqrt{2}}{2}(\ell_x+i\ell_y) = \ell_1^1 \qquad (93)$$

$$\ell_- = \frac{\sqrt{2}}{2}(\ell_x-i\ell_y) = \ell_1^{-1}. \qquad (94)$$

Similar expressions may be defined for the spin angular momentum. The ℓ_1^i are components of a standard spherical tensor of first order. The matrix elements of these tensor operators for the orbital angular momentum operators are given by:

$$\langle LSJM_J|\ell_k^q|LSJM_J\rangle = (-1)^{S+2J+k+\ell-M_J}\sqrt{(2J+1)(2J'+1)}$$

$$\times \begin{Bmatrix} \ell & J & S \\ J' & \ell & k \end{Bmatrix} \begin{pmatrix} J & k & J' \\ -M_J & q & M_J' \end{pmatrix} \langle \ell|||\ell_k|||\ell\rangle \qquad (95)$$

where the symbols are as previously defined. The doubly reduced matrix element $\langle \ell|||\ell_k|||\ell\rangle$ is given by

$$\langle \ell|||\ell_k|||\ell\rangle = [\ell(\ell+1)(2\ell+1)]^{1/2} = \sqrt{30} \ . \qquad (96)$$

The matrix elements of the tensor operator for the spin angular momentum are given by

$$\langle LSJM_J|S_k^q|LSJM_J\rangle = (-1)^{S+2J+k+\ell-M_J}\sqrt{(2J+1)(2J'+1)}$$

$$\times \begin{pmatrix} S & J & \ell \\ J' & S & k \end{pmatrix} \begin{pmatrix} J & k & J' \\ -M_J & q & M_J' \end{pmatrix} \langle S|||S_k|||S\rangle. \qquad (97)$$

The doubly reduced matrix element $\langle S|||S_k|||S\rangle$ is given by

$$\langle S|||S_k|||S\rangle = [S(S+1)(2S+1)]^{1/2} = \sqrt{\tfrac{3}{2}} \qquad (98)$$

The above results are derived in Dieke (1968). The doubly reduced matrix elements for a single particle state are given by Judd (1963).

Using these results, matrix elements of the principle values of the g tensor, g_x, g_y and g_z can be calculated. This

was done and the following expressions for the matrix elements of g were obtained.

$$\langle\psi|g_z|\psi\rangle = 3a_1^2 - \frac{9}{5}a_2^2 - \frac{6}{5}a_3^2 + \frac{3}{5}a_4^2 + \frac{2}{5}a_5^2 + \frac{4}{5}a_2a_3 + \frac{2}{5}\sqrt{6}\,a_4a_5 \tag{99}$$

$$\langle\psi^*|g_z|\psi^*\rangle = -\langle\psi|g_z|\psi\rangle \tag{100}$$

$$\langle\psi|g_z|\psi^*\rangle = 0 \tag{101}$$

$$\langle\psi^*|g_x|\psi\rangle = \frac{6\sqrt{5}}{5}a_1a_2 + \frac{2}{5}\sqrt{5}\,a_1a_3 + \frac{12}{5}\sqrt{2}\,a_2a_4 - \frac{2}{5}\sqrt{3}\,a_2a_5 - \frac{1}{5}\sqrt{2}\,a_3a_4 - \frac{4}{5}\sqrt{3}\,a_3a_5 + \frac{9}{5}a_4^2 + \frac{1}{5}\sqrt{6}\,a_4a_5 - \frac{4}{5}a_5^2 \tag{102}$$

$$\langle\psi|g_x|\psi\rangle = \langle\psi^*|g_x|\psi^*\rangle = 0 \tag{103}$$

$$\langle\psi^*|g_y|\psi\rangle = -\frac{6}{5}\sqrt{5}\,a_1a_2 - \frac{2}{5}\sqrt{5}\,a_1a_3 + \frac{12}{5}\sqrt{2}\,a_2a_4 - \frac{2}{5}\sqrt{3}\,a_2a_5 - \frac{1}{5}\sqrt{2}\,a_3a_4 - \frac{4}{5}\sqrt{3}\,a_3a_5 - \frac{9}{5}a_4^2 - \frac{1}{5}\sqrt{6}\,a_4a_5 + \frac{4}{5}a_5^2 \tag{104}$$

$$\langle\psi|g_y|\psi\rangle = \langle\psi^*|g_y|\psi^*\rangle = 0 \tag{195}$$

These matrix elements can then be used to determine the splitting of the ground state doublet in a magnetic field by degenerate perturbation theory. This was done and the corresponding experimental g values were determined to be $g_x = 2\langle\psi^*|g_x|\psi\rangle$,

$g_y = 2\langle\psi^*|g_y|\psi\rangle$ and $g_z = 2\langle\psi|g_z|\psi\rangle$. These results were used to solve for the coefficients a_i. The resulting wavefunctions and their corresponding energies are given in Table 12. From these wave functions, the matrix elements of the spin operator can be obtained. These are given by

$$\langle\psi|S_x|\psi^*\rangle = \frac{\sqrt{5}}{5} a_1a_2 + \frac{2}{5}\sqrt{5}\, a_1a_3 + \frac{2}{5}\sqrt{2}\, a_2a_4 - \frac{2}{5}\sqrt{3}\, a_2a_5 - \frac{1}{5}\sqrt{2}\, a_3a_4 + \frac{1}{5}\sqrt{3}\, a_3a_5 + \frac{3}{10} a_4^2 + \frac{1}{5}\sqrt{6}\, a_4a_5 + \frac{1}{5} a_5^2 \qquad (106)$$

$$\langle\psi|S_x|\psi\rangle = \langle\psi^*|S_x|\psi^*\rangle = 0 \qquad (107)$$

$$\langle\psi|S_y|\psi^*\rangle = i\left(\frac{1}{5}\sqrt{5}\, a_1a_2 + \frac{2}{5}\sqrt{5}\, a_1a_3 - \frac{2}{5}\sqrt{2}\, a_2a_4 + \frac{2}{5}\sqrt{3}\, a_2a_5 + \frac{1}{5}\sqrt{2}\, a_3a_4 - \frac{1}{5}\sqrt{3}\, a_3a_5 + \frac{3}{10} a_4^2 + \frac{1}{5}\sqrt{6}\, a_4a_5 + \frac{1}{5} a_5^2\right) \qquad (108)$$

$$\langle\psi|S_y|\psi\rangle = \langle\psi^*|S_y|\psi^*\rangle = 0 \qquad (109)$$

$$\langle\psi|S_z|\psi\rangle = \frac{1}{2} a_1^2 - \frac{3}{10} a_2^2 + \frac{3}{10} a_3^2 + \frac{1}{10} a_4^2 - \frac{1}{10} a_5^2 + \frac{4}{5} a_2a_3 + \frac{2}{5}\sqrt{6}\, a_4a_5 \qquad (110)$$

$$\langle\psi^*|S_z|\psi^*\rangle = -\langle\psi|S_z|\psi\rangle \qquad (111)$$

For the ground state doublet the following numerical values were obtained $\langle\psi|S_z|\psi\rangle = .49860$, $\langle\psi|S_z|\psi^*\rangle = .49551$, and $\langle\psi|S_y|\psi^*\rangle = (.49558)i$. The assumption is made that the total wave function, Ψ for the system is equal to the product of the wavefunctions

TABLE 12

Values of the Coefficients a_i for the Cu^{++} Kramers Doublets in in $Cu_2P_2O_7$ and Their Corresponding Energies

energy	a_1	a_2	a_3	a_4	a_5
6355 cm^{-1}	.00039	-.00063	-.00031	.56980	-.82178
5693 cm^{-1}	.19985	.71523	-.66971	.00006	-.00027
3760 cm^{-1}	.63218	-.61632	-.46957	-.00056	.00069
6622 cm^{-1}	.00031	.00014	.00040	-.82178	-.56980
9187 cm^{-1}	.74861	.32954	.57532	-.00063	.00070

associated with the individual magnetic ions. This is a valid assumption provided that the exchange interaction does not perturb the wavefunctions significantly. This is the case for the system of interest since the exchange energy is much less than the energy separation of the Kramers doublets. It is further assumed that the single ion wavefunction ψ_i' refers to the i^{th} site on one sublattice and that $\psi_j'^*$ refers to the j^{th} site on the opposing sublattice. In the absence of the exchange interaction, the system consists of 2N degenerate energy levels, corresponding to the N magnetic ions in the sample. The Heisenberg Hamiltonian is then applied as a perturbation to the system. The degenerate states are now separated in energy and the ground state becomes a doublet consisting of a perfectly aligned antiferromagnet, and its time reversed state, that is where the direction of the spins on opposing sublattices are reversed. These two states are physically identical and hence have the same energy. The remaining states correspond to spin wave excitations. For the purposes of this discussion the system will be assumed to be in its ground state. The ground state doublet is denoted by $|\Psi>$ and $|\Psi^*>$ where

$$\begin{aligned} |\Psi> &= |\psi_1 \cdots \psi_i \cdots \psi_j^* \cdots \psi_N^*> \\ |\Psi^*> &= |\psi_1^* \cdots \psi_i^* \quad\quad \psi_j \quad\quad \psi_N> \ . \end{aligned} \tag{112}$$

In the above approximation the problem can be solved by considering the effect of the exchange interaction on the single ion energy levels. It is necessary to consider the effect of the operator $S_{\alpha i}$ on ψ_i and ψ_i^*. The subscript α refers to the

appropriate component of S_i. By degenerate perturbation theory the solution to this problem is given by

$$\begin{pmatrix} \langle\psi_i|S_{\alpha i}|\psi_i\rangle - \langle S_{\alpha i}\rangle & \langle\psi_i|S_{\alpha i}|\psi_i^*\rangle \\ \langle\psi_i^*|S_{\alpha i}|\psi_i\rangle & \langle\psi_i^*|S_{\alpha i}|\psi_i^*\rangle - \langle S_{\alpha i}\rangle \end{pmatrix} \begin{pmatrix} \psi_i' \\ \psi_i'^* \end{pmatrix} = 0 \quad . \quad (113)$$

The energy of the entire system is then given, relative to the unperturbed Kramers doublet, by

$$E = \sum_{i<j} J_{ij} \langle S_{\alpha i}\rangle\langle S_{\alpha j}\rangle \qquad (114)$$

and for the ground state doublet denoted by Ψ and Ψ^* is given by

$$E = - \sum_{i<j} J_{ij} \langle S_\alpha\rangle^2 \qquad (115)$$

The subscript i has been dropped from S_α since all spins in an antiferromagnet have the same magnitude. It is noted that E is directionally dependent since $\langle S_\alpha\rangle$ depends on the spin direction and is given by $\langle S_\alpha\rangle = .4986$ if the spins are along the direction of the maximum principle value of z and $\langle S_\alpha\rangle = .495$ perpendicular to this direction. This direction is shown in Fig. 22 .

It is evident that this interaction gives rise to an anisotropy energy that is given by

$$E = - \sum_{i<j} J_{ij} [\langle S_\alpha\rangle^2 - \langle S_\beta\rangle^2]. \qquad (116)$$

The equilibrium spin direction, as predicted by this mechanism, occurs in the direction for minimum energy which is along the

direction of the maximum g value. This is 75° away from the measured easy direction for the magnetization, so it may be concluded that this mechanism does not account for the entire anisotropy energy. It should be noted, however, that this mechanism does predict a large anisotropy energy in the plane perpendicular to the b axis of the crystal, and a small anisotropy in the plane defined by the easy direction and the b axis, which is in accordance with experimental results. (Fowlis 1970). The anisotropy in the plane perpendicular to the b axis can be estimated from the measured exchange field H_{ex} from which the exchange constant J can be calculated. The exchange field is defined as the exchange energy divided by the sublattice magnetization and is given by

$$H_{ex} = \frac{2SzJ}{g\mu_o} \quad . \tag{117}$$

J is the average of the nearest neighbour exchange parameters, and z is the number of nearest neighbours. Taking z = 4 and H_{ex} = 900 kOe an average value for J of 34 cm^{-1} is obtained. The value for g is taken to be 2.12 which is the correct value along the easy direction. Using this value for J, an anisotropy energy of $E_{AN} = 1.0\ cm^{-1}$ is obtained. It is noted that this is a considerably larger anisotropy than that due to the dipolar interaction.

It has been assumed throughout the preceding discussion that the exchange tensor J_{ij} is isotropic. The lack of agreement between the experimental spin direction, and that predicted on the basis of dipolar and spin anisotropies would indicate that

this may not be a valid assumption. One description of anisotropic exchange is contained in the pseudo dipolar interaction (Kanamori, 1963). The approximate magnitude of the anisotropic term as compared to the isotropic term is given by $(\lambda/\Delta E)^2$ where λ is the spin orbit coupling parameter and ΔE is the energy separation of the two lowest Kramers doublets. This may also be expressed as being of the order of $(g-2)^2$ which for the case of interest gives a result of about 10%. A detailed calculation of the pseudo dipolar term would be exceedingly difficult because of the complicated nature of the compound studied but it is noted that the interaction is not ruled out by symmetry.

As a final note, there are additional possible contributions to the anisotropy, one of them being the magnetostrictive effects. This arises from spin orbit coupling or from the dependence of the exchange energy on the separation of the magnetic ions. Kanamori also gives a brief description of this effect.

CHAPTER VI

CONCLUSIONS

The spin configurations of $Mn_2P_2O_7$ and $Cu_2P_2O_7$ have been determined by single crystal neutron diffraction. In $Mn_2P_2O_7$ the magnetic unit cell was determined to be commensurate with the chemical unit cell. However the C-centering symmetry is lost in the magnetic unit cell. These results confirmed the work of Collins et al (1970). For $Cu_2P_2O_7$ the magnetic unit cell was assumed to be commensurate with the chemical unit cell. In this compound the magnetic unit cell preserves both the C-centering symmetry and the c glide plane which are symmetry elements of the chemical unit cell. There are two spin configurations which satisfy these criteria, and these two configurations may be distinguished by the presence or absence of the (021) Bragg peak. This peak was found to be present, but its existence can be also explained in terms of a crystallographic phase transition at the Néel temperature. If the peak is assumed to be magnetic in character then the spin configuration consists of antiferromagnetic sheets in the ab plane which are coupled antiferromagnetically to neighbouring sheets. The alternative configuration is identical except that the sheets are ferromagnetically coupled.

The discrepancy between the neutron diffraction measure-

ments on $Mn_2P_2O_7$ and the NMR results of Choh and Stager (1970) has been explained by postulating a low temperature crystallographic phase transition. The NMR data in the paramagnetic and antiferromagnetic phases have been used to estimate the magnitude of the deviation from high temperature symmetry in the low temperature phase. It was found, using a $1/r^{10}$ dependence for the transferred hyperfine interaction, where r is the transferred hyperfine path length, that bond length changes of the order of .01 Å were sufficient to explain the results.

For $Cu_2P_2O_7$ the NMR data were used in a similar manner to calculate transferred hyperfine path length differences. In this compound, however, the distortion from the higher symmetry phase is known from X-ray data (Robertson and Calvo, 1967) and the above results can be compared with this known distortion. It was found that a functional dependence of the transferred hyperfine interaction upon separation of the ions of $1/r^{20}$ gave better agreement with the X-ray data. This result is also consistent with the dependence of the transferred hyperfine interaction upon bond length changes due to thermal expansion.

The anisotropy energy in $Cu_2P_2O_7$ has been discussed. Both dipole anisotropy and spin anisotropy contributions to the anisotropy energy have been considered. Although the spin anisotropy does give approximately the correct anisotropy ratio calculated from antiferromagnetic resonance data (Fowlis, 1970), the correct equilibrium spin direction is not predicted by this

contribution to the anisotropy energy. The dipole anisotropy gives a close approximation to the correct equilibrium spin direction, but does not give the correct anisotropy ratio. It is concluded that the exchange tensor may not be isotropic. The experimental results may be satisfactorily explained in terms of an anisotropic exchange tensor.

BIBLIOGRAPHY

Alperin, H.A. 1960. J. Appl. Phys. 31, 3545.

Atkinson, R.J. 1969. Ph.D. Thesis, McMaster Univ. unpublished.

Atkinson, R.J. and Stager, C.V. 1969. Can. J. Phys. 47, 1557.

Atkinson, R.J., Fowlis, D.C. and Stager, C.V. 1970. Can. J. Phys. 48, 543.

Bacon. G.E. 1962. Neutron diffraction, 2nd ed. (Oxford University Press, Oxford).

Bacon, G.E. and Thewlis, J. 1949. Proc. Roy. Soc. A, 196, 50.

Ballhausen, C.J. 1962. Introduction to Ligand Field Theory (McGraw Hill, New York).

Barnes, R.G. and Smith, W.V. 1954. Phys. Rev. 93, 95.

Benedek, G.B. and Kushida, T. 1960. Phys. Rev. 118, 46.

Born, M. and Huang, K. 1954. Dynamical Theory of Crystal Lattices (Clarendon Press, Oxford).

Calvo, C., Leung, J.S. and Datars, W.R. 1967. J. Chem. Phys. 41, 796.

Chambers, J.G., Datars, W.R. and Calvo, C. 1964. J. Chem. Phys. 41, 806.

Choh S.-H. and Stager, C.V. 1970. Can. J. Phys. 48, 521.

Collins, M.F., Gill, G.S., and Stager, C.V. 1971. Can. J. Phys. 49, 979.

Crawford, M.F. and Schawlow, A.R. 1949. Phys. Rev. 76, 1310.

Dieke, G.H. 1968. Spectra and Energy Levels of Rare Earth Ions in Crystals. (Interscience, New York).

Donnay, G., Corliss, L.M., Donnay, J.D.H., Elliot, N. and Hastings, J.M. 1958. Phys. Rev. 112, 1917.

Dzialoshinski, I. 1958. Phys. and Chem. Solids 4, 241.

Fowlis, D.C. 1970. Ph.D. Thesis, McMaster Univ. unpublished.

Fowlis, D.C. and Stager, C.V. 1969. Can. J. Phys. 47, 371.

Halpern, O. and Johnson, M.H. 1939. Phys. Rev. 55, 898.

Judd, B.R. 1963. Operator Techniques in Atomic Spectroscopy (McGraw Hill, New York).

Kanamori, J. 1963. Magnetism, Vol. 1, edited by G. T. Rado and H. Suhl (Academic Press, New York) Chap. 4.

Lines, M.E. 1967. Phys. Rev. 164, 736.

Long, F. 1972. Private Communication.

Lukaszewics, K. and Smajkiewicz, R. 1961. Rocz. Chem. 35, 741.

Mays, J.M. 1963. Phys. Rev. 131, 38.

Moriya, T. 1963. Magnetism, Vol. 1, edited by G. L. Rado and H. Suhl (Academic Press, New York), Chap.3.

Nagamiya, T., Yosida, K. and Kubo, R. 1955. Advances in Phys. 4, 1.

Opechowski, W. and Guccione, R. (1965). Magnetism, Vol. IIA. Edited by G. L. Rado and H. Suhl (Academic Press, New York).

Owen, J. and STevens, K.W.H. 1953. Nature 171, 636.

Owen, J. and Thornley, J.H.M. 1966. Rep. Prog. Phys. 29, 675.

Riedel, E.P. and Spence, R.D. 1960. Physica, 26, 1174.

Robertson, B.E. and Calvo, C. 1967. Acta Cryst. 22, 665.

Robertson, B.E. and Calvo, C. 1970. Jour. Solid State Chem. 1, 120.

Rotenberg, C. 1959. The 3j and 6j symbols. (Technology Press, M.I.T., Cambridge, Mass.)

Schull, C.G., Strauser, W.A. and Wollan, E.O. 1951. Phys. Rev. 83, 333.

Shulman, R.G. and Jaccarino, V. 1956. Phys. Rev. 103, 1126.

Shulman, R. G. and Jaccarino, V. 1957. Phys. Rev. 108, 1219.

Spence, R.D. and van Dalen, P.A. 1968. Acta Cryst. A24, 494.

Tinkham, M. 1956. Proc. Roy. Soc. A236, 535.

Tondon, V.K. 1971. M.Sc. Thesis, McMaster Univ. unpublished.